Impacts of Base-Case and Post-Contingency Constraint Relaxations on Static and Dynamic Operational Security

by

Ahmed Salloum

A Dissertation Presented in Partial Fulfillment
of the Requirements for the Degree
Doctor of Philosophy

Approved March 2016 by the
Graduate Supervisory Committee:

Vijay Vittal, Co-Chair
Kory Hedman, Co-Chair
Gerald Heydt
Raja Ayyanar

ARIZONA STATE UNIVERSITY

May 2016

ABSTRACT

Constraint relaxation by definition means that certain security, operational, or financial constraints are allowed to be violated in the energy market model for a predetermined penalty price. System operators utilize this mechanism in an effort to impose a price-cap on shadow prices throughout the market. In addition, constraint relaxations can serve as corrective approximations that help in reducing the occurrence of infeasible or extreme solutions in the day-ahead markets. This work aims to capture the impact constraint relaxations have on system operational security. Moreover, this analysis also provides a better understanding of the correlation between DC market models and AC real-time systems and analyzes how relaxations in market models propagate to real-time systems. This information can be used not only to assess the criticality of constraint relaxations, but also as a basis for determining penalty prices more accurately.

Constraint relaxations practice was replicated in this work using a test case and a real-life large-scale system, while capturing both energy market aspects and AC real-time system performance. System performance investigation included static and dynamic security analysis for base-case and post-contingency operating conditions. PJM peak hour loads were dynamically modelled in order to capture delayed voltage recovery and sustained depressed voltage profiles as a result of reactive power deficiency caused by constraint relaxations. Moreover, impacts of constraint relaxations on operational system security were investigated when risk based penalty prices are used. Transmission lines in the PJM system were categorized according to their risk index and each category was assigned a different penalty price accordingly in order to avoid real-time overloads on high risk lines.

This work also extends the investigation of constraint relaxations to post-contingency relaxations, where emergency limits are allowed to be relaxed in energy market models. Various scenarios were investigated to capture and compare between the impacts of base-case and post-contingency relaxations on real-time system performance, including the presence of both relaxations simultaneously. The effect of penalty prices on the number and magnitude of relaxations was investigated as well.

ACKNOWLEDGMENTS

First and foremost, I am immensely grateful to my Creator, to whom I owe my health, patience, and very existence.

My gratitude goes next to my mother, for her boundless and unconditional love and support, for believing in me and showering me with her prayers and blessings.

I would like to express my deep and sincere appreciation to my teacher and advisor, Dr. Vijay Vittal, whom I highly respect and look up to. Dr. Vittal's dedication, knowledge, and wisdom have had a great impact on my personal and academic growth. I also want to thank my advisor, Dr. Kory Hedman, who has inspired me with his enthusiasm and passion. Dr. Hedman's stimulation and patience have made this research experience intriguing and rewarding.

Last but not least, I am extending my thanks to my colleagues and friends who have supported me to complete this work directly or indirectly.

TABLE OF CONTENTS

Page

CHAPTER Page

LIST OF TABLES

Table Page

LIST OF FIGURES

Figure Page

Figure Page

NOMENCLATURE

AC	Alternating current
ACOPF	Alternating current optimal power flow
ACSR	Aluminum-conductor steel-reinforced
B_{im}	Imaginary part of the admittance matrix
b_k	Susceptance of transmission line k
$B(\boldsymbol{x})$	ACOPF barrier function
c	Index of contingencies, $c \in N^g, N^k$
c_g	Operational cost of unit g ($/MWh)
c_g^{NL}	No load generator cost
c_g^{SD}	Generator shutdown cost
c_g^{SU}	Generator startup cost
CAISO	California Independent System Operator
DC	Direct current
DCOPF	Direct current optimal power flow
d_{nt}	Total load at node n during time period t
DT_g	Parameter for the minimum down time requirement for generator g
ERCOT	Electric Reliability Council Of Texas
F_k	Unplanned outage frequency of line k
$f(\boldsymbol{x})$	Nonlinear objective function
g	Parameter for indexing generators
G_{im}	Real part of the admittance matrix
$g(n)$	Set of generators connected to node n

$\boldsymbol{g}(\boldsymbol{x})$	Nonlinear inequality constraints column vector
$\boldsymbol{h}(\boldsymbol{x})$	Nonlinear equality constraints column vector
HVDC	High voltage direct current
I	Index of generator segments, $i \in I$
I_i^*	The conjugate current injected at bus i
IPM	Interior point method
IPP	Independent power producer
J	Jacobian matrix
J_r	Reduced Jacobian matrix
K	Index of transmission lines, $k \in K$
KKT	Karush-Kuhn-Tucker
$L(\boldsymbol{x}, \boldsymbol{\lambda})$	Lagrangian scalar function
LMP	Locational marginal price
LP	Linear programming
LMTF	Load model task force
MISO	Midcontinent Independent System Operator
N	Index for buses, $n \in N$
N^g, N^k	Set of generators and transmission lines contingencies, respectively
N^g, N^k	Set of generators and transmission lines contingencies, respectively
NP	Nonlinear programming
NYISO	New York Independent System Operator
OL_j^{norm}	Normalized post-contingency overload on line j
OL_j^{post}	Post-contingency overload on line j
OL_{MAX}^{post}	Absolute maximum post-contingency overload for all contingencies

OPF	Optimal power flow
P_0	Real power consumed at rated voltage
P_1	Portion of real power modeled as constant impedance
P_2	Portion of real power modeled as constant current
P_3	Portion of real power modeled as constant power
P_g	Generator g supply output
P_g^{max}	Generator g maximum supply output
P_g^{min}	Generator g minimum supply output
P_{gt}	Variable for generator g supply output for time period t
PJM	Pennsylvania Jersey Maryland interconnection
P_i	Injected real power at bus i
P_k	Power flow through branch k
P_k^{max}	Parameter for branch k maximum flow limit, normal rating
$P_k^{max,c}$	Parameter for branch k maximum flow limit, emergency rating
P_{kt}	Variable for power flow through branch k for time period t
PP_M	Penalty price for relaxing base-case transmission constraints (master problem).
PP_S	Penalty price for relaxing post-contingency transmission constraints (slave problem).
PSCOPF	Preventive security optimal power flow
PTDF	power transfer distribution factor
Q_0	Reactive power consumed at rated voltage
Q_1	Portion of reactive power modeled as constant impedance
Q_2	Portion of reactive power modeled as constant current

Q_3	Portion of reactive power modeled as constant power
Q_i	Reactive power consumed at bus *i*
QP	Quadratic programming
R_g^{hr}, R_g^{10}	Max hourly and 10-min ramp rates of unit g, respectively
R_g^{EM}	Emergency ramp rate for generator g
r_{gt}^{SP}	Acquired spinning reserve for generator g during time period t
R_{kj}	Risk index associated with line *k* outage and line *j* overload
r_t^{req}	Required total system reserve during time period t
RTS-96	Reliability test system 1996 version
RUC	reliability unit commitment
s	Feasibility variable
SCED	Security constrained economic dispatch
SCUC	Security constrained unit commitment
S_i	Apparent power consumed at bus *i*
S_{kt}^{M+}, S_{kt}^{M-}	Relaxation variables for base-case thermal limits of transmission asset k during time period t.
$S_{kt}^{NG+}, S_{kt}^{NG-}$	Relaxation variables for post-contingency thermal limits of transmission asset k during time period t, following generation contingency
$S_{kt}^{NK+}, S_{kt}^{NK-}$	Relaxation variables for post-contingency thermal limits of transmission asset k during time period t, following line contingency
SPP	Southwest power pool
t	Parameter used to index time periods
u_{gt}	Variable for status of generator g during time period t
UT_g	Parameter for the minimum up time requirement for generator g

UC	Unit commitment
VAr	Volt ampere reactive
v_{gt}	Variable to startup of generator g during time period t
V_i	Voltage at bus i
w_{gt}	Variable to shutdown of generator g during time period t
$\boldsymbol{x}$	Power system control variables column vector
x_i	Present value of the i-th control variable
x_k	Branch k reactance
$\boldsymbol{x_{max}}$	Maximum limits for system variables $\boldsymbol{x}$ column vector
$\boldsymbol{x_{min}}$	Minimum limits for system variables $\boldsymbol{x}$ column vector
ZIP	Composite static load model
∇_x	Gradient of $\boldsymbol{x}$
α	Deceleration factor
a_{pf}	Real power frequency sensitivity
a_{qf}	Reactive power frequency sensitivity
$\Delta\boldsymbol{x}$	Correction factor
$\boldsymbol{\lambda}$	Lagrange multiplier variables column vector
μ	Barrier parameter
ρ_i	Linear penalty weight for the i-th control variable
$\delta^-(n)$	Set of transmission lines with power flowing out of bus n
$\delta^+(n)$	Set of transmission lines with power flowing into bus n
θ_i	Voltage phase angle at bus i
θ_{nt}	Voltage angle at bus n during time period t

1. INTRODUCTION

1.1 Research Motivation

Electric power system operation is a challenging task that requires system operators to satisfy several objectives while abiding to multiple constraints and limitations. Some of these objectives are even conflicting in nature; for instance, economic objectives push towards full utilization of the power system resources and infrastructure, which in turn results in stressed operating conditions. On the other hand, power system reliability and security become a matter of concern under such stressed operating conditions. Therefore, system operators are continuously solving optimization problems through their energy management systems (EMS) to ensure an economical and secure operation. Mainly, these models allocate resources by determining which generating units are dispatched and the amount of power produced by each generating unit, without violating the system security limits. These optimization problems are referred to as security constrained unit commitment (SCUC) and security constrained economic dispatch (SCED) respectively [1]-[2].

Market models used for resources allocation use several approximations to represent the AC power system as a linear DC system. Furthermore, the resultant DC system is also subjected to additional approximations; for instance, power transfer distribution factors (PTDFs) below a certain threshold are neglected to reduce the optimization problems size and complexity [3]. These approximations are required to obtain near-optimal results in reasonable time and with acceptable computational effort. Considering this approximate nature of the system representation, system operators tend, on some occasions, to

relax certain constraints by defining them as soft limits with a violation penalty price instead of enforcing them as hard limits. This indicates that certain limits are allowed to be violated for a predefined penalty price in the energy market models. These violations are referred to as constraint relaxations. Constraint relaxations are beneficial for avoiding infeasible solutions caused by the several approximations in the market models, as well as an effective mechanism to limit the market clearing prices as will be explained in the succeeding chapters [3]-[4].

This work aims to investigate and identify the critical constraint relaxation practices utilized by system operators and their impacts on system performance and energy markets efficiency. System performance in this context consists of the system reliability, security, and stability, as will be explained in Chapter 4. It is therefore necessary to examine how these constraint relaxations are reflected in real-time and their effect on system operating conditions. Moreover, capturing the impact of constraint relaxations on system performance and energy markets provides a consistent and realistic basis for choosing the proper values for penalty prices associated with constraint relaxations. Penalty prices determination is a critical aspect of constraint relaxations mechanism as they have a direct impact on the number and magnitude of relaxations. Currently, the impacts these constraint relaxations have on the market efficiency and system performance are not considered in determining the related penalty prices. System operators merely choose relatively high penalty prices that are sufficient to ensure that relaxations are infrequent and short-lived.

By utilizing different test cases, including a real-life large-scale system, and investigating the impact of constraint relaxations on the system base-case and post-

contingency operation conditions (static and dynamic behavior), this work captures how constraint relaxations in energy market models are translated into violations in real-time AC system. It also investigates post-contingency constraint relaxations (emergency limits) and compares their impact on markets and system performance with base-case relaxations. Capturing and quantifying the risk associated with various constraint relaxations provides system operators with valuable insight on the real effects of these relaxations, which is crucial in determining realistic and consistent penalty prices in order to control the frequency and magnitude of these relaxations accordingly.

1.2 Literature Survey: Constraint Relaxations

Limited research has been done in the area of constraint relaxations, especially their effect on real-time system performance. System operators provide brief descriptions of constraint relaxations practices in their published operation manuals without providing the bases for choosing their penalty prices or the effect of these relaxations on energy markets and system operating conditions.

The California Independent System Operator (CAISO), for instance, states that the fundamental market design principle for their model is to rely as far as possible on submitted economic bids to clear the market and determine the settlements. However, it has been observed that in some instances depending solely on economic bids, does not yield a complete and feasible solution. In such cases, certain adjustments that are referred to as “uneconomic adjustments” are made in order to obtain a feasible solution. Relaxation of constraints is considered as one of the uneconomic adjustments. The forward and day-ahead, market solution process at CAISO is split into two parts, scheduling run and,

pricing run. When solved, the scheduling run determines the dispatch schedule for the for-ward, day-ahead, market. Penalty prices related to constraint relaxations are assigned extreme high values in order to make these relaxations as few and infrequent as possible. The scheduling run solution, which may include some relaxations, is fed into the pricing run process in order to determine the settlements for the day-ahead market. Constraint relaxations are also allowed through the pricing run process. However, penalty prices are set to lower values compared to the scheduling run. Usually, penalty prices through the pricing run are set to few multiples of the related bid cap. For example, the CAISO penalty price for a transmission relaxation slack variable is currently set to three times the bid cap. Penalty prices are agreed upon by the operator along with their stakeholders and are approved by the utility commission [5]-[6].

Similar practices are adopted by other operators such as the Electric Reliability Council of Texas (ERCOT), Southwest Power Pool (SPP), Midcontinent Independent System Operator (MISO), and New York Independent System Operator (NYISO) [7]-[12]. Instead of using a fixed flat penalty price, ERCOT, for instance, proposes the use of a stepwise penalty price function. The use of a stepwise penalty price function with a variable step width is also proposed by [13]. This multi-step approach gives the market model more flexibility to determine a penalty structure that offers a better compromise between keeping the price excursions down while, at the same time, limiting the number and magnitude of violations.

As for the effect of constraint relaxations on system security, there is no previous work in literature that investigates the direct impacts of energy market models constraint relaxations have on system reliability, stability, and dynamics. Some efforts have been

directed to examine the long-term physical impacts of violating the thermal limits on the transmission lines aluminum conductors. These studies focus on the physical aspects of aluminum-conductor steel-reinforced (ACSR) lines such as loss of strength and sagging [14]-[17].

1.3 Literature Survey: Power System Security

Electric power system security has been widely studied in literature and several definitions have been proposed. Since the early framework proposed by Dy Liacco [18], up to recent online dynamic security assessment (DSA) tools included in sophisticated energy management systems, the core concept of power system security has been regarded as the ability of the system to operate within acceptable and safe operating conditions following an imminent disturbance, without the need of load shedding, generation rejection, or direct human intervention [18]-[24]. The North American Electric Reliability Corporation (NERC) defines power system security as the degree of risk in the power system's ability to withstand sudden disturbances such as short circuit faults or the loss of major components, without interruption of customer service [21]. The International Electrotechnical Commission (IEC) defines power system security as the ability of an electric power system to operate in such a way that credible events do not give rise to: loss of load, stresses of system components beyond their ratings, bus voltages or system frequency outside tolerances, instability, voltage collapse, or cascading sequences [25]. In [24] power system security is simply defined as the art and science of the "survival" of power systems and, in order to ensure their survival, power systems are operated within certain power transfer limits, commonly referred to as security limits.

Although power system security has been studied for decades, it is still considered as a pressing topic with growing importance in the electric power engineering industry. This paramount importance security has stems from its direct impact on power systems planning, operation, and economics. For instance, planners must ensure system security in their expansion and interconnection studies, which is usually a key element in determining the required infrastructure investments [20]. On the other hand, real-time operators must also closely monitor the system and take necessary actions to ensure secure operating conditions. Generation re-dispatch, utilizing generation reserves, and reactive power controls are examples of real-time actions that operators usually take to control lines power flow and voltage magnitudes to ensure secure operating conditions. Therefore, power system security has a direct impact on capital and operational costs, and larger security margins will cost a higher price as a result of underutilizing the system components [19], [20]. On the other hand, power system economics and profit, especially in deregulated power systems, are among the main objectives of power system owners and operators, therefore, a trade-off between security margins and associated costs has to be made. This trade-off between security margins and cost is represented in the form of an optimization problem which solution would ensure operating the system within the security region, while the associated costs are minimized. For instance, security constrained unit commitment usually involves producing the most economic dispatch of generating units while imposing the operational and security constraints [26]. A more detailed discussion of secure unit commitment is provided in Section 2.5 of this dissertation. It should be noted that power system security and economics should not be viewed as conflicting objectives since operating the system outside the security region can result in cat-

astrophic consequences, such as blackouts or equipment damage that are extremely costly.

The relatively recent transformation in the way power systems are structured and operated has imposed new challenges in the field of power system security. Regulated and vertically integrated power systems tended to be more predictable and simpler to operate compared to regulated and open market power system structures [27]-[29]. The integrated planning and operation of generation, transmission, and distribution systems conducted by monopolies, such as government bodies and public utilities. This ensured that the entire system was scaled appropriately and consistently to meet load growth, thereby limiting overloading and extreme operating conditions that may lead to system disturbances [20]. However, reduced operation predictability and stressed operating conditions are not exclusive results of power system restructuring. There are several other factors in literature that are attributed to making power system security a more challenging issue in modern power systems. Examples on such factors are: the aging of transmission infrastructure and the lack of new transmission facilities, large numbers of distributed generation such as renewable resources and their added uncertainty in dispatch levels, and the trend towards multi-area interconnections, which may result in cascading events when information and data are not communicated properly between neighboring interconnected areas [20].

In order to be able to assess the system operational security accurately, operators need to conduct steady state and transient studies to evaluate operating conditions for different states of operation, as well as the security of the paths the system takes between those states [19]. The computations needed to accurately assess the security of a single

defined system condition are technically rigorous and require considerable effort. To date, power systems are usually operated based on the margins obtained by offline studies, which are usually based on deterministic and conservative assumptions, by which all planned conditions and contingencies have to be examined even though most would never actually occur [19]-[20], [27]-[28], [30]. Therefore, online DSA that is run in real-time (or near real-time) would provide operators with more accurate and realistic assessment of system security. When the actual operating margins are known, the system can be operated in more optimal conditions to increase revenue while sustaining system security. Moreover, online DSA would provide operators with early indications of pending trouble and provide the opportunity to take remedial actions as a result of largely eliminating the uncertainty embedded in offline analysis using forecasted conditions. For instance, one of the recommendations (Recommendation 22) in the U.S. – Canada Power System Outage Task Force's final report on the 2003 blackout, states that better real-time tools for operators and reliability coordinators should be evaluated and adopted [31].

Several online DSA schemes and methods can be found in literature, which mainly focus on minimizing the time needed to run DSA for large systems in order to be used in real-time frame. These efforts have been focused on significantly reducing the number of considered contingencies and, on the computational methods used to evaluate system security, especially system transient stability. For instance, risk-based DSA schemes have been proposed in [27]-[28], [30], where the probability and impact of contingent events are used to filter and rank critical contingencies. Therefore, contingencies likelihood and severity are condensed into indices that reflect probabilistic risk. In [28], the probabilistic factors considered include the probability of: fault occurrence, fault type, fault location,

fault clearing time, successful automatic reclosing, fault impedance, and the output of power generators. The impact (or cost) implications used to calculate the total risk are based on several direct and indirect financial costs including equipment replacement, repair and startup, customer interruption, and social and political costs [28]. Depending on the system size under consideration, full simulation methods, such as full power flow solution, time-domain simulation for transient stability, and eigenvalue analysis for small signal stability analysis may not be suitable for real-time DSA. Therefore, approximate methods have been proposed. For instance, trajectory sensitivity analysis is proposed by [32]-[33] for transient stability assessment to avoid numerically solving the large number of nonlinear differential and algebraic equations in a full time-domain simulation. In [24] and [29], energy-based approximation methods are proposed, where the transient stability is evaluated based on the energy acquired at a particular time, which is computed using transient energy functions. Data-driven methods such as decision trees and intelligent system algorithms have also been widely researched. Data-driven methods utilize offline dynamic security database to provide rapid real-time security assessment and preventive control guidelines based on real-time measurements [34]-[36]. It should be noted that DSA results accuracy and credibility depend largely on the validity of the measurements and models used. For instance, the Western Electricity Coordinating Council (WECC) initiated a generator testing requirement and dynamic model validation program following failure of simulations to reproduce events that occurred in the summer of 1996 in the Western Interconnection [37]-[38].

1.4 Dissertation Organization

This dissertation is divided into six chapters. Chapter 2 presents a general theoretical background for the optimization problems and stability topics related to this work. DC power flow is introduced and explained along with its use in unit commitment problems. Two different AC optimization tools that were used in this work and their functionality are explained as well. A brief discussion on Benders' decomposition is provided since it was used in this work to relax post-contingency constraints. An overview of voltage stability and dynamic load modeling are discussed as well. Chapter 3 provides some detailed discussion on constraint relaxations mechanism and the motives system operators have for applying such practice. Chapter 4 presents and explains the system studies performed on the test cases and the results achieved. System studies conducted include static and dynamic base-case and post-contingency analysis. Voltage stability analysis using dynamic load models and risk based penalty price relaxations results are also included in Chapter 4. Impacts of post-contingency constraint (emergency limits) relaxations on real-time system performance and energy markets are investigated in Chapter 5. Conclusions are presented in Chapter 6.

2. THEORETICAL BACKGROUND

2.1 Introduction

This chapter provides a brief theoretical overview of the optimization problems, stability analysis, and dynamic load modeling, which were utilized in this work. A Direct Current Optimal Power Flow (DCOPF) algorithm is presented in the first section along with the various approximations it incorporates. The ACOPF general formulation and solution process is also presented. PSS/E Preventive Security Optimal Power Flow (PSCOPF) tool was utilized in this work to attain an AC *N*-1 secure solution. A description of the PSCOPF algorithm structure and solution procedure is provided next. A general SCUC formulation is also presented and explained. Benders' decomposition technique is also introduced in this chapter as it was utilized throughout this work to allow post-contingency constraint relaxations.

This chapter also provides a theoretical overview of various types of system stability aspects. More detailed discussion on voltage stability is provided herein since test cases with constraint relaxations have significantly more voltage violations compared to non-relaxed cases. Dynamic load modeling overview is also included in this chapter for its significant impact on voltage stability analysis and results.

2.2 Direct Current Optimal Power Flow – DCOPF

DCOPF is widely used by system operators in energy market models in order to determine the generators real power dispatch levels and, statuses in unit commitment problems [1], [39]-[40]. A DC power flow is used as an approximation to the actual AC

power flow to simplify the optimization problem and utilize the linear nature of the DC power flow. This approximation provides acceptable results for the day-ahead market processes while significantly reducing the time and computing resources required to solve large-scale optimization problems. The DC power flow approximation is based on the following assumptions [39], [40]:

- Neglecting the reactive power – voltage (*Q*-*V*) component of the regular AC power flow. This results in a completely linear, non-iterative, power flow algorithm. However, this approximation implies that DC power flow is only good for calculating real power flows on transmission lines and transformers and does not provide any information about the reactive power flows or the voltage profiles.
- All voltages throughout the system are assumed to have an absolute magnitude of 1.0 p.u. This approximation makes the real power flow independent of voltage magnitudes and, therefore, the real power flow is only affected by branches impedances and voltage angles.
- Nonlinear thermal losses are neglected by neglecting branch resistances.
- The difference between voltage angles is assumed to be small enough to use the small angle trigonometric approximation: $(\cos(\theta_i - \theta_j) \approx 1)$, $(\sin(\theta_i - \theta_j) \approx (\theta_i - \theta_j))$.

It should be noted here that these approximations are not necessarily found in all DC power flow formulations. Some of these approximations may not be used in order to achieve a more accurate and realistic solution. For instance, if real power losses are known, these losses can be incorporated in the DC model by adding them to the system loads.

Therefore, a basic lossless DCOPF can be formulated using the DC power flow equations as:

$$minimize \sum_{g} c_g P_g \tag{2.1}$$

$$P_k = \frac{1}{x_k}(\theta_i - \theta_j) \forall k \tag{2.2}$$

$$P_i = \sum_{j}^{N} P_j \, \forall i, j \tag{2.3}$$

$$-P_k^{max} \leq P_k \leq P_k^{max} \forall k \tag{2.4}$$

$$P_g^{min} \leq P_g \leq P_g^{max} \forall g \tag{2.5}$$

where, *i* and *j* are any two buses in the network connected together with at least one branch *k*. Equation (2.1) is the objective function to be minimized, which is in this case the total production cost of all generating units. Equations (2.2) and (2.3) are the DC power flow and power node balance respectively. Equations (2.4) and (2.5) represent the operation limits and ratings of the branches and generating units respectively. More detailed discussion on security limits and constraints will be provided in the security constrained unit commitment section.

2.3 Alternating Current Optimal Power Flow – ACOPF

The Alternating Current Optimal Power Flow (ACOPF) is a large-scale nonlinear optimization problem that has the following general form:

$$obj. \quad \min_{x} f(\boldsymbol{x})$$
$$s.t. \quad \boldsymbol{h}(\boldsymbol{x}) = 0 \tag{2.6}$$
$$\boldsymbol{x_{min}} \leq \boldsymbol{g}(\boldsymbol{x}) \leq \boldsymbol{x_{max}}$$

The optimization problem shown in (2.6) consists of an objective function ***f(x)*** that is to be minimized. In practice, this objective function is usually the total generation cost, which includes other operational costs, such as: startup and shutdown costs. The optimization process is subject to equality and inequality constraints. Equality constraints ***h(x)*** (column vector) in ACOPF include power flow equations, such as bus-power mismatch. Inequality constraints ***g(x)*** are the steady state security constraints, such as transmission lines thermal limits and voltage limits, where $\boldsymbol{x}$ is a column vector of power system variables.

2.3.1 ACOPF Problem Formulation

One of the approaches used to solve the nonlinear system (2.6) is forming a Lagrangian scalar function by linearly combining the objective function and the equality constraints in the following form:

$$L(\boldsymbol{x}, \boldsymbol{\lambda}) = f(\boldsymbol{x}) + [\boldsymbol{\lambda}]^T[\boldsymbol{h}(\boldsymbol{x})] \tag{2.7}$$

where $\boldsymbol{\lambda}$ is a column vector of Lagrange multiplier variables. The Lagrangian formulation in (2.7) transforms the optimization problem into primal-dual problem since it consists of both, power system variable as well as Lagrange multipliers. The equality-constrained optimal solution is obtained by equating the Lagrangian function gradient to zero and solving for $\boldsymbol{x}$ and $\boldsymbol{\lambda}$ in what is known as Karush-Kuhn-Tucker (KKT) optimality condition [41]-[43]. Solving the KKT problem produces a set of optimally defined power system

variables $\boldsymbol{x}$, along with the objective function sensitivities to changes in the constraints $\boldsymbol{\lambda}$. The resultant OPF formulation is always nonlinear and nonconvex due to the presence of the power flow mismatch equations, hence, a global optimal solution cannot be guaranteed. However, since the DC optimal solutions generated by the market model are used as starting points to solve the ACOPF in this work, it can be assumed that the ACOPF provides satisfactory results to represent the AC real-time system operating conditions. The objective function itself can be nonlinear either by explicitly including nonlinear quantities such as power losses, or by implicitly introducing quadratic penalties.

2.3.2 Inequality Constraints and Limits

In order to impose inequality constraints, implicit objective terms that are expressed as a function of the constrained variable are formed. Hard limits are represented as objective terms that are asymptotic to the variables limits, known as barrier terms. Soft limits are represented as penalty objective terms that tend to grow in magnitude as the variable value departs further from its defined limits. Penalty terms can be modeled as linear or quadratic functions. The linear penalty for soft limit constraints is introduced in the objective function in the following form:

$$\sum_{i=1}^{N} \rho_i \left(\max_i \left(0, x_i - x_{max,i}\right) - \min_i \left(0, x_i - x_{min,i}\right) \right) \tag{2.8}$$

where:

N: number of control variables subject to linear penalty

x_i: the present value of the i-th control variable

x_{min}, x_{max}: minimum and maximum control values, respectively

ρ_i: linear penalty weight for the i-th control variable

From (2.8), the penalty is zero whenever the control variable x_i is within its feasible limits (x_{min}, x_{max}). However, a positive penalty term is introduced into the objective function that is directly proportional to the variable's excursion from its defined limit. The penalty terms for soft limit constraints can also be represented in a quadratic form as:

$$\sum_{i=1}^{N} \rho_i \left(x_i - \frac{(x_{min,i} + x_{max,i})}{2} \right)^2 \tag{2.9}$$

The quadratic penalty formulation represented by (2.9) imposes a penalty value on the objective function any time the control variable x_i takes an excursion away from the midpoint of its two limits. The quadratic growth in the penalty value tends to discourage large deviations and possibly infeasible excursions.

Hard limit inequalities are modeled in the Lagrangian function, (2.7), as objective-like functions known as barrier functions. Barrier functions are continuous and asymptotic to the control variable defined limits (x_{min}, x_{max}) and they ensure rigorous enforcement of the associated limits. The entire optimization problem is considered infeasible in the case any control variable x_i violates the feasible region determined by the barrier functions. In PSS/E [41] the barrier functions have the following logarithmic representation:

$$B(\boldsymbol{x}) = -(10^{\mu}) \sum_{i=1}^{N} \left[\log(x_i - x_{min,i}) + \log(x_{max,i} - x_i) \right] \tag{2.10}$$

where, μ is defined as the barrier parameter. The smaller the barrier parameter, the closer the control variables can approach their limits. Therefore, μ is assigned a relatively high value at the beginning of the optimization process, and then it is reduced systematically

during each iteration. This entire process is referred to as the interior point method (IPM) [41]-[43] since representing the barrier function as part of the objective function, ensures that the minimum of the combined objective function ($f(\boldsymbol{x})+B(\boldsymbol{x})$) is always inside the limits represented by (x_{min}, x_{max}). The augmented Lagrangian function has the following formulation:

$$L`(\boldsymbol{x},\boldsymbol{\lambda}) = f(\boldsymbol{x}) + B(\boldsymbol{x}) + [\boldsymbol{\lambda}]^T[\boldsymbol{h}(\boldsymbol{x})] \tag{2.11}$$

2.3.3 The Solution Process

Invoking the KKT optimality conditions to the augmented Lagrangian function in (2.11) results in the following:

$$\begin{bmatrix} \nabla_x\nabla_x L`(\boldsymbol{x},\boldsymbol{\lambda}) & \nabla_x\nabla_\lambda L`(\boldsymbol{x},\boldsymbol{\lambda}) \\ \nabla_\lambda\nabla_x L`(\boldsymbol{x},\boldsymbol{\lambda}) & \nabla_\lambda\nabla_\lambda L`(\boldsymbol{x},\boldsymbol{\lambda}) \end{bmatrix} \begin{bmatrix} \Delta\boldsymbol{x} \\ \Delta\boldsymbol{\lambda} \end{bmatrix} = \begin{bmatrix} -\nabla_x L`(\boldsymbol{x},\boldsymbol{\lambda}) \\ -\nabla_\lambda L`(\boldsymbol{x},\boldsymbol{\lambda}) \end{bmatrix} \tag{2.12}$$

The left-hand side KKT matrix is composed of four sub-matrices. The upper diagonal sub-matrix ($\nabla_x\nabla_x L`(\boldsymbol{x},\boldsymbol{\lambda})$) is a second-order partial derivative square matrix, known as the Hessian matrix. The off-diagonal sub-matrices ($\nabla_x\nabla_\lambda L`(\boldsymbol{x},\boldsymbol{\lambda})$ and $\nabla_\lambda\nabla_x L`(\boldsymbol{x},\boldsymbol{\lambda})$) are the Jacobian matrix and its inverse respectively and, they are merely derivatives of the equality constraint equations in terms of the power system variables. The lower diagonal sub-matrix ($\nabla_\lambda\nabla_\lambda L`(\boldsymbol{x},\boldsymbol{\lambda})$) is uniquely zero since the Lagrangian function is linear in $\boldsymbol{\lambda}$. The right-hand side vector in (2.12) has a length equal to the summation of the number of power system variables and the number of equality constraints. The $\boldsymbol{x}$-gradient term ($-\nabla_x L`(\boldsymbol{x},\boldsymbol{\lambda})$) and $\boldsymbol{\lambda}$-gradient term ($-\nabla_\lambda L`(\boldsymbol{x},\boldsymbol{\lambda})$) encourage $\boldsymbol{x}$ to move in a direction that minimizes the mismatch and the combined objective value, respectively.

The KKT system in (2.12) is solved iteratively using Newton's method. Newton's method solves a quadratic approximation to the nonlinear system starting from estimated values for $\boldsymbol{x}$ and $\boldsymbol{\lambda}$. By solving the quadratic approximated combined objective function, the correction factor $\Delta\boldsymbol{x}$ is obtained. The value of this correction factor is driven by the right-hand side of (2.12). $\boldsymbol{x}$ and $\boldsymbol{\lambda}$ are updated with the correction factor as:

$$\begin{aligned} \boldsymbol{x}_k &= \boldsymbol{x}_{k-1} + \alpha\Delta\boldsymbol{x} \\ \boldsymbol{\lambda}_k &= \boldsymbol{\lambda}_{k-1} + \alpha\Delta\boldsymbol{x} \end{aligned} \tag{2.13}$$

where, k denotes the present number of iteration and α is a deceleration (or scaling) factor (normally set to 1.0).

The computed correction factor $\Delta\boldsymbol{x}$ when added to $\boldsymbol{x}$ from the previous iteration determines the new minimum of the quadratic equation. From this point on, a new quadratic equation is developed and a new correction factor is computed. As the updated $\boldsymbol{x}$ approaches its nonlinear optimum, the minimum of the quadratic equation converges to the minimum of the nonlinear combined objective. In the case where the quadratic solution estimate for $\boldsymbol{x}$ is far from the optimum, the correction factor $\Delta\boldsymbol{x}$ may force some elements of $\boldsymbol{x}$ to violate their limits. In such cases, the deceleration factor α comes into play and its value is reduced in order to ensure that all system variables remain inside the limits (x_{min}, x_{max}). In PSS/E [41] this iterative process is considered to have converged if the following criteria is satisfied:

- Number of maximum allowed iterations is not exceeded
- The power mismatch does not exceed a user-defined tolerance
- The final value of the barrier parameter μ in Equation (2.10) is reached (default value for 10^{μ}: 0.00001)

- The final iteration has a deceleration factor α equals to 1.0.

2.4 Preventive Security Constrained Optimal Power Flow – PSCOPF

Throughout this work it was desired to operate the test system under consideration at *N*-1 secure conditions. *N*-1 secure operating conditions imply that following a single contingency, the system does not suffer any type of voltage or flow violations. *N*-1 contingency can be represented as the failure or unplanned outage of any element in the system (transmission line, transformer or generating unit). Since no post-contingency adjustment or operator intervention is required, this type of operation security is considered as preventive security. Achieving *N*-1 preventive security conditions manually is a very tedious and inconsistent process and, even infeasible for large systems. For instance, securing the system against a specific contingency might worsen the violations of another contingency or introduce new violations, even in the base-case. Therefore, the built-in PSCOPF tool in PSS/E was used in order to perform this task.

2.4.1 PSCOPF Objective Function and Constraints

PSCOPF is a special class of the OPF formulation that takes into consideration predefined security constrains and a set of critical contingencies. However, the PSCOPF objective function is not cost-related as in regular OPF problems. The objective of PSCOPF is to minimize the number and magnitude of adjustments of the system controls. These controls comprise of:

- On-line and off-line generators power output and scheduled voltage
- Transformers tap settings

- Switched shunts
- Phase shifters
- Load controls.

The equality and inequality constraints for PSCOPF are very similar to the constraints in the regular OPF. However, since PSCOPF considers post-contingency conditions as well as base-case conditions, it is possible to define a different set of operation limits as emergency limits. These emergency limits will only be enforced following the event of a contingency. PSCOPF constraints include:

- Power balance equations for pre- and post-contingency cases
- Operation limits for pre- and post-contingency cases
- System controls limits.

2.4.2 PSCOPF Objective Function and Constraints

The PSCOPF iterative solution process can be split into two parts for each iteration:

a) Part-1: Identifying the set of critical contingencies and building the Benders' cuts
b) Part-2: Solving the master problem, determining the optimal settings of the various controls. and updating the base-case.

a) Part-1

For large systems with a large number of contingencies to be considered, PSCOPF quickly becomes a large-scale nonlinear optimization problem. Solving this problem by imposing all post-contingency constraints simultaneously might not be feasible due to the limited computing resources available. In PSCOPF, Benders' decomposi-

tion is used to decompose the initial problem into several sub-problems that can be solved separately and iteratively. In Benders' decomposition, the master problem is modeled using the base-case conditions while the cuts represent the different contingencies considered. In this identification process, PSCOPF also tries to choose the dominant contingency among a set of related contingencies. Therefore, securing the system against the most severe dominant contingency will ensure secure post-contingency conditions for other related less severe non-dominant contingencies. A more detailed discussion on Benders' decomposition and the required characteristics of its sub-problems are provided in Section 2.6. The flow chart in Figure 2.1 illustrates the steps of Part-1 of the PSCOPF process [41].

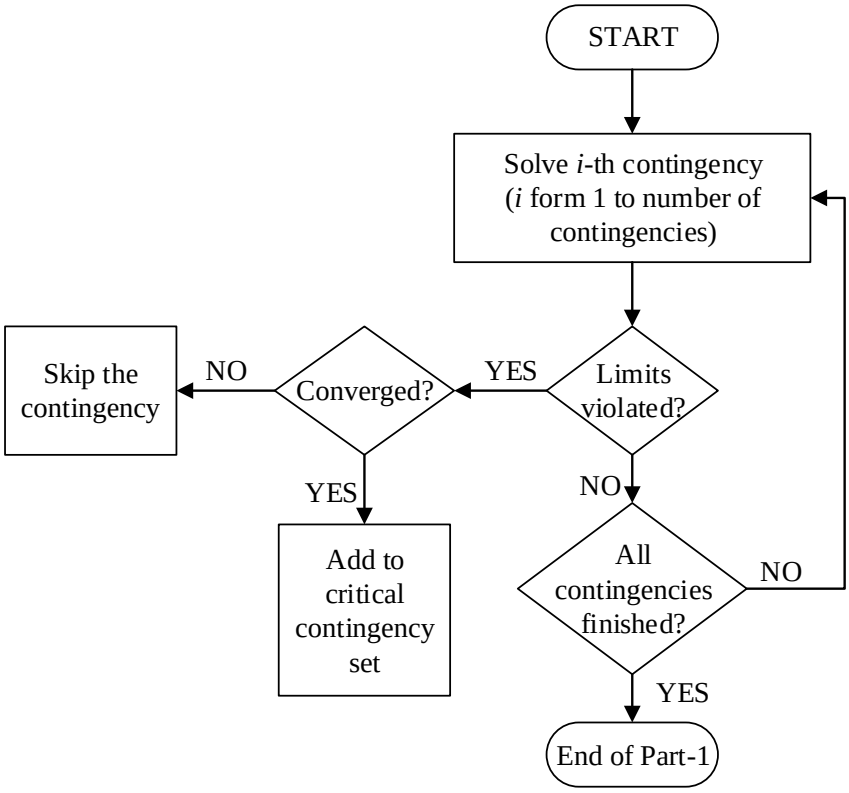

Figure 2.1. PSCOPF Part-1 Flow Chart [41].

b) Part-2

In this part, Benders' cuts for each violation associated with each contingency are created. In PSCOPF, Benders' cuts are represented as linear constraints that are added to the master problem. Using the available controls and operation constraints along with Benders' cuts, the master problem is built. The master problem is solved using successive linear programming (SLP) by which the required adjustments are determined and the base-case is updated. The AC power flow of the updated base-case is obtained and this new operating condition is used to test the predefined contingencies. If new violations appear under the new base-case operating conditions, the Benders' cuts are updated and the whole process is repeated all over again. Otherwise, if all contingency sets are tested and no violations are reported, Part-2 of PSCOPF is terminated and the system is considered conforming to *N-1* preventive security under the new base-case operating conditions. Figure 2.2 illustrates the steps of Part-2 of PSCOPF process [41].

2.5 Security Constrained Unit Commitment – SCUC

Unit commitment (UC) is the process by which power system operators determine the status (committed or de-committed) and power production levels of generating units in their generation fleet. The main objective of unit commitment is to commit enough generation for a certain period of time to ensure that the load demand is met reliably and economically. Since reliability and economics are contradicting objectives in this problem, unit commitment is considered an optimization problem. Committing enough generating units to supply the load is a basic constraint in the unit commitment problem, however, it is not the only constraint. Several other security constraints could be added to this

problem in order to claim an optimal and secure solution. These constraints are related to the network model used to represent the real network, the capability and characteristics of the generating units, and to several other operational and security conditions.

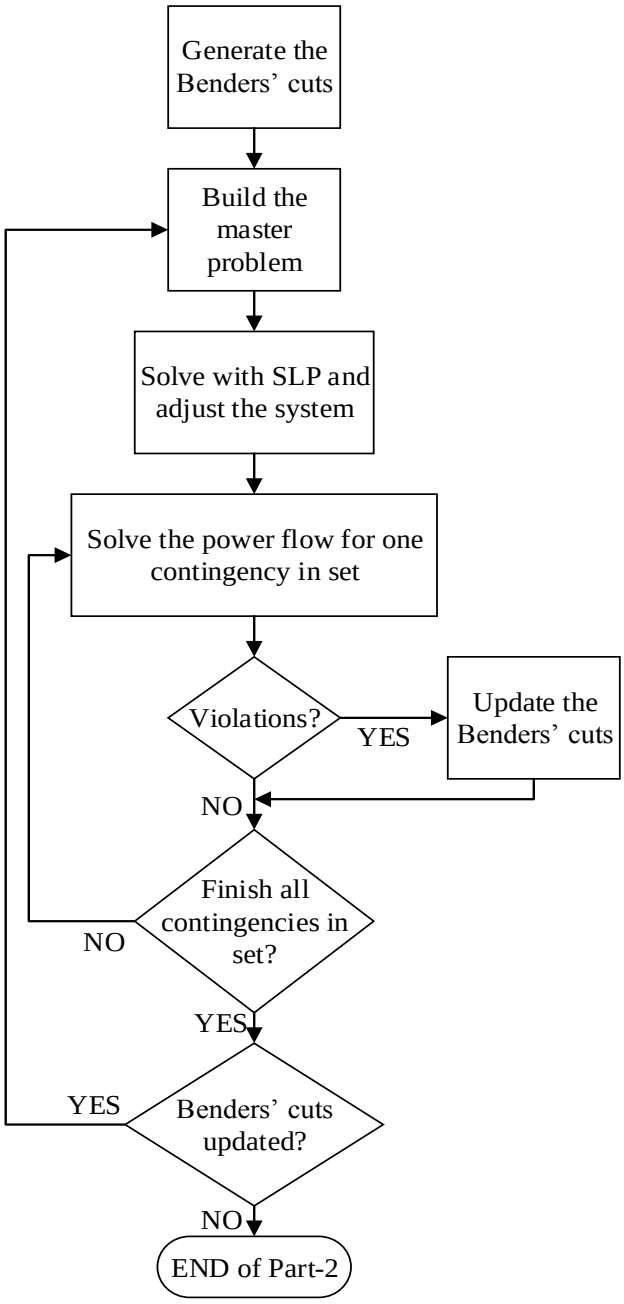

Figure 2.2. PSCOPF Part-2 Flow Chart [41].

When these security constraints are incorporated in the unit commitment problem, security constrained unit commitment model is formulated. Some of the commonly used security constraints are presented in the next subsection [39], [44].

2.5.1 Unit Commitment Security Constrains

It should be noted at this point that the presented SCUC formulation is not unique. The model presented in this subsection was chosen to serve the purpose of this particular work.

Objective function:

The objective function of the SCUC problem can be written as:

$$minimize \ \sum_g \sum_t c_g P_{gt} + c_g^{NL} u_{gt} + c_g^{SU} v_{gt} + c_g^{SD} w_{gt} \quad (2.14)$$

The objective of a SCUC problem is to minimize the overall cost incorporated in operating a set of generating units over a certain time frame. As (2.14) indicates, the total cost for this SCUC problem consists of active power production cost, no load cost, start-up, and shut-down costs respectively.

Generators and branches limits

As indicated in (2.5), each generating unit has minimum and maximum production limits that must be satisfied for any committed unit. Similarly, (2.4) indicates that branches (transmission lines and transformers) also have thermal ratings that typically must not be exceeded. These constraints are presented respectively in the SCUC formulation as:

$$u_{gt} P_g^{min} \leq P_{gt} + r_{gt}^{SP} \leq u_{gt} P_g^{max} \qquad \forall g, t \ (2.15)$$

$$-P_k^{max} \leq P_k \leq P_k^{max} \qquad \forall k \text{ (2.16)}$$

Equation (2.15) enforces each generator production limits while accounting for spinning reserve allocation as will be explained in the following discussion.

Spinning reserve

Reserve in general (spinning and non-spinning) is required to ensure acceptable frequency response in the event of losing a portion of the generating units in any possible contingency event. Reserve allocation consists of the amount and location of reserve throughout the system to ensure that the required reserve could be utilized when needed through the available transmission capacity. The typical reserve amount is usually a percentage of the forecasted peak demand. The reserve could also be calculated to make-up for the loss of major heavily loaded generating units or, as a probability function of not having enough supply to meet the load. Usually such reserve rules are defined by regional reliability councils. The following formulas show how spinning reserve constraints are incorporated in the SCUC problem:

$$r_t^{req} \geq \sum_g 0.07\, d_{nt} \qquad \forall g, t \text{ (2.17)}$$

$$P_{gt} + r_{gt}^{SP} \leq r_t^{req} \qquad \forall g, t \text{ (2.18)}$$

The constraint enforced by (2.17) states that the required total reserve over a certain time period should not be less than 7% of the total load for that time period [45]. Moreover, (2.18) ensures that the allocated reserve is sufficient to cover the loss of any single unit. The left side of the inequality in (2.18) combines the present production and the designated spinning reserve for that particular unit since both will be lost in the event

of losing that unit. In order to model spinning reserve availability more accurately, the ramp rate capability of each unit could also be considered. Ramp rate effect on spinning reserve availability is represented in the following constraint:

$$r_{gt}^{SP} \leq R_g^{EM} u_{gt} \qquad \forall g, t \text{ (2.19)}$$

Equation (2.19) states that the specified spinning reserve of any committed unit in the specified time period should not exceed the emergency ramp rate of that unit. The emergency ramp rate is the maximum increase in power generation a unit can produce in a short period of time. Usually the emergency ramp rate is specified over a 10 minute period. The required total reserve is usually a combination of spinning and non-spinning reserve. Spinning reserve is the available generation from all committed and synchronized generating units in the system, minus the load and losses being supplied. On the other hand, non-spinning reserve is typically assigned to fast start units. Fast start units are typically gas-turbine or hydro units that can be brought online and synchronized in relatively short time. Such fast start unit capacity can be included in the total required reserve as long as the time needed to bring them up to their full capacity is accounted for.

Ramp rates

Ramp rate constraints are considered as coupling constraints since they are imposed over consecutive time periods (usually over consecutive hours). Generating units, especially large nuclear units, have limited capability of changing their production levels within a certain time period. This limitation needs to be captured when solving the SCUC over several successive time periods. Ramp rates can be represented by the following constraints:

$$u_{gt-1}R_g^{HR} + v_{gt}R_g^{SU} \geq P_{gt} - P_{gt-1} \qquad \forall g, t \text{ (2.20)}$$

$$u_{gt}R_g^{HR} + w_{gt}R_g^{SD} \geq P_{gt-1} - P_{gt} \qquad \forall g, t \text{ (2.21)}$$

Equation (2.20) and (2.21) represent ramp-up and ramp-down constraints respectively, taking into account start-up and shut-down ramp rates.

Minimum-up and minimum-down time

Thermal units must have gradual temperature changes in both directions (when fired-up and turned-off). Therefore, once a thermal unit is brought online, it must stay online for a certain amount of time (minimum-up time). On the other hand, once a thermal unit is turned off, it must stay off for a certain amount of time before being fired up again (minimum-down time). Minimum-up and minimum-down time constraints are also considered as coupling constraints since they link consecutive time periods together. Minimum-up and minimum-down time are represented in (2.22) and (2.23) respectively:

$$\sum_{s=t-UT_g+1}^{t} v_{gt} \leq u_{gt} \qquad \forall g, t \text{ (2.22)}$$

$$\sum_{s=t-DT_g+1}^{t} w_{gt} \leq 1 - u_{gt} \qquad \forall g, t \text{ (2.23)}$$

Binary variables

In unit commitment problems binary variables are used to indicate the status of generating units (u_{gt}), startup variable (v_{gt}), and shutdown variable (w_{gt}). While the unit status variable (u_{gt}) is enforced to be binary, the startup and shutdown variables are guaranteed to be binary through the following constraints:

$$v_{gt} \geq u_{gt} - u_{gt-1} \qquad \forall g, t \text{ (2.24)}$$

$$w_{gt} \geq u_{gt-1} - u_{gt} \qquad \forall g, t \text{ (2.25)}$$

DC power flow

The DC power flow and node balance equality constraints, Equation (2.2) and Equation (2.3) presented in Section (2.1) respectively, are also included in the used SCUC formulation.

2.6 Benders' Decomposition

Benders' decomposition is one of the commonly used mathematical decomposition techniques in solving particular large-scale optimization problems. The main idea of Benders' decomposition and other multistage optimization algorithms, is to partition the decision making process into several stages as opposed to the traditional approach of considering all variables and constraints simultaneously by solving a monolithic optimization problem. The decision making process usually consists of one or more optimization problems along with feasibility checks. For optimization problems with the appropriate structure, decomposition techniques usually reap significant computational benefits because typically the computation complexity growth of these large scale problems is not linear [46]. Moreover, Benders' decomposition facilitates the use of parallel computing which in turn could provide flexibility and utilize available computing resources efficiently [46]-[47]. However, Benders' decomposition serves its purpose only for certain types of problems as will be explained in the forthcoming discussion. Benders' decompo-

sition is used in power systems decision problems such as security constraints unit commitment and maintenance scheduling, as well as other applications [46], [48].

The first component of Benders' decomposition is the master problem. The master problem is usually an optimization problem that could be of various types, such as: linear programing (LP), mixed integer programming (MIP) or nonlinear programming (NL). Depending on the structure of the decomposition the master problem evaluates a lower bound solution by solving for all variables or for a subset of variables. The master problem therefore has fewer constraints or variables or both. The solution is then fixed and passed to the sub-problems to check its feasibility and optimality in case sub-optimization problems are present [47].

In a feasibility sub-problem the initial solution is checked against additional constraints. The goal of the feasibility check is to ensure that for the generated master problem solution, there exists a feasible solution for the sub-problem. In the event of infeasibility, the dual information is used to introduce additional constraints on the master problem to ensure feasibility in the next iteration. These additional constraints are called Benders' feasibility cuts. Therefore, sub-problems in Benders' decomposition are required to be convex problems in order to ensure that the generated cuts create a new feasibility region for the master problem that would remove the related violations in the next iteration [46]. The feasibility check is performed by introducing slack variables to relax the coupling constraints. The problem is considered feasible only if the summation of these slack variables is zero. After passing the feasibility check the sub-optimization problems evaluate the upper limit solution and modify the master problem through optimality Benders' cuts if the gap between the lower and upper limits exceeds a predefined

value. Typically this entire process is performed iteratively until a feasible solution within a desired optimality gap is obtained. It should be noted here that the application and structure of the problem dictate whether both feasibility and sub-optimization slave problems are required or just one of them. Moreover, depending on the relationship between sub-problems, decomposition can be either time (sequential) or functional based [46].

Benders' decomposition efficiency and, even viability, rely on the ability to distinguish the variables and their separability in order to form the master and slave problems. An efficient and successful decomposition synthesizes Benders' cuts that rule out a large class of trial values in the master problem. This is critical because Benders' cuts add additional constraints to the master problem at each iteration. Therefore, adding an excessive number of additional constraints would increase the size of the master problem to the point where the decomposition loses its purpose or even makes the problem more complicated. Hence, Benders' decomposition efficiency relies on the localization of variables, i.e. the ability to separate the variables among the constraints in a way that generates sub-problems with strong intra-coupling and weak inter-coupling correlation [49].

2.7 Voltage Stability

This section provides a brief overview of power system stability in general as it is the basic building block in assessing system security and reliability. For the purpose of this study, a detailed discussion on voltage stability is provided herein since test cases with constraint relaxations have significantly more voltage violations compared to non-relaxed cases. Power system stability can be classified into three main categories according to their physical nature [50]:

- Rotor angle stability: this type of stability is related to the ability to maintain or restore equilibrium between mechanical torque and electric torque in synchronous machines following a disturbance. Consequently, instability in this regard refers to growing deviation or oscillation of one machine with respect to other machines, resulting in loss of synchronism.
- Voltage stability: the ability of a power system to maintain steady and acceptable voltages at all buses in the system under normal operating conditions after being subjected to a disturbance.
- Frequency stability: refers to system ability to maintain or restore its frequency within an acceptable range following a major disturbance. Frequency stability is related to the equilibrium between generation and load throughout the system. Frequency instability usually appears as sustained or growing frequency swings resulting is generation and/or load loss.

Disturbances could be large, such as major transmission lines faults, generating units tripping, loss of major components, or small, such as a gradual change in load. Voltage instability occurs when one bus or more in the system suffers from progressive and uncontrolled change in the voltage magnitude, usually in the form of voltage decrease. Voltage instability can cause prolonged periods of voltage depression conditions (brown-out), or even a voltage collapse and blackout, depending on the available reactive power and load dynamics. Although voltage instability is essentially a local phenomenon, voltage collapse, which is more complex than simple voltage instability and is usually the result of a sequence of events, is a condition that affects large areas of the system [51].

Rotor angle stability had been the primary aspect of stability studies for decades. However, recent events of abnormal voltage magnitudes and voltage collapse incidents in some large interconnected power systems have sparked an interest in the voltage stability phenomenon [52]-[53]. Rotor stability was believed to be responsible for voltage instability conditions. This case is true since a gradual loss of synchronism between two groups of machines as their rotor angles approach or exceed 180° would result in very low voltages at intermediate points in the network. However, this is not the case if the disturbance was close to load centers and the voltage depression was rather caused by reactive power deficiency and/or load dynamics. Therefore, voltage instability may occur when rotor stability is not an issue. Actually, sustained voltage instability conditions can cause rotor instability.

Several recent factors and operating conditions have also caused the voltage instability problem to become more prevalent, such as [54]-[55]:

- Power systems in general and specifically transmission lines tend to be operated under more stressed conditions. These stressed operating conditions are not only due to continuous and significant load growth, but also because of major changes and restructuring of energy markets, as well as unconventional practices such as constraint relaxations. Stressed transmission lines have less capability of delivering reactive power to demanding load centers because of the high reactive power losses. Transmission lines (especially long ones) with a relatively large voltage angle difference between sending and receiving ends also have limited capability of reactive power delivery.

- High rates of induction and single phase motor penetration, especially those used in air conditioning systems, heat pumps and refrigeration. These motors are known as low inertia machines. As a result they have fast response to disturbances and can decelerate or even stall rapidly. Voltage instability issues are directly affected by dynamic behavior of motors.
- Excessive reliance on shunt connected capacitor banks for reactive power compensation. In heavily shunt capacitor compensated systems, the voltage regulation tends to be poor. Another disadvantage for shunt capacitors is that the reactive power support they provide is directly proportional to the square of the voltage. Therefore, at low voltages when the reactive power support is most needed, the VAr output of the capacitor banks drops.
- High penetration of electronic loads which have significant discontinuous response to variations in voltage magnitude.
- The use of HVDC tie lines to transfer large amounts of electric power. The convertors associated with these lines consume significant amounts of reactive power.

2.7.1 Voltage Stability Classification

It is useful to classify voltage stability into subclasses in order to better understand system behavior under voltage instability conditions. Classification also helps choosing the right analytical strategies depending on the nature of phenomenon of interest. Voltage stability is classified here according to the magnitude of the disturbance affecting the system into two subclasses:

- Small disturbance voltage stability: also called small-signal or steady state voltage stability. This type of voltage stability is related to small and possibly gradual perturbations in the system, such as small changes in the load. Small-signal stability is determined by the characteristics of load and continuous and discrete controls at a specific instant of time. A criterion for this type of voltage stability is that at a given operating condition, for every bus in the system, the bus voltage magnitude increases as the injected reactive power at the same bus is increased. When analyzing small disturbance voltage stability, usually either midterm (10 seconds to few minutes) or long-term (few minutes to tens of minutes) studies are performed [50]-[51].
- Large disturbance voltage stability: also called transient voltage stability. Large disturbance here refers to major changes in operating conditions. These changes could be major faults on transmission lines, generating units tripping, transmission lines tripping, or other large disturbances. The transient voltage stability is determined by the load characteristics, continuous and discrete controls, as well as the protection systems. However, in order to capture the nonlinear dynamic interactions between the different system components and their effect on transient voltage stability, a dynamic time domain analysis should be performed. This type of analysis is referred to as short-term voltage stability analysis (typically 0 to 10 seconds). A criterion for large disturbance voltage stability is that following a large disturbance and after the actions of system control devices, voltages at all buses reach acceptable steady state levels [50]-[51].

2.7.2 Voltage Stability Analysis

From the previous discussion, it is apparent that each type of voltage stability has its own characteristics and nature, therefore, each type has to be approached and analyzed using the appropriate analytical tool. In general, voltage stability problems are studied using two approaches [50], [55]:

- Static analysis
- Time domain dynamic analysis.

Static analysis studies are used for steady state voltage stability problems initiated by small disturbances. The system dynamics affecting voltage stability in the event of small disturbances are usually quite slow and much of the problem can be effectively analyzed using the static approaches that examine the viability of a specific operating point of the power system. Power flow is used for this type of study, where snapshots are captured from different system conditions at certain time instants. At each of these time frames, system dynamic equations are linearized, and time derivatives of the state variables are assumed to be zero, while state variables take their numerical values at that time instant. Therefore, the resultant system equations are simple algebraic equations that can be solved using power flow simulation. Static analysis can be performed faster than dynamic simulations and need fewer modeling details. However, with the presence of fast acting components such as motors and solid state devices (such as HVDC convertors), the dynamic effect and the interactions between controllers and protection systems must be included in the voltage stability analysis to capture the actual behavior of the system.

Steady state static studies are not only useful in the determination of the voltage stability of a given operating condition, but they also provide information about the proximity of these conditions to voltage instability as well as voltage sensitivity. Static analysis has been solved by different approaches [50], [56]:

Q/V sensitivity analysis: The linearized region provided by power flow analysis around a given point is used to indicate the relation sensitivity between the voltage and reactive power. This sensitivity is described by the elements of the Jacobian matrix. The power equations (polar form) for any node *i* can be written as,

$$S_i = P_i + jQ_i = V_i I_i^* \tag{2.25}$$

where, S_i, P_i, Q_i are the complex, real, and reactive power injections at bus *i* respectively. The term V_i is the bus voltage, and I_i^* is the conjugate current injected at bus *i*.

Power flow equations (real form) of bus *i* with respect to the rest of the system are written as,

$$P_i = V_i \sum_{m=1}^{n} (G_{im} V_m cos\theta_{im} + B_{im} V_m sin\theta_{im}) \tag{2.26}$$

$$Q_i = V_i \sum_{m=1}^{n} (G_{im} V_m sin\theta_{im} - B_{im} V_m cos\theta_{im}) \tag{2.27}$$

where, *G* and *B* are the real and imaginary parts of the admittance matrix, respectively. θ_{im} is the voltage angle difference between buses *i* and *m*. The Jacobian matrix is used to achieve the following linearized form,

$$\begin{bmatrix} \Delta P \\ \Delta Q \end{bmatrix} = \begin{bmatrix} J_{P\theta} & J_{PV} \\ J_{Q\theta} & J_{QV} \end{bmatrix} \begin{bmatrix} \Delta\theta \\ \Delta V \end{bmatrix} \tag{2.28}$$

where, $\Delta P, \Delta Q, \Delta\theta, \Delta V$ are the incremental changes is bus real power, reactive power injection, voltage angle, and voltage magnitude, respectively. Although system stability is

affected by real power, it is possible to keep *P* constant in order to evaluate the sensitivity only between the reactive power and voltage magnitude. Therefore, by setting $\Delta P = 0$,

$$\Delta Q = J_R \Delta V \tag{2.29}$$

where, J_R is the reduced Jacobian matrix of the system and can be written as,

$$J_R = [J_{QV} - J_{Q\theta} J_{P\theta}^{-1} J_{PV}]. \tag{2.30}$$

The *Q/V* sensitivity at a bus represents the slope of the *Q/V* curve at a given operating point. A positive value for the sensitivity indicates stable conditions. The larger the sensitivity index, the closer the operating point is to instability. The value of infinity represents stability limit or the critical point. Negative values for sensitivity indicate unstable conditions, with very small negative values representing highly unstable conditions.

Q/V modal analysis: This analysis approach has the advantage of providing the mechanism of instability at the critical point. The eigenvalues and eigenvectors of the reduced Jacobian matrix are evaluated and used to indicate voltage stability. Positive eigenvalues represent stable voltage conditions, and the smaller the magnitude, the closer the relevant modal voltage is to being unstable. Compared to *Q/V* sensitivity analysis, *Q/V* modal analysis is more capable of identifying the critical voltage stability areas and elements that participate in each mode once the system reaches the critical voltage stability point; hence, *Q/V* modal analysis can describe the mechanism of voltage instability. *Q/V* sensitivity analysis is not able to identify individual voltage collapse modes; instead it only provides information regarding the combined effects of all modes of voltage-reactive power variations.

Q/V curve analysis: *Q/V* curves show the relationship between the reactive power support at a certain bus and the voltage of that same bus. For large power systems these

curves are obtained by a series of power flow simulations. A fictitious synchronous condenser with unlimited reactive power capability is placed at the test bus and the voltage magnitude is varied through the simulation [57]. *Q/V* curves are useful in determining the amount of reactive power needed to be injected at a certain bus in order to obtain a desired voltage level. Therefore, these curves can be used for both voltage stability indication purposes and shunt compensation sizing. However, it should be noted that *Q/V* curves are only valid for steady state analysis [51]. It should also be noted that power flow equations tend to diverge around the voltage stability critical point; therefore, special techniques have to be used to overcome the divergence problem, such as continuation power flow.

Dynamic analysis provides the most accurate results for voltage stability phenomenon using time domain simulations which capture the real dynamic nature of the system without any approximations. Nonlinear dynamic simulation is, therefore, very useful and effective for short term voltage stability studies and fast voltage collapse situations following large disturbances. However, as a price for this accuracy, dynamic simulations are more complicated than static studies since the overall system equations include first-order differential equations that have to be solved as well as the regular algebraic equations. Solving these equations requires significant computational capacity and is relatively time consuming. The accuracy of dynamic simulation results depends mainly on the models used; therefore, system components have to be modeled in detail and with high accuracy. The set of system differential equations can be expressed as follows [50]-[51],

$$\dot{x} = f(x, V) \tag{2.31}$$

and the set of algebraic equations as,

$$I(x, V) = Y_N V \tag{2.32}$$

where x: state vector of the system, V: bus voltage vector, current injection vector, Y_N: bus admittance matrix and (x_o, V_0) are the initial conditions.

Although no expression for time appears explicitly in the previous equations, Y_N is a function of both voltage and time since certain time varying components such as transformer tap changes, phase shift angle controls, and topology are included in it. Also, the relation between I and x can be a function of time. Numerical integration alongside power flow analysis is usually used to solve the nonlinear dynamic equations in the time domain.

2.8 Load Modeling

Loads in transient stability studies are generally defined as active power consuming devices connected to the network at bulk power delivery points. These devices are formed by aggregating a large number of load components and representing them as a single entity [58]-[59]. A load model is a mathematical representation that takes the voltage and possibly frequency as inputs and gives the load active and reactive power consumption as its output [60]. In traditional power flow and steady state analysis studies, a single mathematical model that describes the behavior of these load components is assigned for each load aggregation. This grid-level approach has greatly reduced the complexity associated with representing load in power system studies and made it possible to perform these computer studies within reasonable time and with acceptable accuracy [61].

However, with the growing complexity of load behavior as a result of introducing new and more sophisticated load components, such as: solid state electronic devices, discharge lighting, control and protection technologies, and motors, the grid-level representation approach previously mentioned appears to be missing out a significant amount of important details for the sake of simplifying the behavior of large number of different load devices into one single mathematical model. This negative aspect has started to surface in the form of inconsistencies between simulation results using these simplified load models and the actual (measured) behavior of the system for certain events. The shortfall of simple load models is even more evident when delayed voltage recovery events and sustained depressed voltage magnitudes are investigated [58], [62]-[64].

As computer-based dynamic simulations have become an essential tool used by power system operators for planning purposes and to ensure operational security, the need for a different load representation that would provide more accurate results has become more pressing [65]. This concern is magnified by the fact that power systems operating conditions are also changing and moving towards the edge of operational stability margins in order to satisfy the growing demand and to maximize profits [60]. Therefore, accurate DSA studies are needed to avoid possible costly outages and/or damages.

Despite the research conducted in the field of load modeling and the improvements achieved, it is still considered a challenging and non-trivial problem due to the nature of loads which can be described by the following [58], [60],[62]:

- A large number of load components with highly diverse characteristics and behavior.

- Load composition and magnitude are constantly changing with time. The scope of time change here is within day, week, and season. This introduces a statistical characteristic for actual loads which makes it difficult to represent using deterministic methods.
- Lack of data describing the load since most of the load is located at the customer side which makes it inaccessible to electric utilities.
- Lack of dynamic measurements, because artificial disturbances initiated by utilities such as changing transformers tap settings, are too small to reveal the discontinuous nature of load behavior. On the other hand, uncontrolled large disturbances could take place outside the loading conditions of interest.
- In the distribution system, loads are connected with a myriad of continuous and discrete control and protection devices, which affect the load behavior significantly under voltage and/or frequency disturbances.

2.8.1 Load Model Requirements

Before proceeding to the development of new load models, the requirements expected from these models should be determined. These requirements are extracted from the need for results with high accuracy levels for simulations and DSA studies. A successful and effective load model should be able to [60]-[61]:

- Capture and reproduce the behavior of aggregated load components when subjected to practical variations in system voltage and/or frequency with an acceptable accuracy. This includes the ability of representing events such as:

voltage recovery delays, voltage collapse, and oscillations in transient and steady state time frame.

- Represent rotating loads (motors) dynamically, which makes it capable of capturing motor stalling conditions and their impact on voltage recovery. It should also capture the sensitivities of motor real and reactive power requirements with respect to applied voltage.
- Represent the effect of components lost in the lumped loads such as: thermal protection devices, under-voltage contactors, distribution transformers and feeders, and shunt capacitors.

However, the load model should not be overly complex or cause simulations to become a computational burden. The model should also be physically based, which makes it possible to derive the load model and modify it using information which is relatively easily obtained [60].

2.8.2 Static Composite Load Model

More than one single static load model is needed to describe the behavior of load aggregation. This is due to the fact that different load components with different characteristics were embodied into a single entity [58]-[59], [66]. Static composite load model was developed to represent the complex relation between power and voltage magnitude through an algebraic relation that combines the three different static load models (constant impedance *Z*, constant current *I*, constant power *P*); hence, it is sometimes called ZIP model.

A polynomial equation is usually used to represent the composite static load model as:

$$P = P_0\left(P_1\left(V/V_0\right)^2 + P_2\left(V/V_0\right) + P_3\right)\left(1 + a_{pf}\Delta f\right) \tag{2.33}$$

$$Q = Q_0\left(Q_1\left(V/V_0\right)^2 + Q_2\left(V/V_0\right) + Q_3\right)\left(1 + a_{qf}\Delta f\right) \tag{2.34}$$

where V_0 is the rated (or initial) voltage, P_0 and Q_0 are the active and reactive power consumed at V_0, respectively. P_1, P_2, and P_3 are coefficients that specify the portions of load that are represented as constant impedance, constant current, and constant power respectively. The summation of these coefficients equals one. Q_1, Q_2, and Q_3 are the corresponding reactive power coefficients. It can be noticed that a frequency dependency linear term has been added to both equations to capture frequency change effect on power consumption response. Δf is the deviation in frequency from nominal value, a_{pf} and a_{qf} are the frequency sensitivity of active and reactive power, respectively.

The polynomial model has limited flexibility in representing highly voltage sensitive and nonlinear loads. For example the reactive power of discharge lighting is proportional to voltage to the power four [67]. Therefore, an exponential model which provides more flexibility can be used. The exponential composite static model is represented as:

$$P = P_0\left(P_1\left(V/V_0\right)^{P_{e1}} + P_2\left(V/V_0\right)^{P_{e2}} + P_3\right)\left(1 + a_{pf}\Delta f\right) \tag{2.35}$$

$$Q = Q_0\left(Q_1\left(V/V_0\right)^{Q_{e1}} + Q_2\left(V/V_0\right)^{Q_{e2}} + Q_3\right)\left(1 + a_{qf}\Delta f\right) \tag{2.36}$$

where, P_e and Q_e are the active and reactive power exponential coefficients, respectively.

2.8.3 Motor Modeling

Rotating loads, which consist of all different types of motors, are mainly responsible for the dynamic behavior loads exhibit during transients. Static models, however, are not able to capture these dynamics due to the high nonlinearity and discontinuity in motors behavior under depressed voltage levels. Motors can constitute around 72% of the total load [68], especially in areas with summer load peak where air conditioners (A/C) are intensively used. Most of the industrial load is also comprised of large motors. In extreme cases, industrial motor loads can represent around 98% of the total load [69]. Therefore, with such high motor load penetration, motors dynamic behavior becomes very significant and important to capture in transient studies, especially in short term voltage stability analysis. Voltage recovery delay, or even collapse, following a fault is directly related to decelerating and stalling motors as will be explained next. Three phase induction motors and single phase A/C motors, which are discussed here, are the most commonly used motors, and have the largest impact over voltage stability [59], [63].

In steady state operation, the motor electrical torque is equal to the mechanical torque of the mechanical load connected to it. However, under voltage disturbance (usually depressed voltage magnitude due to a fault) the generated electrical torque is reduced depending on the voltage magnitude, since the electrical torque is proportional to the voltage squared. This state of non-equilibrium between electrical and mechanical torque will cause the motor to decelerate. The deceleration rate depends on the applied voltage level and on the mechanical load characteristics. Mechanical load torque can be either speed dependent, like fans and pumps, or constant, like reciprocating and rotary compressors. Naturally, constant load torque will cause higher deceleration rate. During decelera-

tion the slip will proportionally increase causing the motor to draw high current at low power factor. The increased consumption of reactive power is responsible for delaying the voltage recovery and can even result in a voltage collapse. If the fault is not cleared promptly, and there is not enough reactive power, motors will decelerate till they stall. The key factors in determining a motor active and reactive power response to voltage variations are the inertia (motor and load shaft inertia) and rotor flux time constant [58]. Therefore, small motors with low inertia values, such as single phase A/C motors, tend to decelerate and stall faster than large motors.

The dominant power consuming part of the single phase A/C units is the compressor motor, which consumes up to 87% of the total unit consumption [62]. Therefore, this type of motors have to be modeled and considered in transient stability studies, especially in areas that have summer load peaks. Single phase A/C motors are prone to stall because of their low inertia and the mechanical characteristics of the compressor they drive [64], [70]; therefore, they are directly responsible for the delayed voltage recovery phenomenon. Under stall conditions (i.e. slip=100%) motors draw very high current with a very low power factor. Stall current magnitude is only determined by motors rated locked-rotor current and the applied voltage. In some cases this current can be as high as 8.5 p.u. for residential A/C motors [70]. Under reduced voltage conditions the electrical torque will start to drop down causing the motor to decelerate. The motor will continue to decelerate until it is unable to overcome the pressure applied by the compressor, at this point the motor stalls. Usually single phase A/C motors stall if the voltage falls to between 50 – 65 % of nominal voltage for more than 3 cycles [71]. Stalling voltage depends

on other factors, such as: ambient temperature and humidity. Figure 2.3 shows the reactive power consumption of a stalled A/C motor.

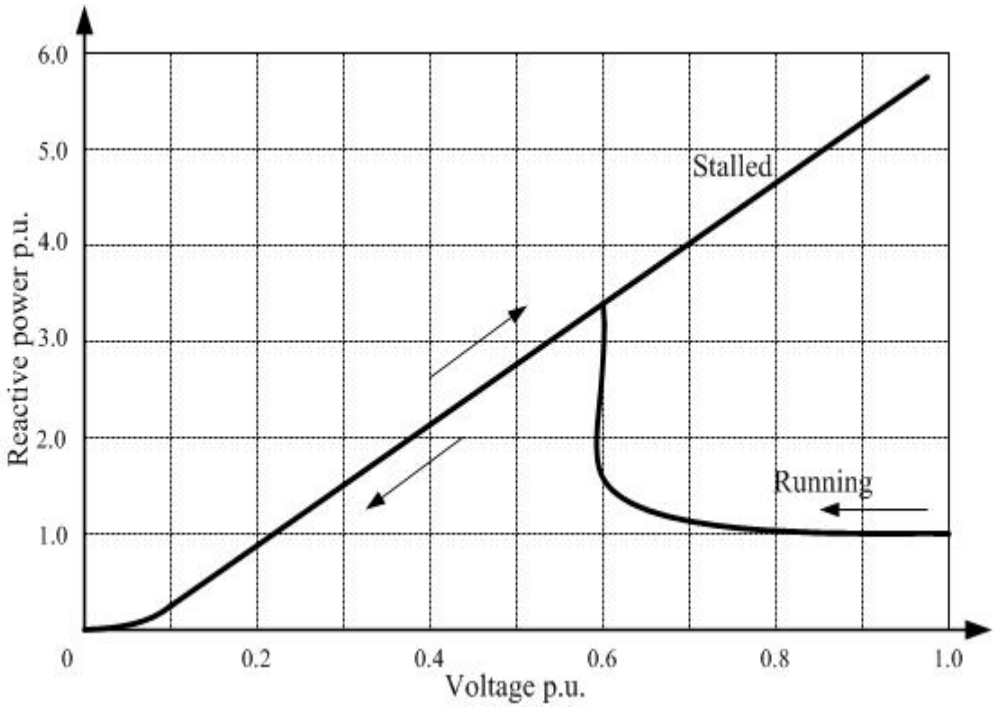

Figure 2.3. Reactive Power Consumption of a Stalled Single Phase Induction A/C Motor.

Stalled A/C motors can in some cases re-accelerate if the voltage recovers to a certain level (roughly above 70%). However, re-accelerating after stall condition depends on the type of compressor connected to the motor. Single phase A/C motors are also equipped with under-voltage and thermal relays which should be included in the model as they significantly affect the dynamic behavior of these motors. Thermal relays usually operate in response to the high current drawn during stall conditions. The time required for thermal relays to operate depends on the drawn current. Thermal tripping could happen for an individual unit or for a whole feeder that is supplying many stalled motors. Under-voltage protection contactors operate faster than thermal ones; under-voltage con-

tactors open almost instantaneously at low voltages (35 – 45 %), and can reclose at voltages above 50% [62].

The characteristics of single phase A/C motors discussed above have significant impact on short term voltage stability analysis and must be included in the model. The controls and protection schemes should also be included in the load model since they control tripping and reconnecting the units. Laboratory tests and offline simulations have proved that conventional three phase induction motor model is not adequate to capture the dynamic response of single phase A/C motors [61], especially the stalling conditions. However, the steady state behavior of both motors is very similar and a three phase induction motor can be suitable to capture the behavior of single phase A/C motor in steady state conditions. To include the stalling conditions, a fictitious shunt component is connected in parallel with the motor to replace it with the locked-rotor impedance representing a constant impedance model. This approach is called "hybrid performance based modeling" [71].

2.8.4 Composite Load Model Structure

The WECC developed an interim composite load model that was used for planning and operation studies in early 2002 [62]. This model was represented by 80% of load as static, and 20% as induction motor load. This interim model was unable to represent delayed voltage recovery events following a major transmission fault. Simulations using this interim model indicated instantaneous voltage recovery contrary to the real recorded event. Therefore, WECC formed a load modeling task force (LMTF) to improve

the interim model and develop a more accurate and comprehensive one. The LMTF acknowledged the following factors in the improved composite load model:

- The electrical distance between the point where the load is connected in simulations (usually transmission or sub-transmission level) and the point where the physical load is connected (distribution level). Therefore, the improved model should include the network components such as: feeders and transformers impedance, shunt devices, protection, and transformer taps.
- Single phase A/C motors have significant impact on voltage stability and should be included in the new model explicitly since the induction motor model is not adequate to represent their characteristics. This will allow the new composite model to capture the dynamic behavior of these motors such as: decelerating, stalling, and tripping.
- Induction motors vary widely in characteristics depending on size, number of phases and mechanical torque they drive. Therefore, the new model should differentiate between the different types of induction motors. This provides more flexibility and accuracy in representing motor loads.

Figure 2.4 shows LMTF proposed composite load model.

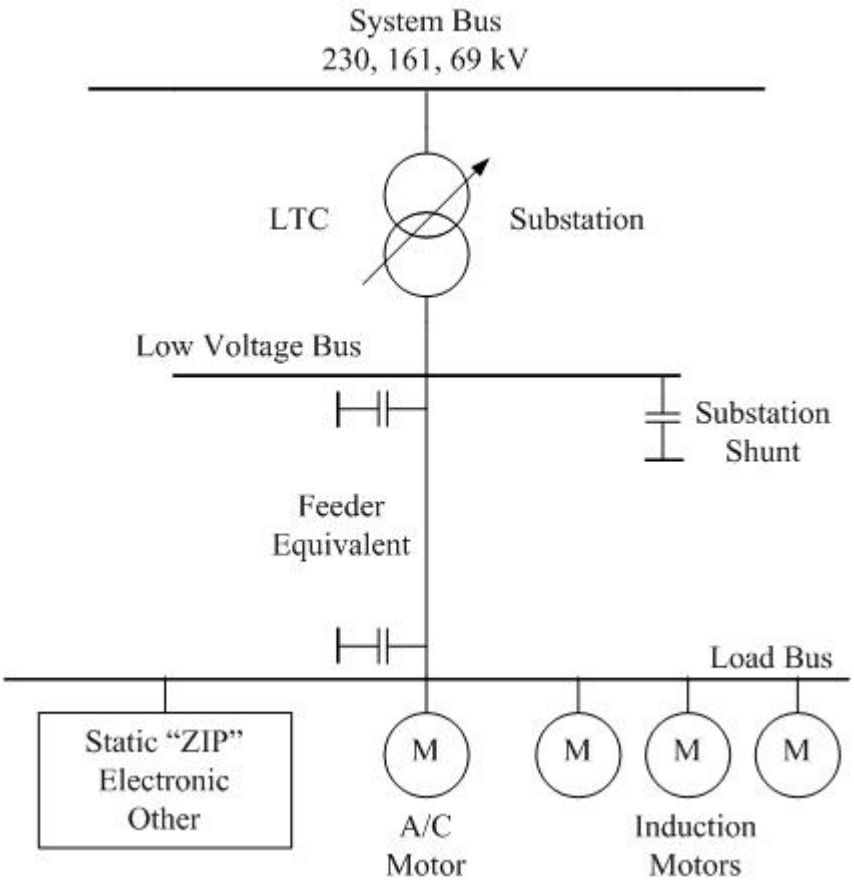

Figure 2.4. LMTF Proposed Composite Load Model

3. CONSTRAINT RELAXATIONS

3.1 Overview

System operators use energy market models to perform several procedures that are required to ensure that the energy demand in their control areas is satisfied reliably and economically. Security constrained unit commitment (SCUC), security constrained economic dispatch (SCED), and reliability unit commitment (RUC) are examples of these procedures. The electric power network is represented in these energy market models as a linear approximate DC system. This approximation is required in order to solve the optimization problems associated with the energy market operations without incurring prohibitive processing times and complexity. The constraint relaxation process, which is defined as allowing certain constraints in the optimization problem to be violated for a set penalty price, is considered as a type of approximation. Similar to other approximations, operators use constraint relaxation mechanisms to achieve various gains, such as: facilitating the optimization solution and controlling locational marginal prices (LMPs) [72]. An analytical illustration of how constraint relaxations are incorporated in the optimization problem and their direct effect on LMPs is presented in this chapter. Further discussion on the potential benefits achieved by employing constraint relaxation mechanism is presented as well.

3.2 Effect of Constraint Relaxations on LMPs

One of the major motivations system operators have for applying constraint relaxations is the direct impact this mechanism has over LMPs. Previously, market models

were designed to use bid caps as the only means for limiting the LMPs throughout the system. Bid caps are the maximum prices independent power producers (IPPs) are allowed to bid for their offered supply in the day-ahead market. However, the LMPs which are used to determine the different payments made to generators are not limited by bid caps. The following general optimization example illustrates the effect constraint relaxations have on the duals (LMPs) of the primary problem [73].

$$\begin{array}{ll} \multicolumn{2}{c}{min\ c_1x_1 + c_2x_2} \\ s.t. & \\ a_{11}x_1 + a_{12}x_2 \geq b_1 & (\lambda_1) \\ a_{21}x_1 + a_{22}x_2 \geq b_2 & (\lambda_2) \\ x_1 \geq 0 & \\ x_2 \geq 0 & \end{array} \qquad \begin{array}{ll} \multicolumn{2}{c}{max\ b_1\lambda_1 + b_2\lambda_2} \\ s.t. & \\ a_{11}\lambda_1 + a_{21}\lambda_2 \leq c_1 & (x_1) \\ a_{12}\lambda_1 + a_{22}\lambda_2 \leq c_2 & (x_2) \\ \lambda_1 \geq 0 & \\ \lambda_2 \geq 0 & \end{array} \tag{3.1}$$

The optimization problem represented by (3.1) represents the standard primal problem and its corresponding dual formulation for a general optimization problem where no constraint relaxations are allowed. The constraints in this representation can be relaxed by introducing the slack variables s_1 and s_2. The relaxed optimization problem and its dual formulation are presented in the following set of equations:

$$\begin{array}{ll} \multicolumn{2}{c}{min\ c_1x_1 + c_2x_2 + P_1s_1 + P_2s_2} \\ s.t. & \\ a_{11}x_1 + a_{12}x_2 \geq b_1 - s_1 & (\lambda_1) \\ a_{21}x_1 + a_{22}x_2 \geq b_2 - s_2 & (\lambda_2) \\ x_1 \geq 0 & \\ x_2 \geq 0 & \\ s_1 \geq 0 & \\ s_2 \geq 0 & \end{array} \qquad \begin{array}{ll} \multicolumn{2}{c}{max\ b_1\lambda_1 + b_2\lambda_2} \\ s.t. & \\ a_{11}\lambda_1 + a_{21}\lambda_2 \leq c_1 & (x_1) \\ a_{12}\lambda_1 + a_{22}\lambda_2 \leq c_2 & (x_2) \\ \lambda_1 \leq P_1\ (s_1) & \\ \lambda_2 \leq P_2\ (s_2) & \\ \lambda_1 \geq 0 & \\ \lambda_2 \geq 0 & \end{array} \tag{3.2}$$

Since there is a penalty price associated with each constraint violation, the penalty prices P_1 and P_2 are added to the objective function in order to limit the value and duration of these violations. When comparing the structure of non-relaxed and relaxed formu-

lations in (3.1) and (3.2) respectively, it can be observed that the dual variables λ_1 and λ_2 in the non-relaxed system have only a lower limit and can theoretically grow to any value. On the other hand, the dual variables in the relaxed formulation have upper bounds that are equal to the penalty prices. Therefore, it can be concluded that the upper limit of the dual variables (LMPs) can be directly enforced by relaxing the optimization problem constraints (node-balance) and defining the corresponding penalty prices. It should be noted here that different types of constraints could be relaxed including those variables that cannot be physically relaxed, such as node-balance. Such physically unrealizable relaxations are expected to serve the purpose of relaxation in the market model, while appearing as different types of violations in the physical system or disappearing as a result of the various approximations in the model.

3.3 Constraint Relaxation Motivations

In addition to controlling LMPs, system operators utilize a constraint relaxation mechanism as a measure to ensure that their market models produce acceptable and feasible solutions. Attaining a feasible solution with good results can be a matter of concern because of the various approximations introduced in the energy market models. In such cases, constraint relaxations can be considered as corrective approximations that are required to avoid infeasibility or unrealistic solution values. Furthermore, the relatively high penalty price values associated with constraint relaxations imply substantial gains in social welfare in the event of a slight constraint violation. This is the result of introducing a significantly high penalty price for each constraint violation regardless of the magnitude of that violation.

4. METHODOLOGY AND RESULTS

4.1 Introduction

Constraint relaxations, by definition, mean that certain security, operational, or financial constraints are allowed to be violated in the energy market models for a predetermined penalty price. Some of these relaxations are physically unrealizable, such as the node balance constraints. Other relaxations, however, are physically achievable, such as branches thermal limits and, therefore, could appear in the AC real-time system as actual violations. Even physically unrealizable relaxations could appear in the real-time system as violations in other forms since these relaxations are a form of approximation. Therefore, in order to assess the true risk associated with allowing certain constraints to be relaxed, the impact of these relaxations on real-time system performance was investigated. Capturing the impact of constraint relaxations on real-time system performance provides operators with a better understanding on how relaxations in the energy market models are translated into physical violations. This information can be used not only to assess the criticality of constraint relaxations, but also as a basis for determining penalty prices more accurately. In this chapter power system performance criteria are presented and defined. The methodology of the analysis conducted is discussed, followed by the results.

4.2 Power System Performance Definition

Power system performance is defined by the following concepts:

- Reliability: NERC defines power system reliability as: “the degree to which the performance of the elements of that system results in power being delivered to consumers within accepted standards and in the amount desired. The degree of reliability may be measured by the frequency, duration, and magnitude of adverse effects on consumer service” [74]. Hence, power system reliability can be regarded as the probability of satisfactory operation over an extended time period.
- Security: power system security is related to the robustness of the system following imminent disturbances (contingencies). NERC defines power system security as the degree of risk in the power system ability to withstand sudden disturbances such as short circuit faults or the loss of major components, without interruption of customer service. Security, therefore, depends on the system operating conditions as well as the probability of contingent events [21].
- Stability: power system stability can be defined as “the ability of an electric power system, for a given initial operating condition, to regain a state of operating equilibrium after being subjected to a physical disturbance, with most system variables bounded so that practically the entire system remains intact” [21]. Power system stability depends on the severity and the physical nature of contingent events as well as the system operating conditions.

Power system performance aspects (reliability, security, and stability) are interrelated as all of them refer to system robustness and satisfactory operation. For instance, a power system cannot be considered reliable if it is insecure and it cannot be considered secure if it is unstable. Hence, reliability is the overall objective in power system planning and operation because it spans long period of time and comprises all other aspects.

The distinction between power system security and stability is that security is more general, as it factors in the probability of contingent events. Power system security also accounts for contingencies that are not classified as stability events, such as equipment failure or sabotage. Power system security also considers post-contingency operating conditions, such that a system could be stable following a contingency but insecure due to post-contingency overloads or voltage violations.

4.3 Power System Performance Analysis and Results

In this section, a detailed description of the test cases used to conduct this work is provided. Also the analysis methodology used to investigate the impact of constraint relaxations on real-time system overall operational security along with the results are presented.

4.3.1 Test Case Description

In order to capture the direct effect of constraint relaxations on system security and reliability as well as on related energy market aspects, the constraint relaxations process practiced by system operators was replicated using two test cases: the RTS-96 test case [75] and the PJM system. The RTS-96 test case was chosen for this part of the analysis because of the significant number of generators in this test case, which provide a suitable platform for studies related to this type of work such as security constrained unit commitment, security constrained economic dispatch and optimal power flow (ACOPF and PSCOPF). The RTS-96 test case is comprised of three identical areas where each ar-

ea is connected to the other two areas (ring configuration). Table 4.1 shows the overall RTS-96 test case components.

Table 4.1. RTS-96 System Components.

Component	Number
Areas	3
Buses	73
Generators	99
Shunts	3
Lines	104
Transformers	16
Load Aggregations	51
Max. Load (MW)	9405

The PJM test case is a large-scale real-life system. PJM provided hourly detailed power flow and dynamic data for one week in July 2013. The provided data includes PJM control areas as well as the neighboring areas. Representing neighboring areas is required in this type of analysis in order to capture the power transfers between PJM control areas and other areas, as well as the dynamics of neighboring areas that could affect PJM control areas. PJM also provided their market data for that week, which was used in this work to obtain market solutions based on realistic and practical bidding data. Table 4.2 lists the overall components of PJM control areas as well as the neighboring areas. It should be noted here that the topology of the PJM test case changes from one time period to another.

For each test case, market SCUC solutions were obtained and used as starting points to represent the AC real-time system. This process was conducted twice, once with no constraint relaxations and another time allowing certain constraints to be relaxed. This approach facilitated the comparison between the two different scenarios while ensuring high consistency between them. PSS/E ACOPF [41] was used to obtain a base-case AC

feasible solution that is as close as possible to the market solution. Therefore, the same economic data and constraints used in the energy market models were used in ACOPF. Running ACOPF provided an accurate and consistent transition from the dispatch schedules generated by the DC market models to an AC feasible solution. Losses were distributed in an economic manner rather than being picked up by the slack bus. Other controls, such as scheduled voltages, transformers tap settings, and switched shunts, were adjusted optimally as well.

Table 4.2. PJM System Components (Peak Hour).

Component	PJM	Neighboring areas
Areas	24	24
Buses	10150	5128
Generators	1682	1185
Shunts	810	786
Lines	8653	5899
Transformers	4201	1999
Load Aggregations	8101	3764
Max. Load (MW)	144340	134974

The output of the ACOPF is a base-case AC feasible system. However, this is not always the case because some cases needed out-of-market corrections to overcome AC infeasibility. Usually AC infeasibilities are voltage related since voltage and reactive power are not represented in DC energy market models. In order to achieve AC feasibility with the least number of out-of-market corrections, a limited number of generators were turned on in areas that were causing infeasibility. It should be noted that more out-of-market corrections were needed for cases with constraint relaxations. This can be explained by the lower number of committed generating units compared to cases with no constraint relaxations that resulted in less reactive power availability. In order to assess

the impact of constraint relaxations on overall system performance, several static and time-domain studies were conducted, as will be presented in the following discussion.

4.3.2 Static Analysis and Results (RTS-96)

Since the goal here is to capture the impacts of constraint relaxations on real-time system performance, constraint relaxations that are physically realizable were allowed to appear as actual violations in the AC system. This approach also ensured that the cases with relaxed constraints have the least amount of out-of-market corrections and are as close as possible to market SCUC solutions. However, for cases that do not have constraint relaxations, PSS/E ACOPF and PSCOPF were both used to obtain AC feasible base-case and post-contingency solutions, which resulted in feasible and *N*-1 secure cases that were used as benchmarks to compare with corresponding cases with relaxed constraints.

Several modifications were made to the RTS-96 test case throughout this work. Some modifications such as increasing the original loads by 10%, de-rating the transmission lines thermal capacity by 10%, and tripping the HVDC line were made in order to stress the system and, therefore, obtain appropriate constraint relaxations. Other modifications consisted of enabling transformers tap setting adjustments and adding switched shunts in order to introduce more control capabilities within the system that will be used in the succeeding steps to ensure a secure base-case and *N-1* operating conditions.

Static analysis was used to investigate base-case and post-contingency line flows and bus voltage violations. Table 4.3 lists the market relaxations and their corresponding violations in the AC real-time system. It should be noted that the relaxed lines (line IDs

25, 65, and 104) shown in Table 4.3 are identical lines since the RTS-96 test case is comprised of three identical areas, and each one of them is in a different area. Those relaxed lines are major transmission lines that connect between several generating units and large load pockets.

Table 4.3. RTS-96 AC Line Flow Violations.

Time period	Relaxed line ID	DC flow % (market solution)	AC flow % (real-time solution)
7:00	65	110.3%	116.9%
	104	104.5%	108.2%
8:00	104	105.0%	111.0%
22:00	25	103.2%	105.1%
23:00	65	108.3%	115.8%
	104	105.4%	110.8%

From Table 4.3, it can be seen that all line flow relaxations in the market solution have appeared as actual flow violations in the AC real-time system. It can be also noticed that the AC violations are higher in magnitude than corresponding market relaxations. Discrepancies between DC and AC solutions are expected since the DC market solution is approximate. For instance, reactive power flow and thermal losses are not represented in the DC market model and, therefore, line flows are most likely to be higher in the AC system. However, this is not always the case. In large scale complicated cases, the relationship between DC and AC line flows cannot be deduced intuitively as will be shown in the PJM test case.

Table 4.4 shows the number of voltage violations corresponding to the relaxed cases shown in Table 4.3. A bus voltage is considered in violation if it falls outside the tolerance range of 0.95 – 1.05 p.u. Table 4.4 also shows the number of committed generators for the relaxed cases and the corresponding non-relaxed cases. The number of addi-

tional generators needed to make the non-relaxed market solution feasible and *N*-1 secure is also displayed; hence, no voltage violations are present. From Table 4.4 it can be seen that the cases (time periods) with more relaxations (hours 7:00 and 23:00) tend to have more voltage violations compared to cases with fewer relaxations. It can also be noticed that relaxed cases usually have fewer number of committed generators compared to cases with no relaxations, which explains voltage violations due to reactive power deficiency. It should be noted here that all voltage violations listed in Table 4.4 are low voltage violations.

Table 4.4. RTS-96 Voltage Violations and Out-Of-Market Corrections.

Time period	Relaxed		No relaxations	
	Committed generators	Voltage violations	Committed generators (market)	Added generators (out-of-market)
7:00	56	6	58	4
8:00	64	5	65	1
22:00	63	2	63	0
23:0	55	6	59	1

From the results in Table 4.3 and Table 4.4, it is apparent that cases with relaxed constraints sustained both line flow and bus voltage violations in the base-case. The next and final step in RTS-96 static analysis is to investigate the impact of constraint relaxations on post-contingency line flow and bus voltage violations. The post-contingency operating conditions were determined by running an exhaustive *N*-1 contingency analysis. Post-contingency analysis was conducted for cases with constraint relaxations and for their corresponding non-relaxed cases. Table 4.5 summarizes the post-contingency results.

Table 4.5. RTS-96 Post-Contingency Violations.

Time period	Relaxed		
	Voltage violations	Line flow violations	Unsolved contingencies
7:00	62	13	9
8:00	14	9	5
22:00	26	7	1
23:00	22	8	15

For post-contingency analysis, the bus voltage tolerance range is 0.90 – 1.10 p.u. Also, line emergency thermal limits (Rate-C) were used. As can be seen in Table 4.5 there are a significant number of post-contingency violations and, therefore, the relaxed cases are not secure without out-of-market corrections. Unsolved contingencies indicate that the power flow for some contingencies was not successfully solved, usually because of excessive reactive power mismatches. Consequently, there were additional violations that were not reported due to those unsolved contingencies. Additionally, special attention was given to the relaxed lines, i.e. the lines with AC line flow violations in the base-case, since those lines were already overloaded. Table 4.6 shows the post-contingency power flow on those relaxed lines.

Table 4.6. RTS-96 Post-Contingency Relaxed Lines Flows.

Time period	Relaxed line ID	Post-contingency AC flow %	
		Relaxed	No relaxation
7:00	65	103.0%	98.7%
	104	115.6%	96.8%
8:00	104	116.6%	94.5%
22:00	25	109.5%	100%
23:00	65	103.2%	99.3%
	104	118.0%	99.9%

Table 4.6 shows that the relaxed lines were vulnerable to high flow violations following certain contingencies. Similar to Table 4.5, emergency thermal limits are used in

Table 4.6, which also lists the flows on the same lines for cases with no relaxations. As expected, there were no post-contingency violations for those cases since they were *N*-1 secured.

4.3.3 Dynamic Analysis and Results (RTS-96)

Following the RTS-96 test case static analysis, the dynamic behavior of the relaxed cases was investigated and compared to corresponding cases with no relaxations. The original RTS-96 dynamic data only consisted of classical machine models. Therefore, realistic and detailed dynamic data was created and used for this analysis. The detailed dynamic data included synchronous machine models, exciter models and governor models. Each generator size and type were considered throughout this dynamic modeling process. Time periods 8:00 and 23:00 were chosen for this analysis since the post-contingency line flow violations were the highest in those time periods as shown in Table 4.6. The sequence of contingent events was started by placing a three-phase fault at one terminal of the line that corresponds to the contingency causing the relaxed lines to be overloaded. After 5 cycles the fault was cleared and the first line was tripped. After one second, the overloaded relaxed line was tripped. This sequence of events represents an *N*-2 contingency. The same process was repeated for the non-relaxed cases and rotor angles of the most affected generators were plotted and compared. Figure 4.1 and Figure 4.2 show the relative rotor angle plots for the relaxed and non-relaxed cases, respectively, for time period 8:00.

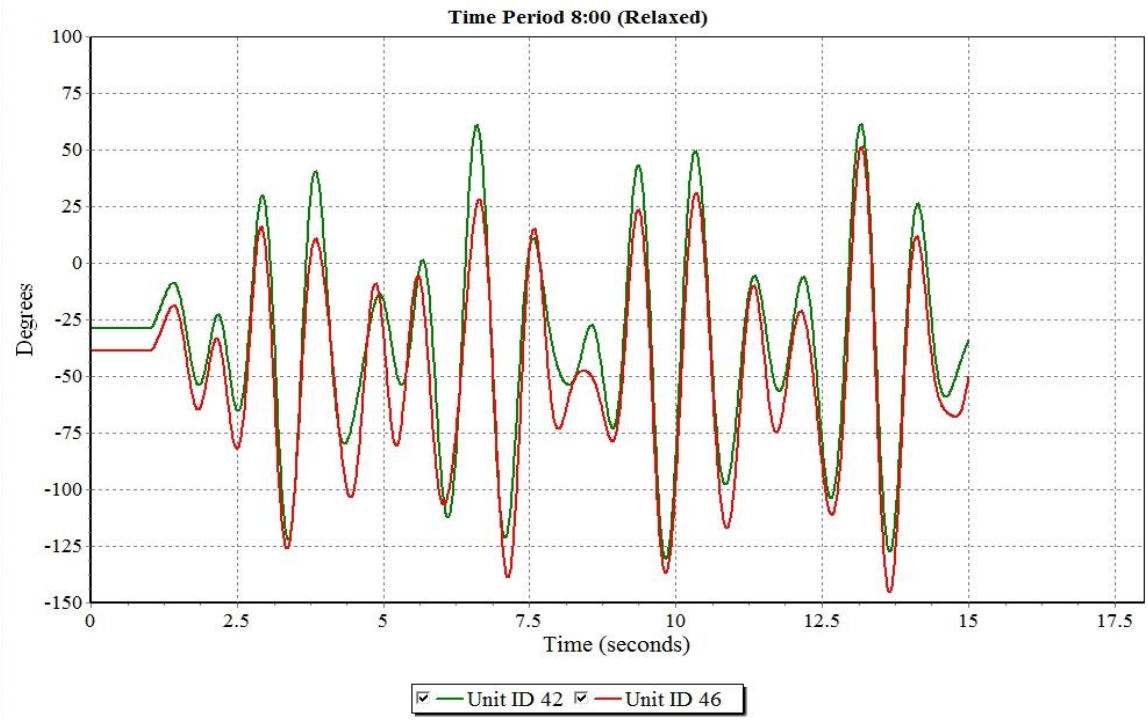

Figure 4.1. RTS-96 Rotor Angles – Time Period 8:00 (Relaxed).

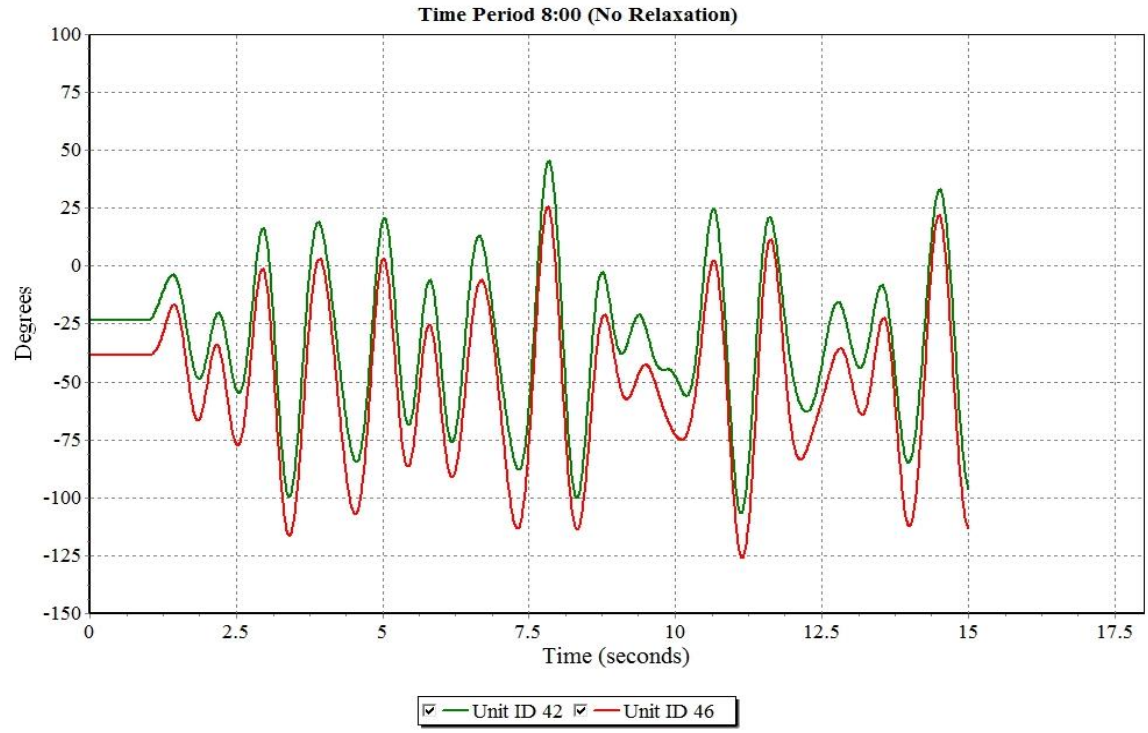

Figure 4.2. RTS-96 Rotor Angles – Time Period 8:00 (No Relaxations).

Figure 4.1 and Figure 4.2 show the relative rotor angle plots for generating units 42 and 46, which were most affected by the imposed contingency. Despite the sustained oscillations in both cases, which indicate poor damping, it can be noticed that the oscillations in the relaxed case have higher magnitudes compared to the non-relaxed case. Although both cases are considered stable, the higher oscillations imply that the relaxed case is more prone to stability problems. The same analysis was conducted for time period 23:00. Relative rotor angle plots are shown in Figure 4.3 and Figure 4.4 for the relaxed and non-relaxed cases respectively.

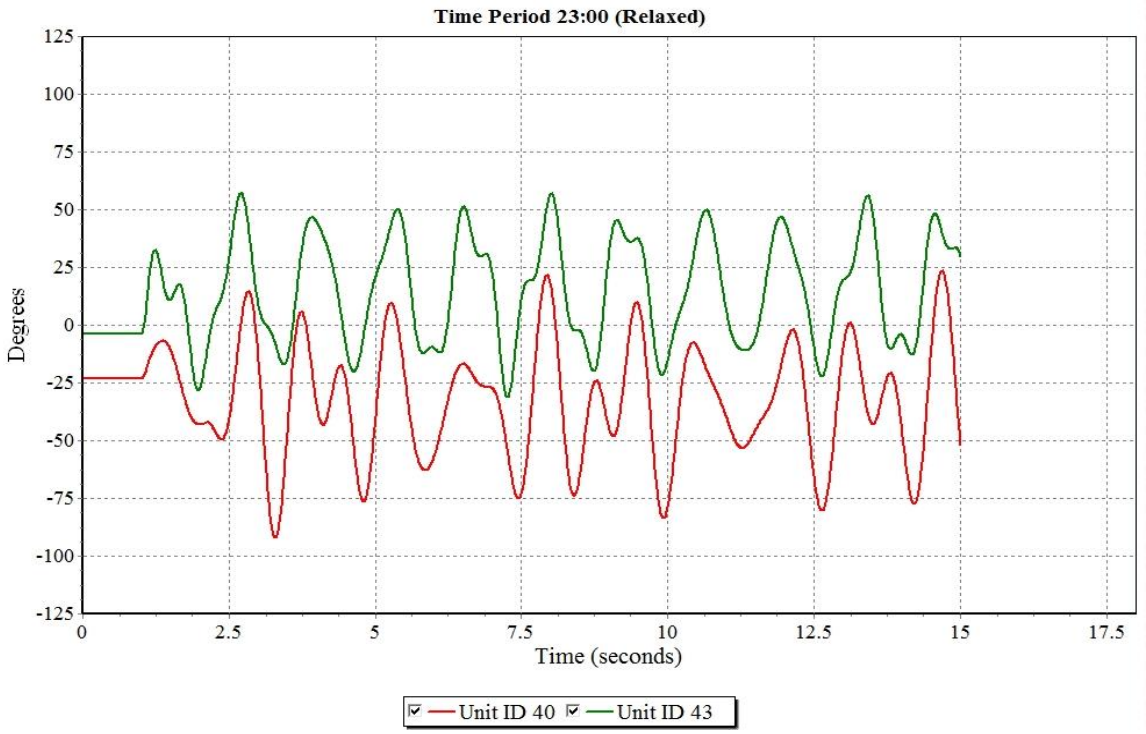

Figure 4.3. RTS-96 Rotor Angels – Time Period 23:00 (Relaxed).

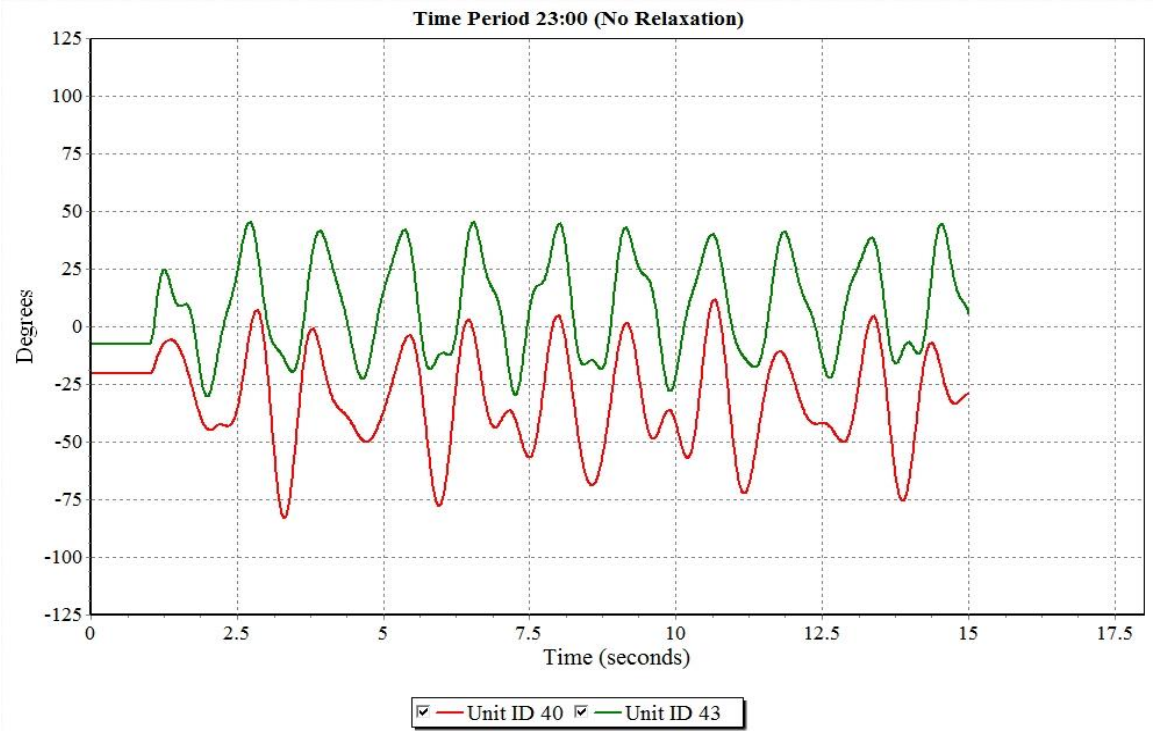

Figure 4.4. RTS-96 Rotor Angles – Time Period 23:00 (No Relaxations).

Figure 4.3 and Figure 4.4 show the relative rotor angle plots for generating units 40 and 43 were most affected by the imposed contingency. Similar to time period 8:00, higher oscillations were observed in the relaxed case compared to the non-relaxed case for time period 23:00. The higher oscillations are not an exclusive result of constraint relaxations from the proposed market solution. Out-of-market corrections that directly affect operating conditions also have an impact on the dynamic behavior of the cases under study.

It was also desired to investigate the dynamic voltage profiles of the relaxed cases following a large disturbance. A full *N*-1 contingency analysis was conducted for the relaxed cases in order to identify the contingencies causing the most severe post-contingency voltage violations. Table 4.7 shows the contingencies resulting in the most severe voltage violations along with the post-contingency voltage and affected buses.

Table 4.7. RTS-96 Post-Contingency Voltage Violations.

Time period	Contingency ID	Lowest voltage bus ID	Voltage p.u.	Voltage base kV
7:00	57	207	0.74	138
23:00	103	307	0.77	138

For each time period listed in Table 4.7, time-domain dynamic analysis was conducted to investigate the dynamic post-contingency voltage profiles. A three-phase fault was placed at one terminal of the lines corresponding to the contingencies shown i n Table 4.7. After 5 cycles, the fault was cleared and the line was tripped, resulting in the post-contingency low voltage violations shown. The analysis was conducted for the cases with no relaxations as well in order to demonstrate the differences between the two scenarios. Figure 4.5 and Figure 4.6 show the voltage plots for the relaxed and non-relaxed cases respectively for time period 7:00.

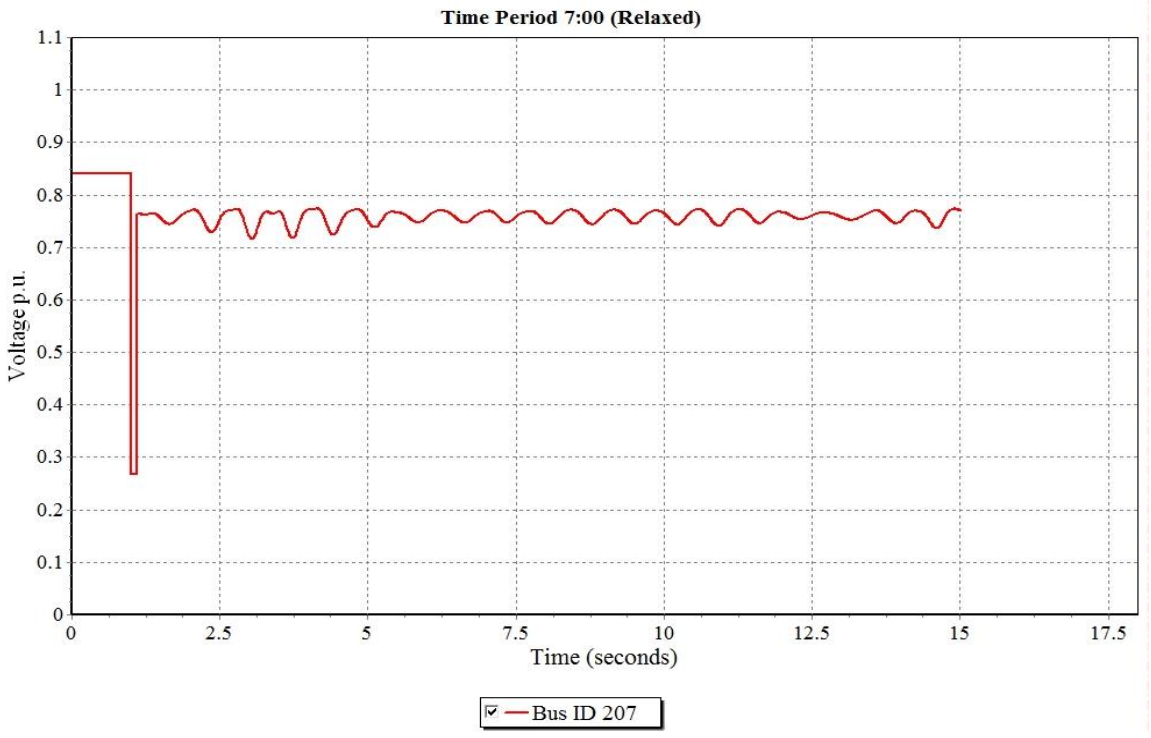

Figure 4.5. Bus ID 207 Voltage Profile – Time Period 7:00 (Relaxed).

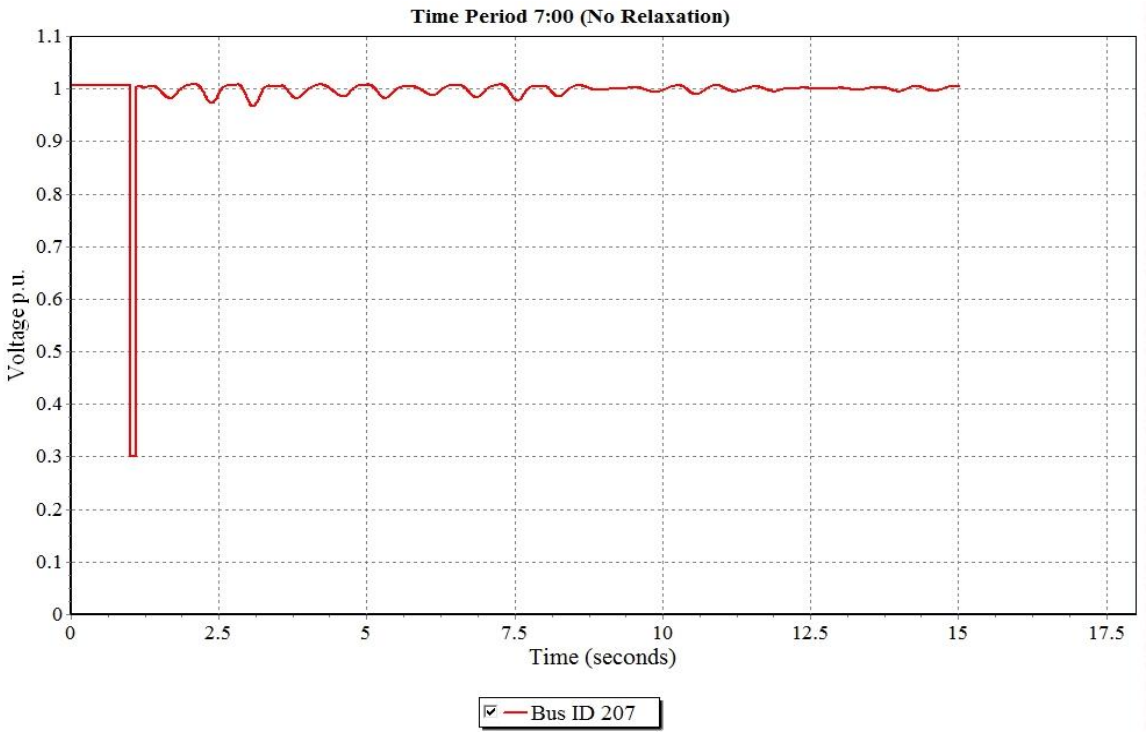

Figure 4.6. Bus ID 207 Voltage Profile – Time Period 7:00 (No Relaxation).

Figure 4.5 and Figure 4.6 show a significant difference in voltage magnitude between the relaxed and non-relaxed cases. It can be noticed that bus ID 207 had a base-case low voltage violation in the relaxed case and it sustained an even lower voltage following the imposed contingency. On the other hand, there were no voltage violations in the non-relaxed case since it was *N*-1 secured. Figure 4.7 and Figure 4.8 show the voltage plots for the relaxed and non-relaxed cases, respectively, for time period 23:00.

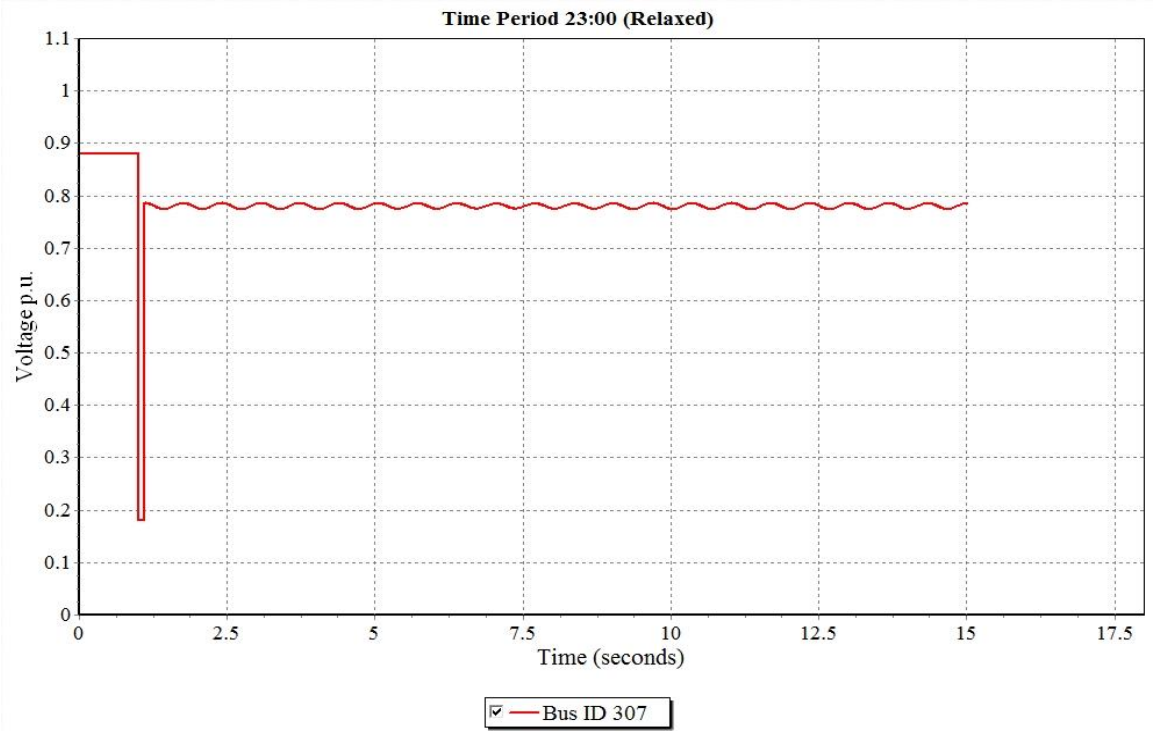

Figure 4.7. Bus ID 307 Voltage Profile – Time Period 23:00 (Relaxed).

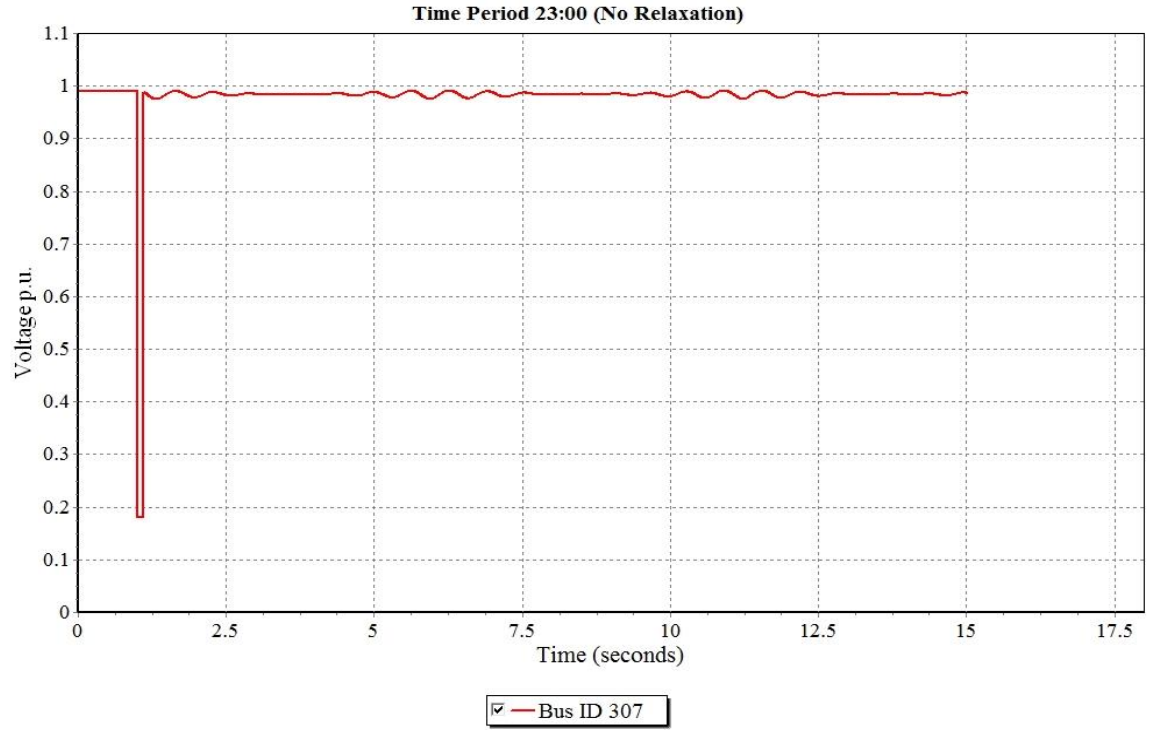

Figure 4.8. Bus ID 307 Voltage Profile – Time Period 23:00 (No Relaxation).

Similar to time period 7:00, Figure 4.7 shows that the relaxed case for time period 23:00 had a sustained depressed voltage profile following the imposed contingency with base-case low voltage violation as well. On the other hand, Figure 4.8 shows normal base-case and post-contingency voltage magnitudes for the non-relaxed case. The voltage plots presented in Figure 4.5 - Figure 4.8 indicate reactive power deficiency in the relaxed cases compared to cases with no relaxations for both time periods. This difference in reactive power availability is due to the larger number of committed generators in the non-relaxed cases as a result of the market solution as well as the out-of-market corrections as shown in Table 4.4.

4.3.4 Static Analysis and Results (PJM)

PJM test case performance was investigated in a similar manner to RTS-96. However, due to the size and complexity of PJM test case and the lack of specialized commercial tools, only two time periods (hours) were investigated. An off-peak and on-peak time periods were chosen to represent light and heavy load conditions respectively. Relaxed market SCUC solutions for those two time periods along with their corresponding non-relaxed cases were used as starting points to achieve an AC feasible solution. However, for the PJM test case out-of-market corrections were required for all cases (relaxed and non-relaxed) as a first step to obtain a successful power flow. Intensive out-of-market correction analyses using PSS/E ACOPF and PSCOPF were conducted on the non-relaxed cases to achieve AC feasibility and *N*-1 security. On the other hand, limited out-of-market corrections were applied to the relaxed cases in order to sustain the line relaxations in the real-time system and keep the final solution as close as possible to the market

solution. Table 4.8 lists the market relaxations and their corresponding violations in the AC real-time system.

Table 4.8. PJM AC Line Flow Violations.

Time period	Line ID	DC flow % (market solution)	AC flow % (real-time solution)
Off-peak	878	159%	140%
	1464	252%	252%
	4605	106%	97%
	4649	102%	96%
	5020	103%	96%
	9048	No relaxation	101%
	9049	No relaxation	101%
	10519	117%	130%
	11115	109%	110%
	11255	129%	102%
On-peak	190	101%	92%
	878	210%	187%
	1464	148%	87%
	1703	101%	107%
	3460	No relaxation	106%
	5020	No relaxation	101%
	5590	No relaxation	102%
	6470	107%	99%
	7318	No relaxation	105%
	7557	108%	101%
	9965	105%	104%
	10519	118%	143%
	11001	101%	106%
	11049	No relaxation	106%
	11111	No relaxation	106%
	11255	109%	109%

From Table 4.8, it can be seen that not all AC line flow violations were originated from the market solution as constraint relaxations and, equally, not all line relaxations in the market solution were realized as actual AC line flow violations in the real-time system. This discrepancy between market solution and actual AC solution is expected since the DC market models contain several approximations, which include neglecting thermal losses and reactive power. For large-scale systems such as the PJM test case, the effect of

these approximations is more evident compared to small test systems such as RTS-96. However, Table 4.8 shows that AC line flow violations that are not associated with market relaxations tend to have relatively small magnitudes compared to the lines that were relaxed in the market solution. It can also be noticed that line relaxations in the market models most likely will appear as AC flow violations in real-time.

Table 4.9 shows the number of voltage violations in the relaxed cases shown in Table 4.8. A bus voltage is considered in violation if it falls outside the tolerance range of 0.90 – 1.10 p.u. It also shows the number of committed generators for the relaxed cases and the corresponding non-relaxed cases. The number of additional generators needed to make the non-relaxed market solution feasible and *N*-1 secure is also displayed; hence, no voltage violations are present.

Table 4.9. PJM Voltage Violations and Out-Of-Market Corrections.

Time period	Relaxed			No relaxations	
	Committed generators (market)	Added generators	Voltage violations	Committed generators (market)	Added generators
Off-peak	1395	17	60	1445	63
On-peak	1837	26	52	1935	84

As shown in Table 4.9, 17 and 26 out-of-market generators had to be turned on in the relaxed off-peak and peak time periods, respectively, to attain a base-case AC feasible solution. Base-case voltage violations were found in both relaxed time periods. It should be noted here that most of the voltage violations in the off-peak case are high voltage violations. A greater number of generators had to be turned on in the non-relaxed off-peak and peak time periods (63 and 84 generators respectively) to attain AC feasible and *N*-1 secure cases. Similar to the RTS-96 test case, the PJM relaxed solutions had fewer committed generators compared to their corresponding non-relaxed cases.

For *N*-1 contingency analysis, line flow violations, voltage violations, and unsolved contingencies were reported in the relaxed cases. Table 4.10 presents the post-contingency flows on the lines that had originally base-case flow violations.

Table 4.10. PJM Post-Contingency Relaxed Lines Flows.

Time period	Relaxed line ID	Post-contingency AC flow %	
		Relaxed	No relaxation
Off-peak	878	175%	100%
	1464	315%	98%
	10519	285%	100%
	11115	97%	38%
	11255	120%	42%
On-peak	878	234%	100%
	1703	102%	73%
	7557	104%	87%
	9965	86%	84%
	10519	380%	100%
	11001	115%	22%
	11255	140%	60%

As can be seen from Table 4.10, relaxed lines had significant post-contingency flow violations. Table 4.10 also shows that there were no post-contingency flow violations in the non-relaxed cases, as they were *N*-1 secure. Therefore, relaxed lines with AC flow violations were more vulnerable to excessive post-contingency flow violations. It should be noted here that the *N*-1 analysis included lines that have a voltage base of 138 kV and above. Moreover, post-contingency thermal ratings (Rate-C) were used to conduct the post-contingency analysis.

In order to assess the reactive power sufficiency and availability, *Q/V* analysis was conducted. *Q/V* analysis provides an informative tool to compare reactive power availability between relaxed and non-relaxed cases and can also be used as a tool to estimate the reactive power injection needed in order to obtain a local desired voltage level.

Therefore *Q/V* curves can be used for both voltage stability indication purposes, and shunt compensation sizing. A 13.8 kV bus that is directly connected to the 138 kV level through a transformer was chosen to conduct this analysis. This bus was chosen because it suffered from a significantly depressed voltage magnitude (around 0.82 p.u.). The PSS/E *Q/V* analysis tool places a fictitious synchronous condenser with unlimited reactive power capability at the test bus, and the voltage magnitude is varied from 0.9 p.u. to 1.1 p.u. in 0.02 p.u. steps. This process was applied to the base-case as well as to the *N*-1 post-contingency operating conditions. The same analysis was conducted for cases with no relaxations. Figure 4.9 and Figure 4.10 show the base-case *Q/V* curves for relaxed and non-relaxed cases, respectively.

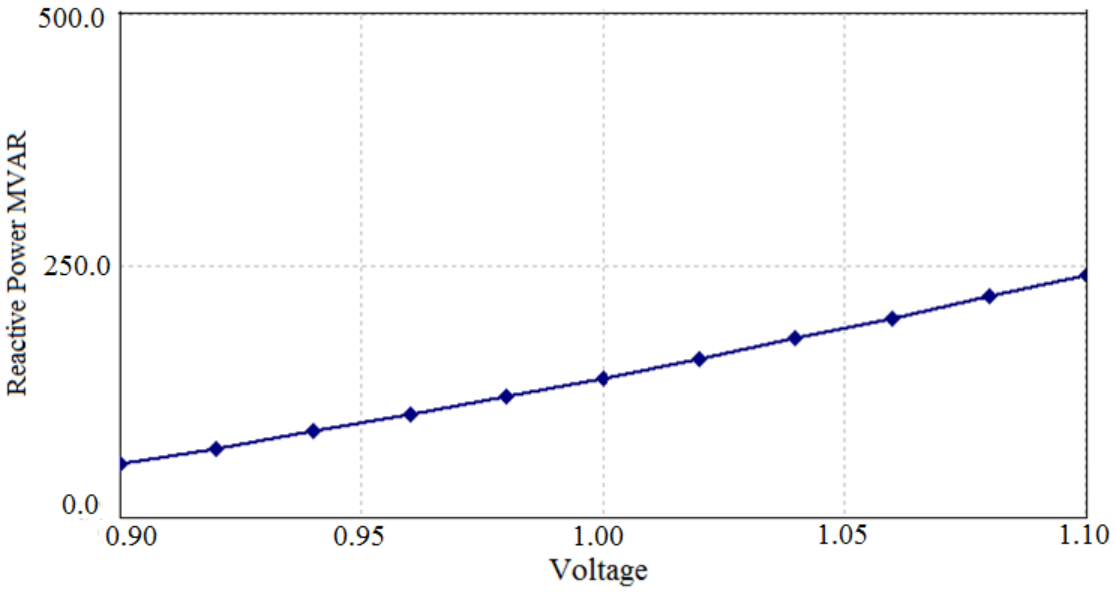

Figure 4.9. Base-Case Q/V Curve (Relaxed).

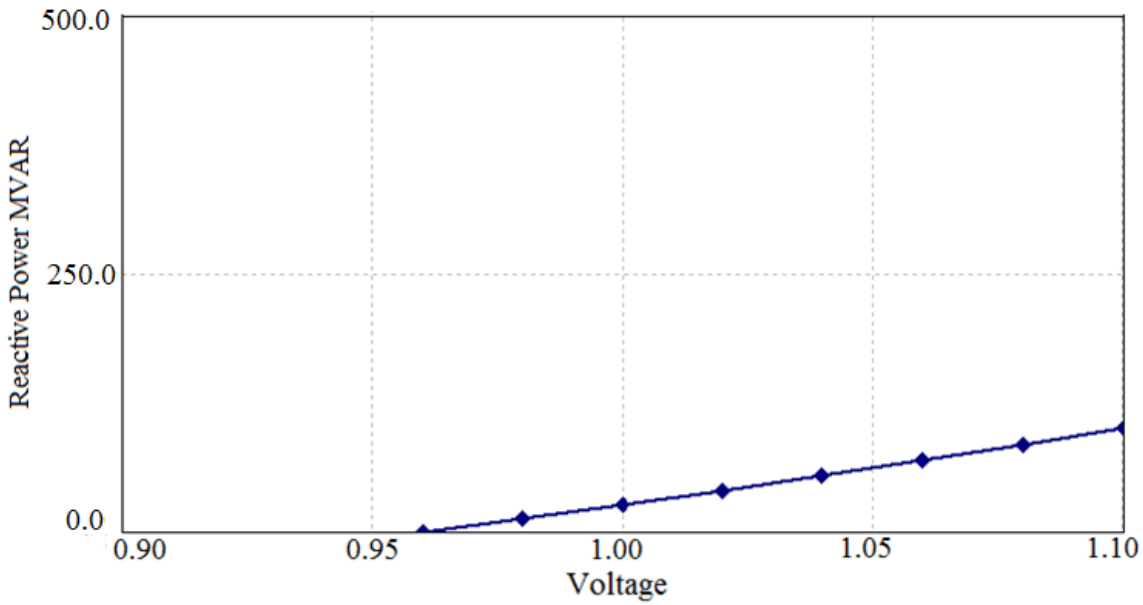

Figure 4.10. Base-Case Q/V Curve (No Relaxation).

As can be seen from Figure 4.9 and Figure 4.10, more reactive power was needed in the relaxed case to obtain the various voltage magnitudes at the test bus. Figure 4.9 shows that around 138 MVAR were needed to obtain a 1.0 p.u. voltage in the relaxed case while in Figure 4.10, only 26 MVAR were needed to obtain the same voltage level in the case with no relaxations. This result clearly implies less reactive power availability in the relaxed case compared to the case with no relaxations, which makes the relaxed case more prone to voltage stability issues. Figure 4.11 and Figure 4.12 extend the *Q/V* analysis to post-contingency operating conditions in order to investigate the effect of reactive power availability on the system following a contingency.

Table 4.9 shows the number of voltage violations in the relaxed cases shown in Table 4.8. A bus voltage is considered in violation if it falls outside the tolerance range of 0.90 – 1.10 p.u. It also shows the number of committed generators for the relaxed cases and the corresponding non-relaxed cases. The number of additional generators needed to

make the non-relaxed market solution feasible and *N*-1 secure is also displayed; hence, no voltage violations are present.

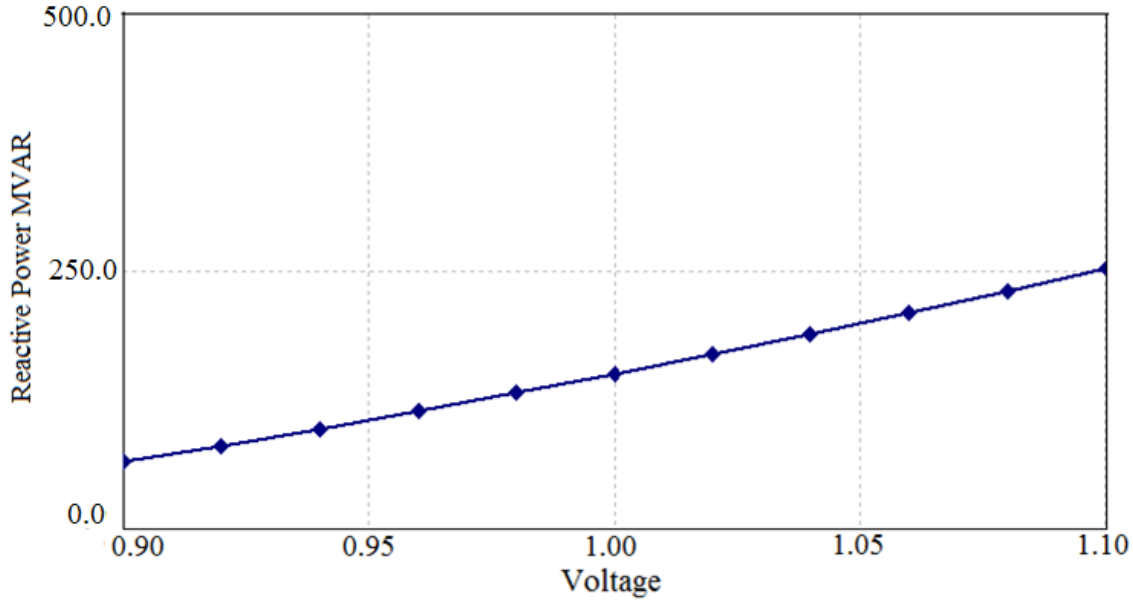

Figure 4.11. Post-Contingency Q/V Curve (Relaxed).

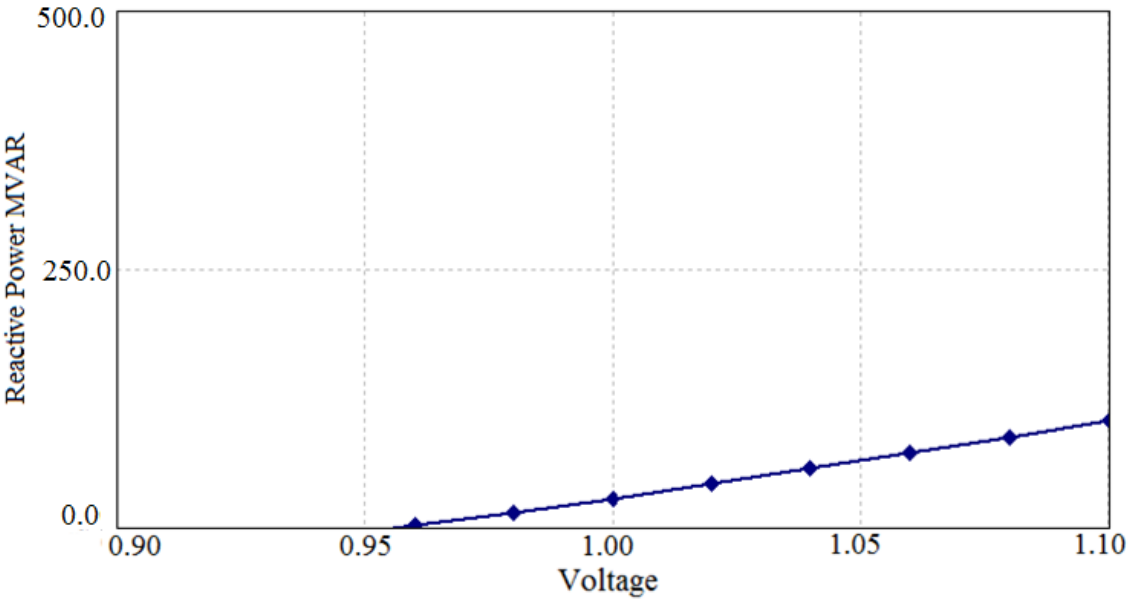

Figure 4.12. Post-Contingency Q/V Curve (No Relaxation).

4.3.5 Dynamic Analysis and Results (PJM)

The test case provided by PJM included detailed dynamic models data that were used to investigate the dynamic behavior of the PJM test case. Similar to the static analysis presented here, dynamic analysis was conducted on the relaxed cases and the corresponding cases with no relaxations in order to show the impact of relaxations on system dynamics. Rotor angle stability following a large disturbance was first checked. A full *N*-1 contingency analysis was conducted for the relaxed peak time period (on-peak hour) and the contingencies were ranked according to their severity and impact on the relaxed lines. The peak time period was chosen to conduct this type of analysis since it has more stressed operating conditions and is more likely to witness stability problems. The three most severe contingencies that appear in Table 4.10 were chosen for this analysis, as shown in Table 4.11.

Table 4.11. PJM Post-Contingency Flow Highest Violations.

Contingency ID	Relaxed line affected ID	Voltage base kV	Post-contingency flow %
710	878	230	234%
4592	10519	500	380%
5006	11255	138	140%

It should be noted here that the contingencies shown in Table 4.11 are all single line loss events. A sequence of contingent events was initiated in order to exploit those contingencies and examine the system dynamic post-contingency response. A three-phase fault was first placed at one terminal of the lines corresponding to the contingencies shown in Table 4.11. After 5 cycles the fault was cleared and the line was tripped resulting in the post-contingency flows shown in Table 4.11. After 1 second the relaxed line

with the excessive post-contingency flow was tripped. Therefore, this series of events can be considered an *N*-2 contingency. The same contingencies were also applied to the cases with no relaxations and results were compared. Figure 4.13 and Figure 4.14 show the rotor angle plots for the most affected generators for the relaxed and non-relaxed, respectively, following contingency 710 (Table 4.11). It should be noted that all considered contingencies here represent transmission line outages.

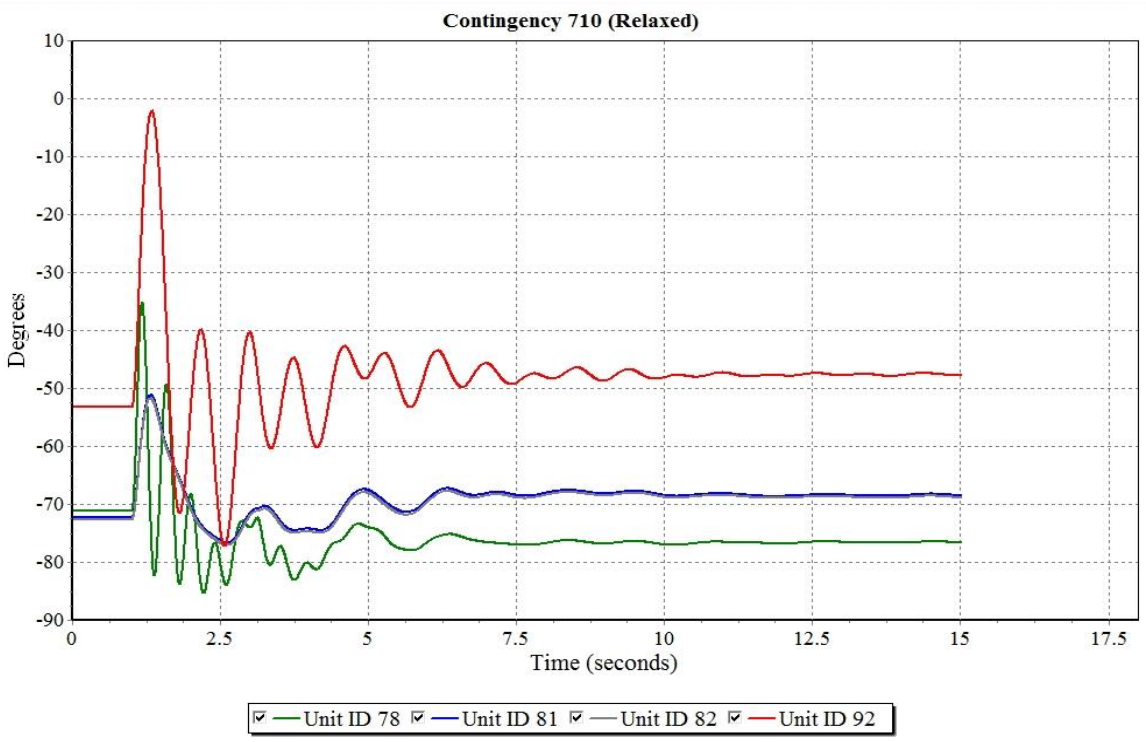

Figure 4.13. Rotor Angles Following Contingency 710 (Relaxed).

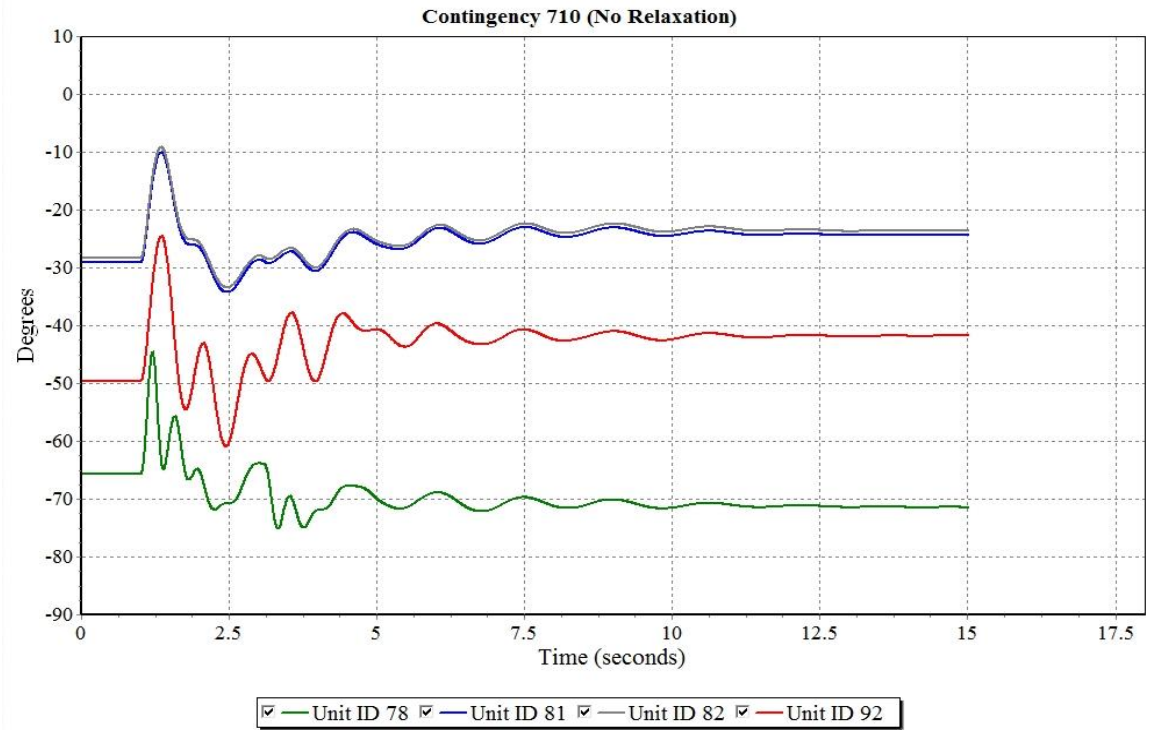

Figure 4.14. Rotor Angles Following Contingency 710 (No Relaxation).

Figure 4.13 and Figure 4.14 show that the system is stable following the sequence of contingent events for relaxed and non-relaxed cases. However, it can be seen that the oscillations for rotor angles in the relaxed case are higher compared to the non-relaxed case. Moreover, the settling time is larger for the relaxed case. This indicates that although both systems are stable, the relaxed case is closer to its stability margins and is more likely to suffer from stability related problems. Figure 4.15 – Figure 4.18 show the same analysis for contingencies 4592 and 5006.

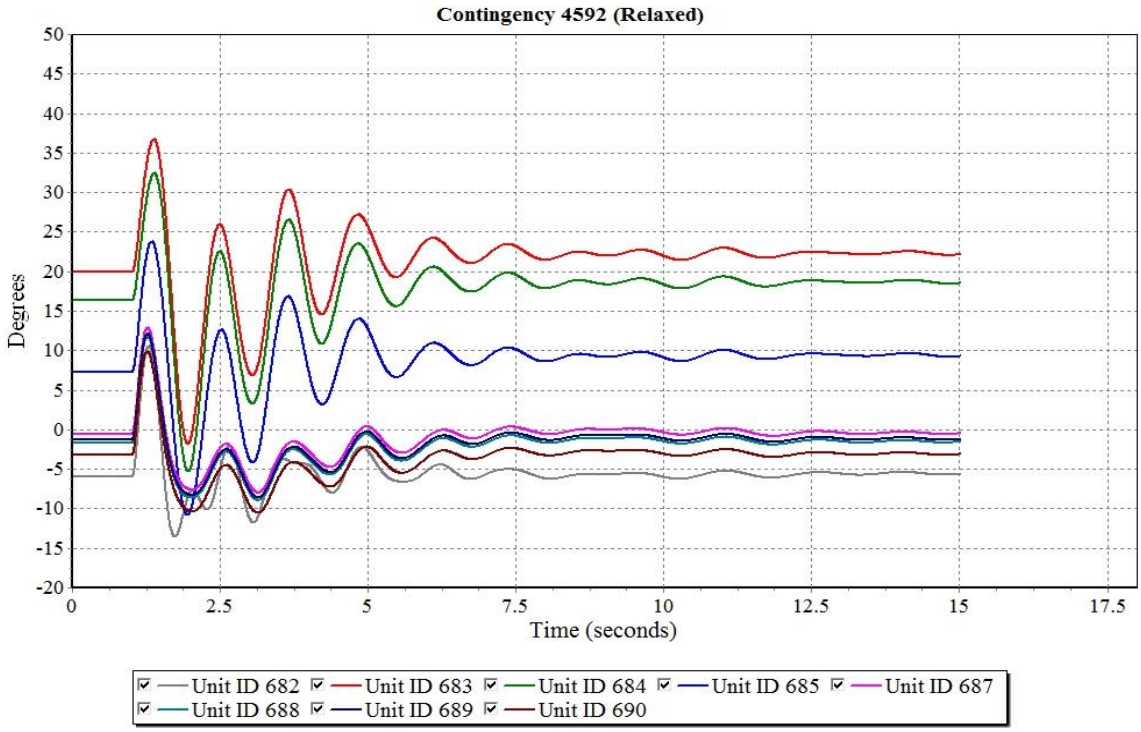

Figure 4.15. Rotor Angels Following Contingency 4592 (Relaxed).

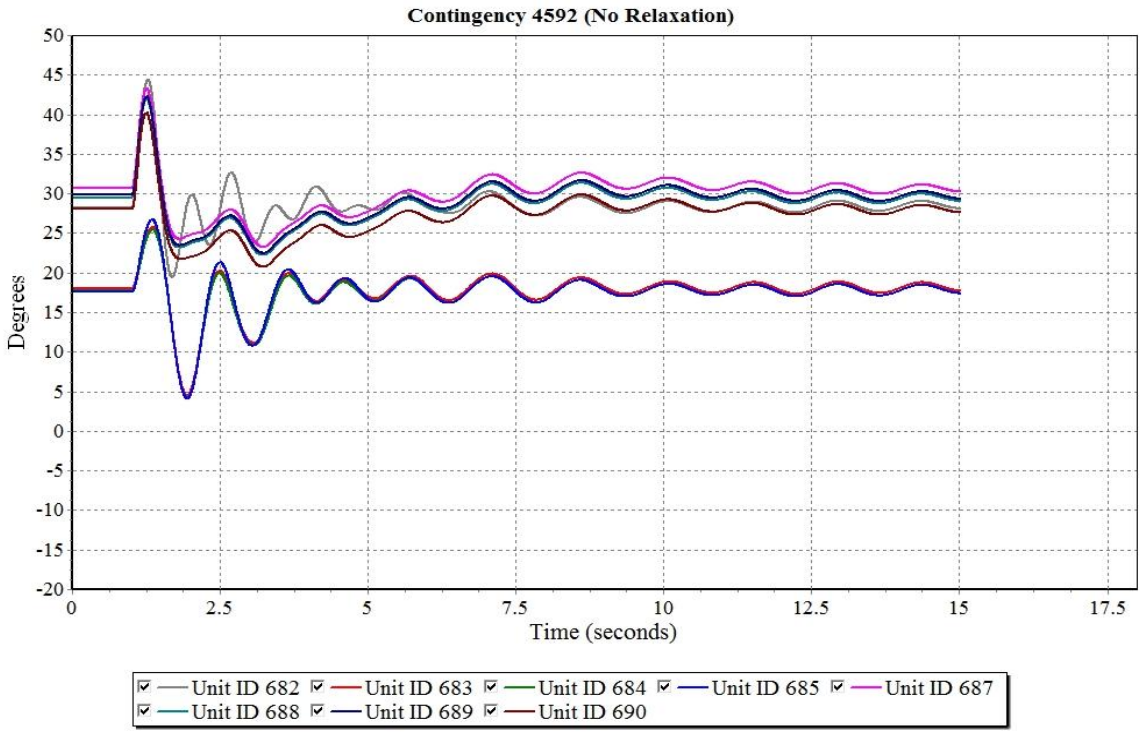

Figure 4.16. Rotor Angles Following Contingency 4592 (No Relaxation).

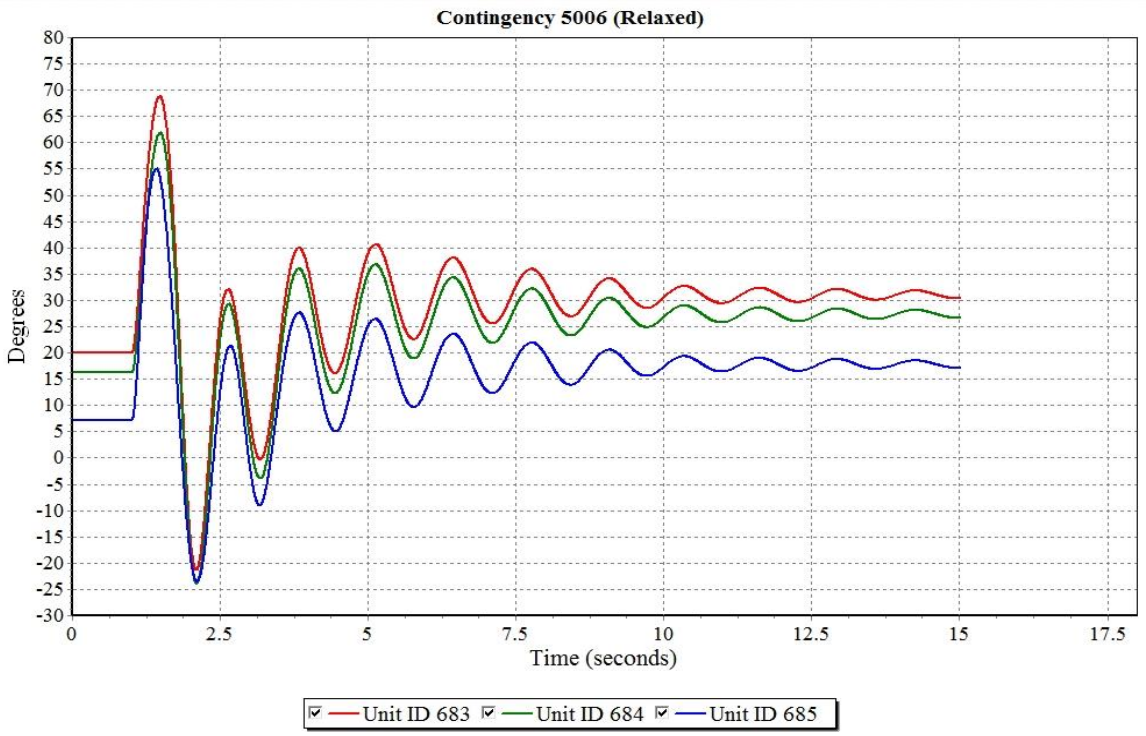

Figure 4.17. Rotor Angles Following Contingency 5006 (Relaxed).

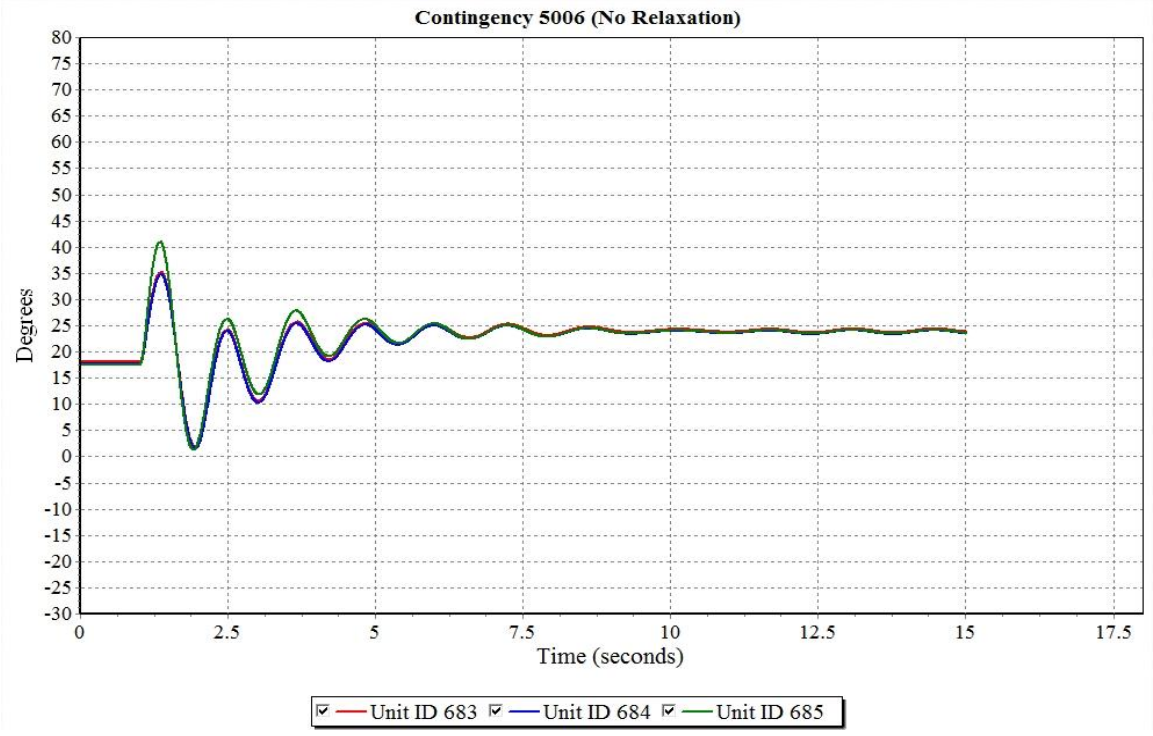

Figure 4.18. Rotor Angles Following Contingency 5006 (No Relaxation).

The same dynamic response trend observed in contingency 710 was repeated in the other two contingencies. It can be seen from Figure 4.15 – Figure 4.18 that the magnitude of the oscillations and settling time were higher for relaxed cases compared to cases with no relaxations. However, this dynamic response is not an exclusive result of constraint relaxations. The particular operating conditions of the test cases are what determine the difference in post-contingency dynamic behavior between relaxed and non-relaxed cases. Moreover, out-of-market corrections affect operating conditions and, therefore, will also affect the post-contingency dynamic behavior.

A similar analysis was conducted to assess the dynamic post-contingency voltages. A full *N*-1 contingency analysis was conducted for the same relaxed peak time period (on-peak hour) and the contingencies that caused post-contingency low voltages were ranked according to their severity. The three most severe contingencies are listed in Table 4.12.

Table 4.12. PJM Post-Contingency Lowest Voltages.

Contingency no.	Lowest voltage bus ID	Voltage p.u.	Voltage base kV
2427	546	0.82	138
5471	436	0.83	138
1941	1166	0.87	138

For each contingency listed in Table 4.12, time-domain dynamic analysis was conducted to investigate the dynamic post-contingency voltage profiles. A three-phase fault was placed at one terminal of the lines corresponding to the contingencies shown in Table 4.12. After 5 cycles, the fault was cleared and the line was tripped, resulting in the post-contingency low voltage violations shown. The analysis was conducted for the case with no relaxations as well in order to point out the differences between the two scenari-

os. Figure 4.19 and Figure 4.20 show the voltage plots of the most affected buses corresponding to contingency 2427 for the relaxed and non-relaxed cases, respectively.

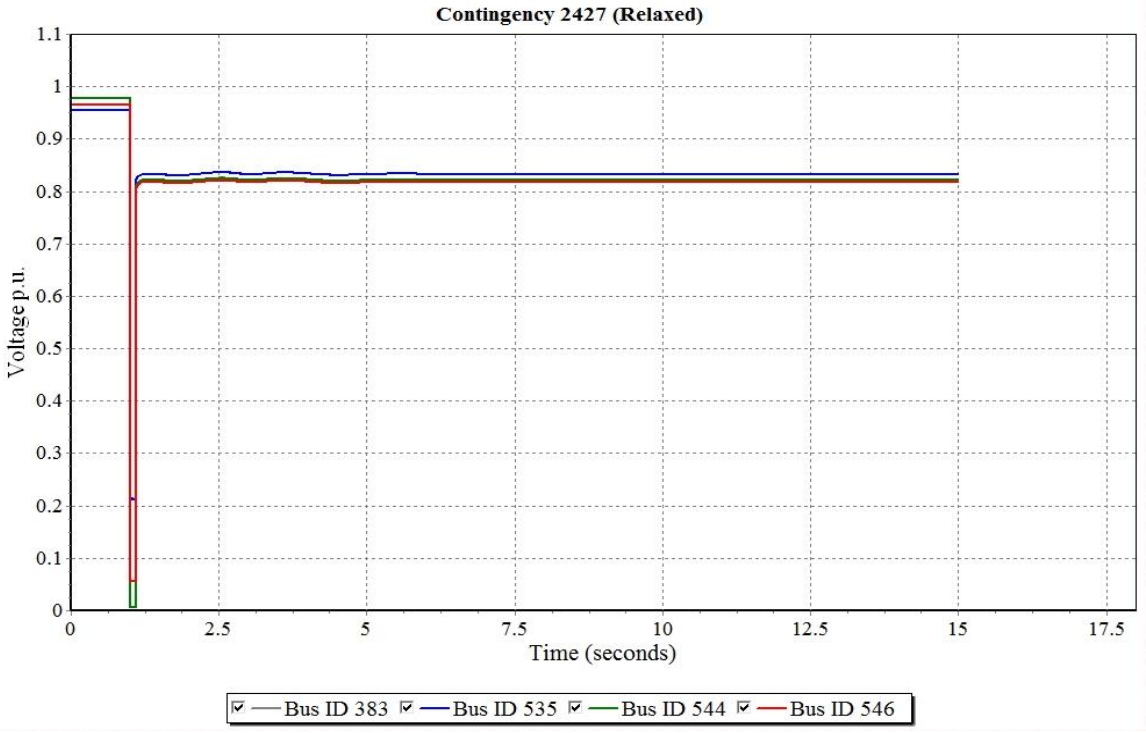

Figure 4.19. Voltage Profiles Following Contingency 2427 (Relaxed).

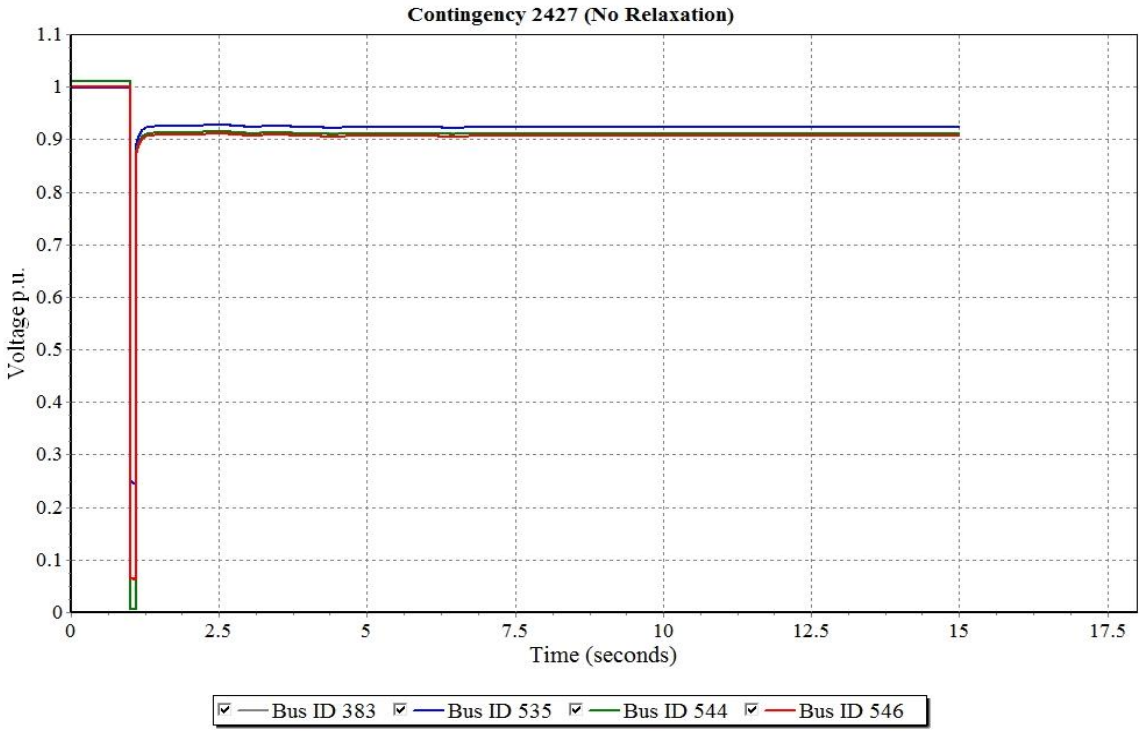

Figure 4.20. Voltage Profiles Following Contingency 2427 (No Relaxation).

Figure 4.19 indicates post-contingency voltage violation, as the voltage is 0.82 p.u. as shown in Table 4.12 as well. On the other hand, Figure 4.20 shows that the voltage for the same bus following the same contingency in the non-relaxed case is approximately 0.9 p.u. This result is expected since the non-relaxed case is *N*-1 secure. The same analysis was conducted for the other two contingencies listed in Table 4.12. Figure 4.21 - Figure 4.24 show the corresponding voltage plots for relaxed and non-relaxed cases.

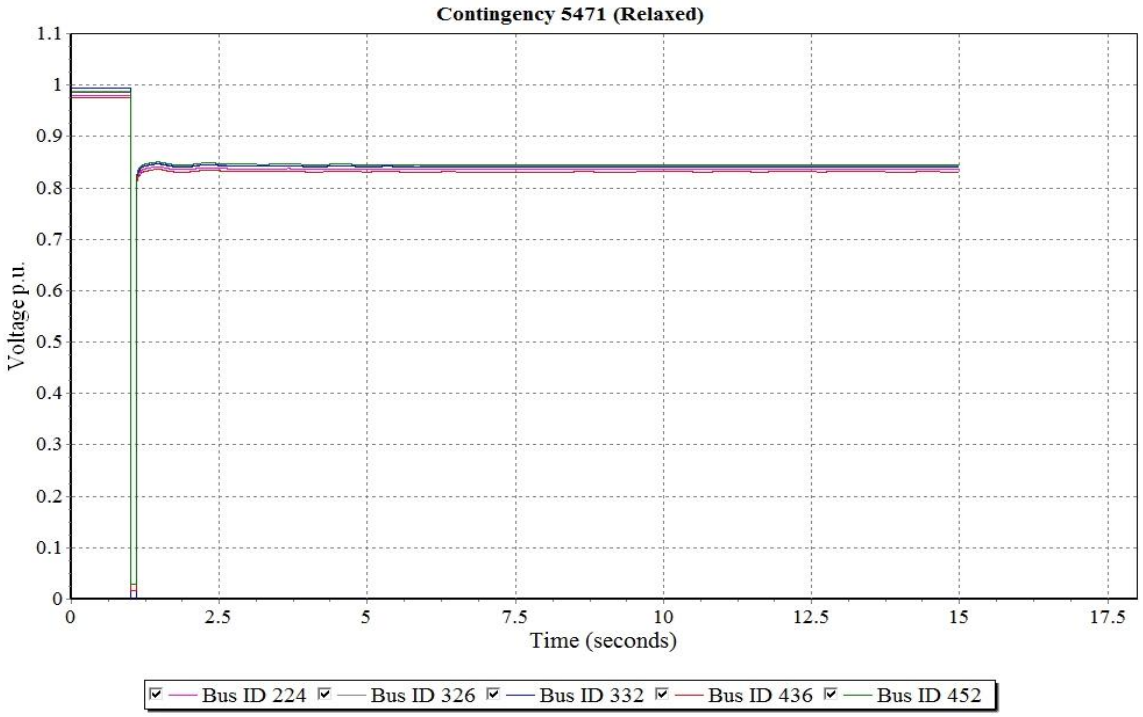

Figure 4.21. Voltage Profiles Following Contingency 5471 (Relaxed).

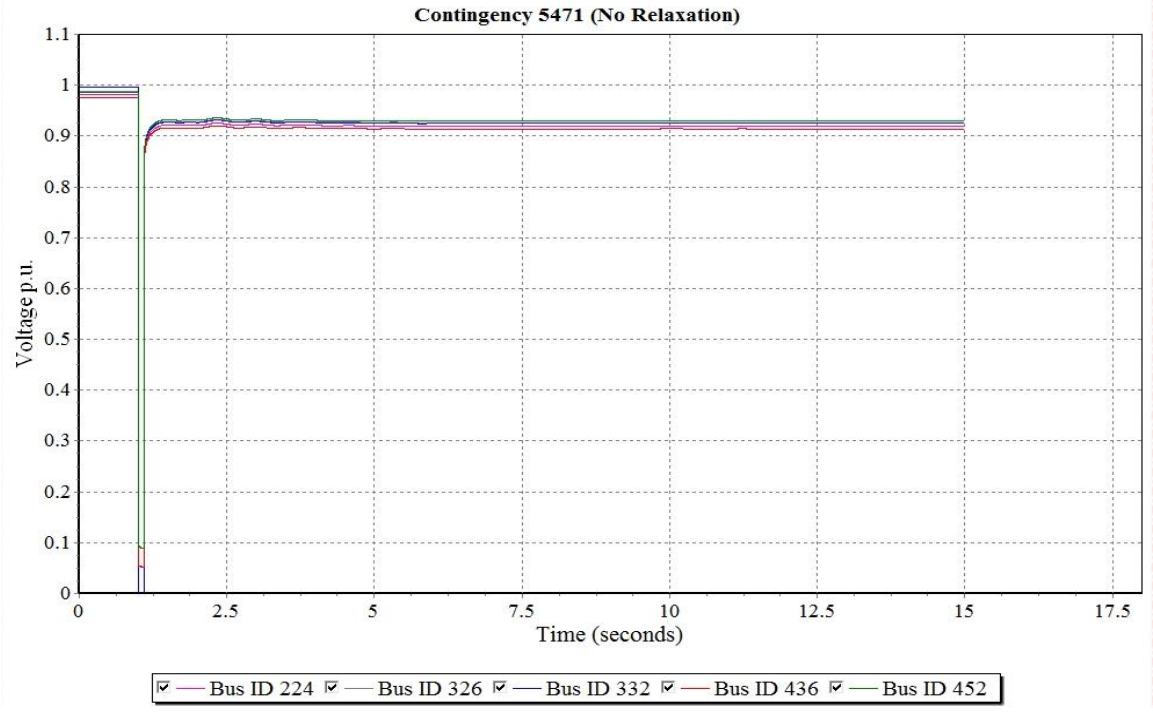

Figure 4.22. Voltage Profiles Following Contingency 5471 (No Relaxation).

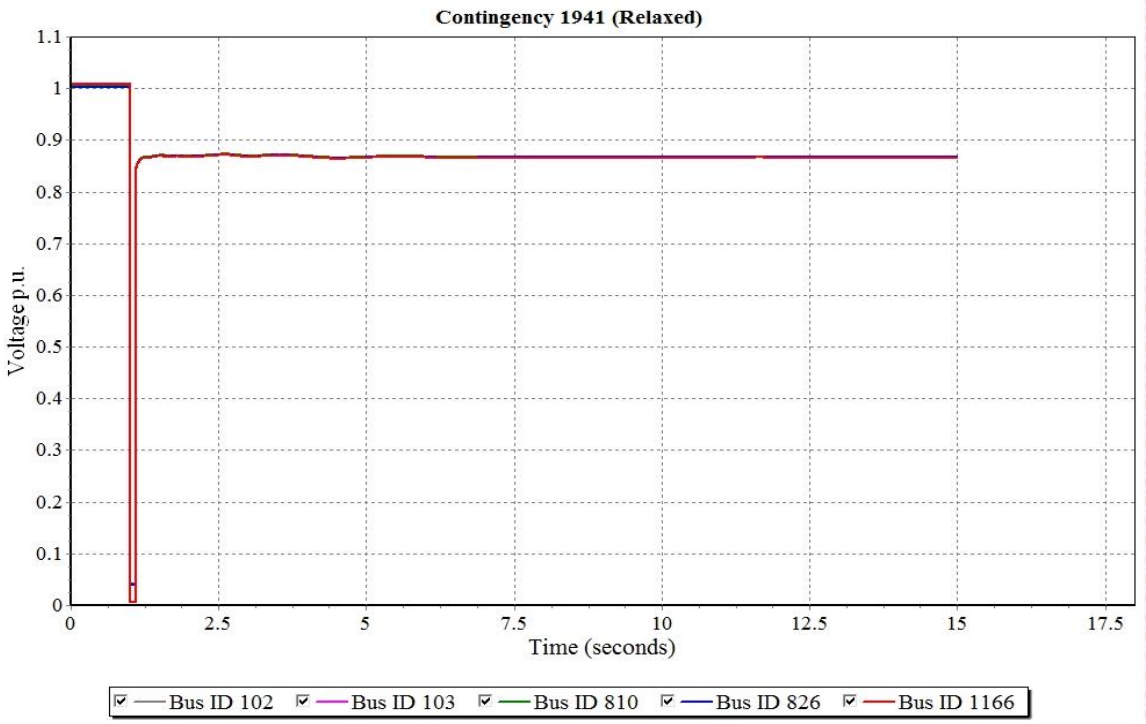

Figure 4.23. Voltage Profiles Following Contingency 1941 (Relaxed).

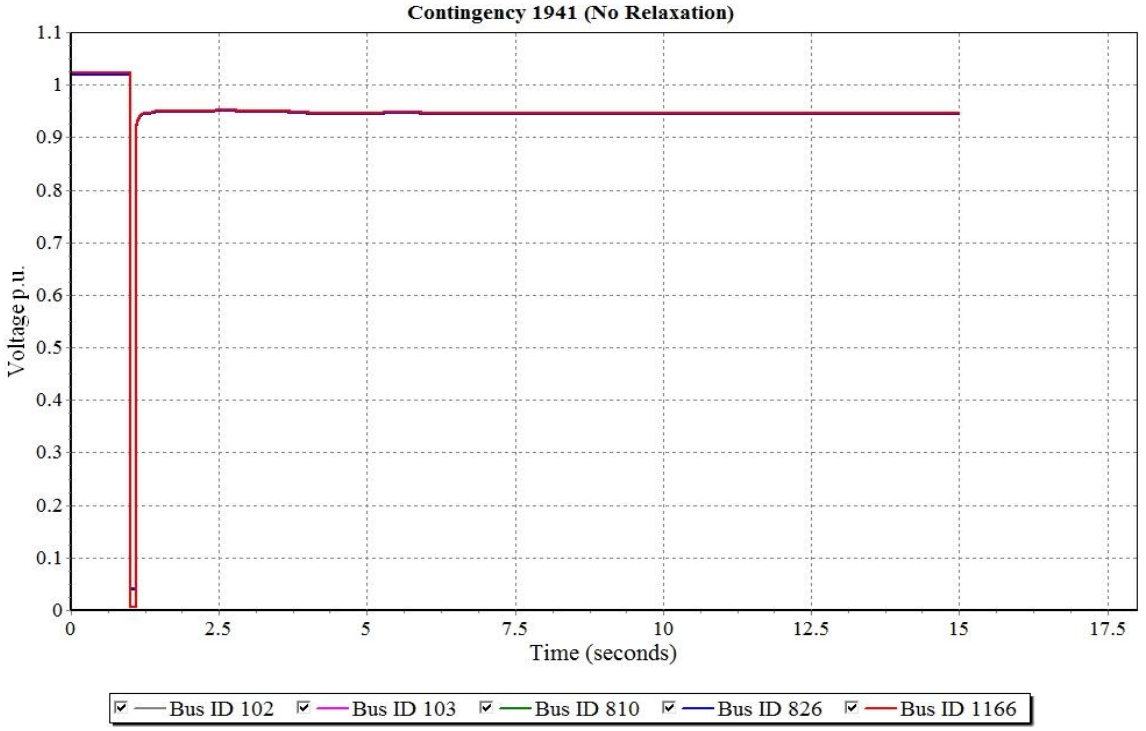

Figure 4.24. Voltage Profiles Following Contingency 1941 (No Relaxation).

Figure 4.21 - Figure 4.24 show that in the relaxed cases the voltage sustained depressed values (less than 0.9 p.u.) following certain severe contingencies. On the other hand, there were no post-contingency steady state voltage violations in the non-relaxed cases as the final voltage value was higher than 0.9 p.u. for all tested contingencies. The provided PJM dynamic models data does not include dynamic load models; thus, the voltage recovers instantaneously following the fault clearance. The depressed voltage magnitudes in the relaxed cases compared to the cases with no relaxations imply reactive power deficiency in those cases. The dynamic voltage analysis conducted here confirms the *Q/V* analysis results shown in the static analysis part. Reactive power deficiency in the relaxed case can be directly related to the relatively smaller number of committed generators compared to non-relaxed cases. Moreover, the non-relaxed cases were subject to intensive out-of-market corrections that resulted in increasing the number of committed generators.

4.3.6 PJM Voltage Stability - Dynamic Load Models

In order to achieve more accurate and realistic voltage stability analysis results, the loads in the PJM system were dynamically modeled. Figure 4.19 - Figure 4.24 show instantaneous voltage recovery as well as final voltage magnitudes that are identical to static results shown in Table 4.12, which is expected since static load models were used. Constant current and constant impedance models were used to represent the load active and reactive power parts, respectively. Dynamic models were used in this work to conduct further voltage stability analysis in order to investigate the impacts of reactive power deficiency caused by constraint relaxations on a real system that includes realistic dynam-

ic loads such as the PJM system. Moreover, as discussed in Section 2.8, motor loads have significant impact on voltage stability, especially under low voltage conditions.

A recent dynamic load modeling document released by PJM Planning Committee [76], was used to provide guidance on PJM dynamic load models requirements and the commercial models under consideration. According to [76], the main objective of dynamic load modeling efforts is to capture the dynamic behavior of complex and induction motor loads during peak load hours. PSS/E complex load model (CLODxx) [41], is identified as a robust, commonly used, and adequate model to be used in the PJM system, while more detailed models can be added if necessary [76]. CLODxx model as shown in Figure 4.25 [41], is capable of modeling different motor sizes, discharge lighting, static loads (ZIP), as well as electrical distance parameters (feeder and transformer).

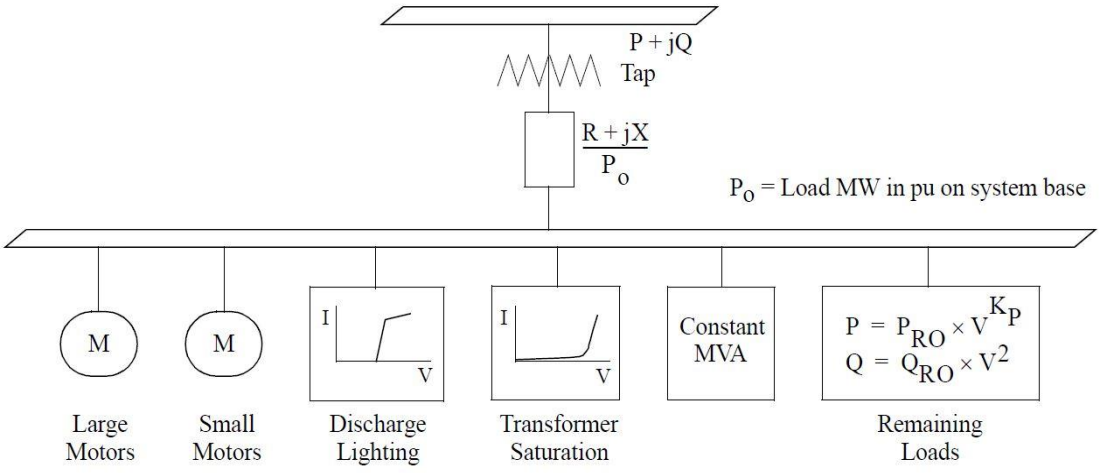

Figure 4.25. PSS/E Complex Load Model (CLODxx) [41].

The parameters of any dynamic load model, depend on the classes and composition of the load under consideration. Therefore, it is not uncommon for utilities and operators to use different parameters for different areas within their own system. Load data

from various operators indicate that motor loads can comprise around 50% the total load during peak load hours [77]-[79]. A mix of residential and commercial load classes was assumed in this work, as the load pockets are relatively small and distributed in the areas used for voltage stability analysis. Several time domain simulation were conducted to test different motor load penetration levels. However, it was noticed that in relaxed cases which have reactive power deficiency, loads with high motor penetration levels (50%) resulted in voltage collapse. Therefore, small motors and large motors were modeled as 30% and 10% of total load, respectively.

Same PJM voltage stability analysis, which was conducted previously, was repeated after dynamic load models were included. For each contingency listed in Table 4.12, time-domain dynamic analysis was conducted to investigate the dynamic post-contingency voltage profiles. A three-phase fault was placed at one terminal of the lines corresponding to the contingencies shown in Table 4.12. After 5 cycles, the fault was cleared and the line was tripped, resulting in the post-contingency low voltage violations shown. The analysis was conducted for the case with no relaxations as well in order to point out the differences between the two scenarios. Figure 4.26 and Figure 4.27 show the voltage plots of the most affected buses corresponding to contingency 2427 for the relaxed and non-relaxed cases, respectively.

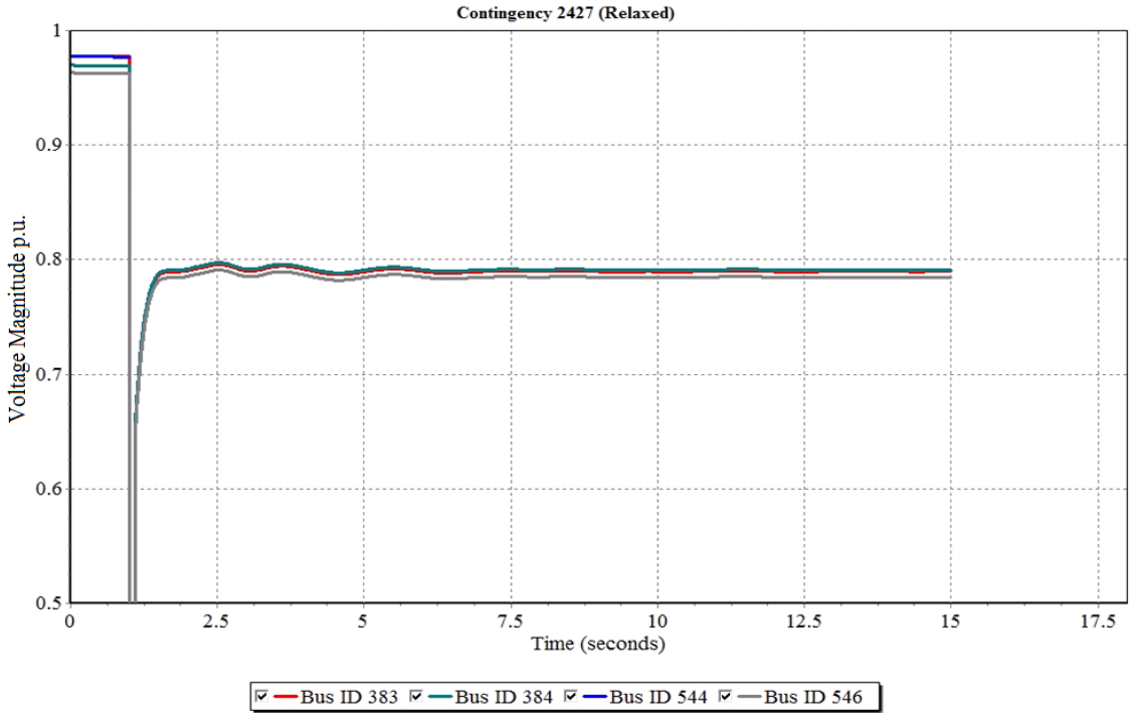

Figure 4.26. Voltage Profiles Following Contingency 2427 (Relaxed).

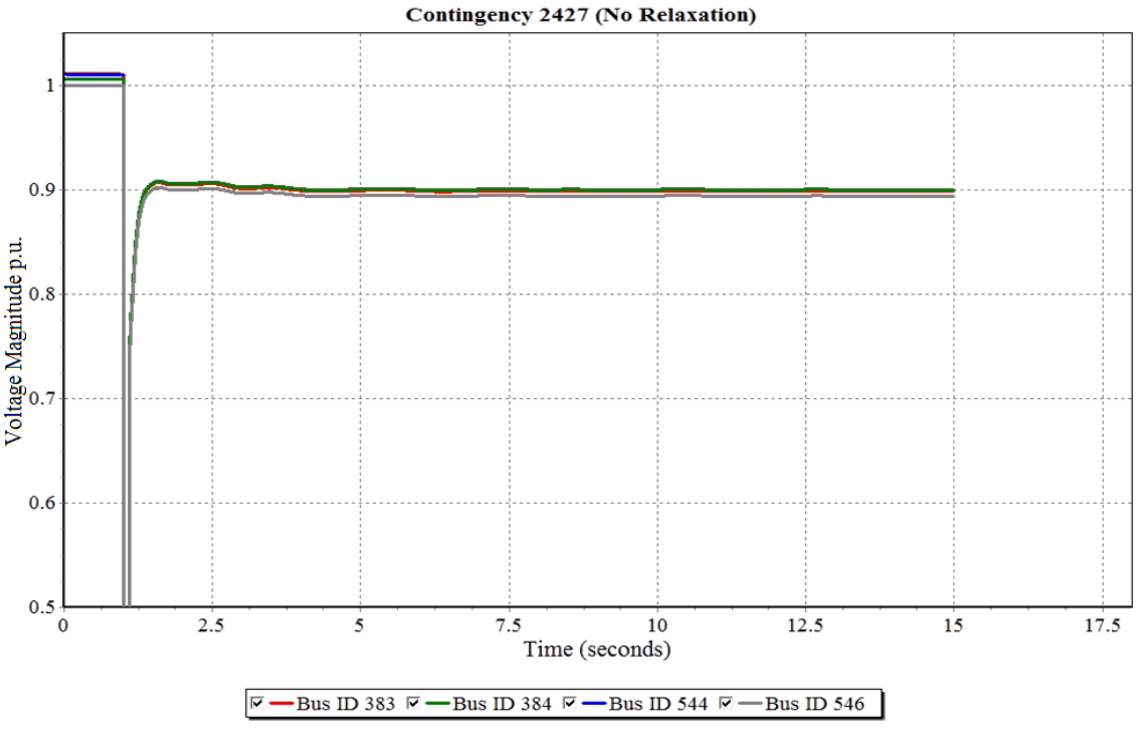

Figure 4.27. Voltage Profiles Following Contingency 2427 (No Relaxation).

As can be seen in Figure 4.26 - Figure 4.27, voltage recovery in relaxed and non-relaxed scenarios was slightly delayed compared to the instantaneous voltage recovery shown previously. Moreover, it can be noticed that the final value of the voltage magnitude is lower as well especially, for the relaxed case. Although the static analysis showed a steady state voltage magnitude of 0.82 p.u. (shown in Table 4.12), the actual voltage magnitude is 0.78 p.u. when dynamic models are used, as shown in Figure 4.26. The delayed voltage recovery and depressed voltage magnitudes can be explained mainly as a result of motors stalling and increased reactive power consumption, which worsened the inherent reactive power deficiency conditions in the relaxed cases. The same analysis was conducted for the other two contingencies listed in Table 4.12. Figure 4.28 - Figure 4.31 show the corresponding voltage plots for relaxed and non-relaxed cases.

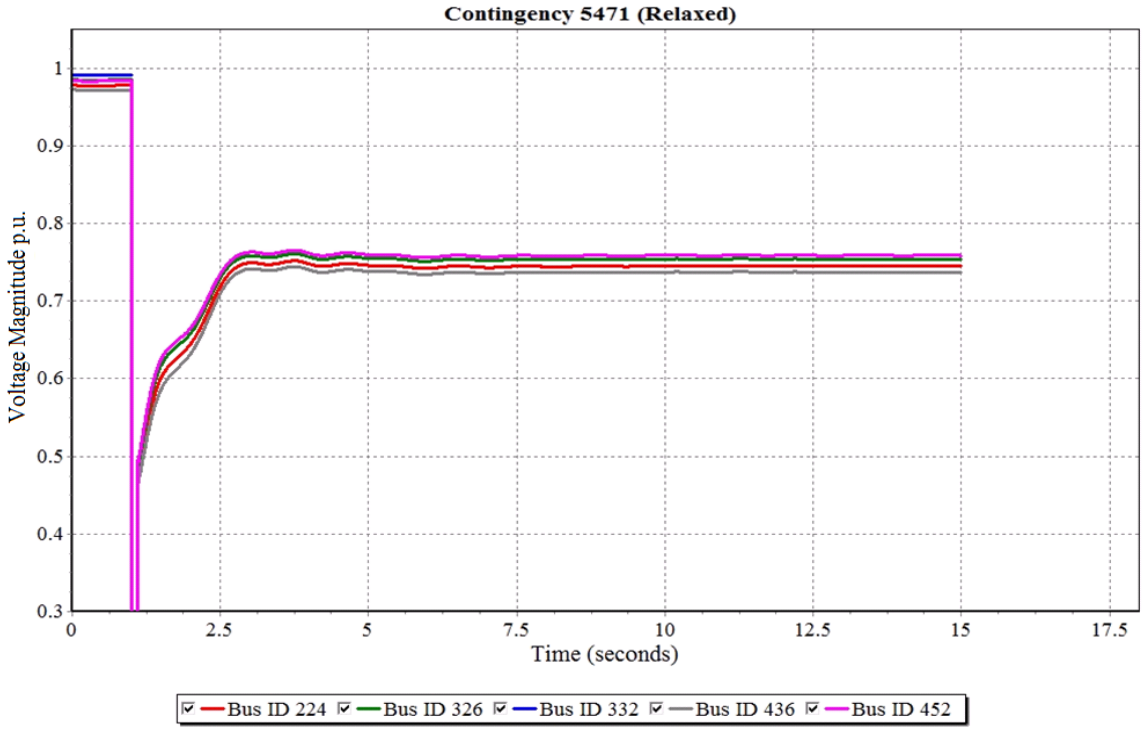

Figure 4.28. Voltage Profiles Following Contingency 5471 (Relaxed).

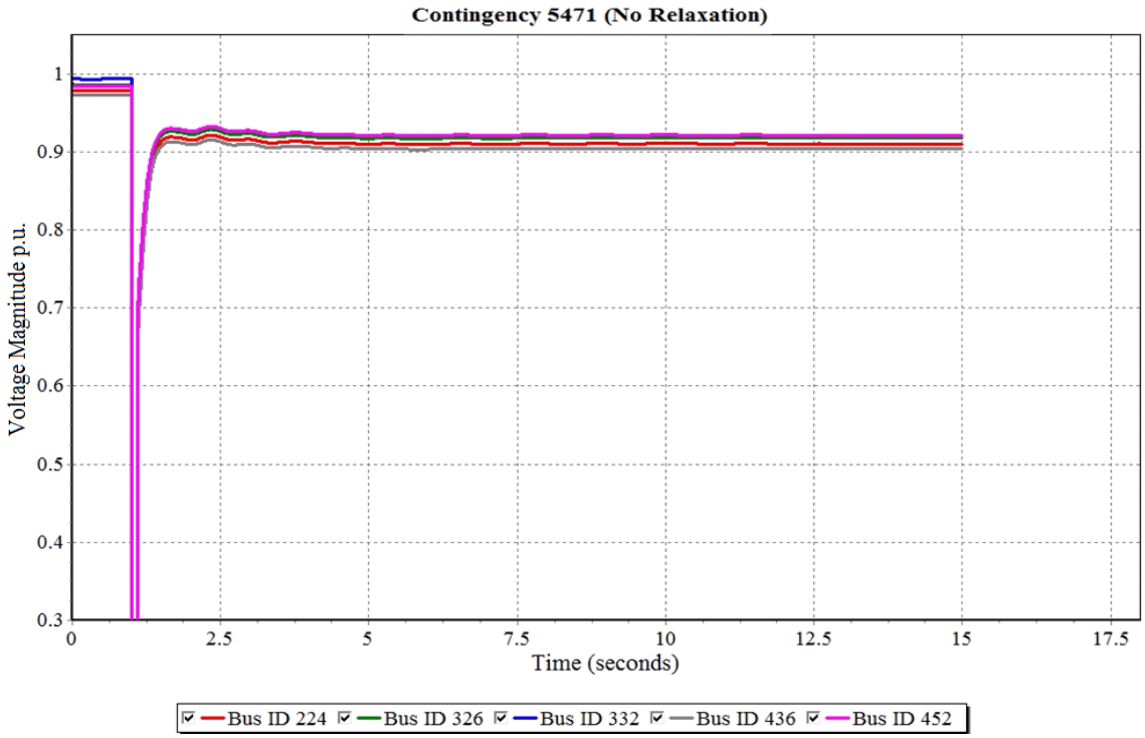

Figure 4.29. Voltage Profiles Following Contingency 5471 (No Relaxation).

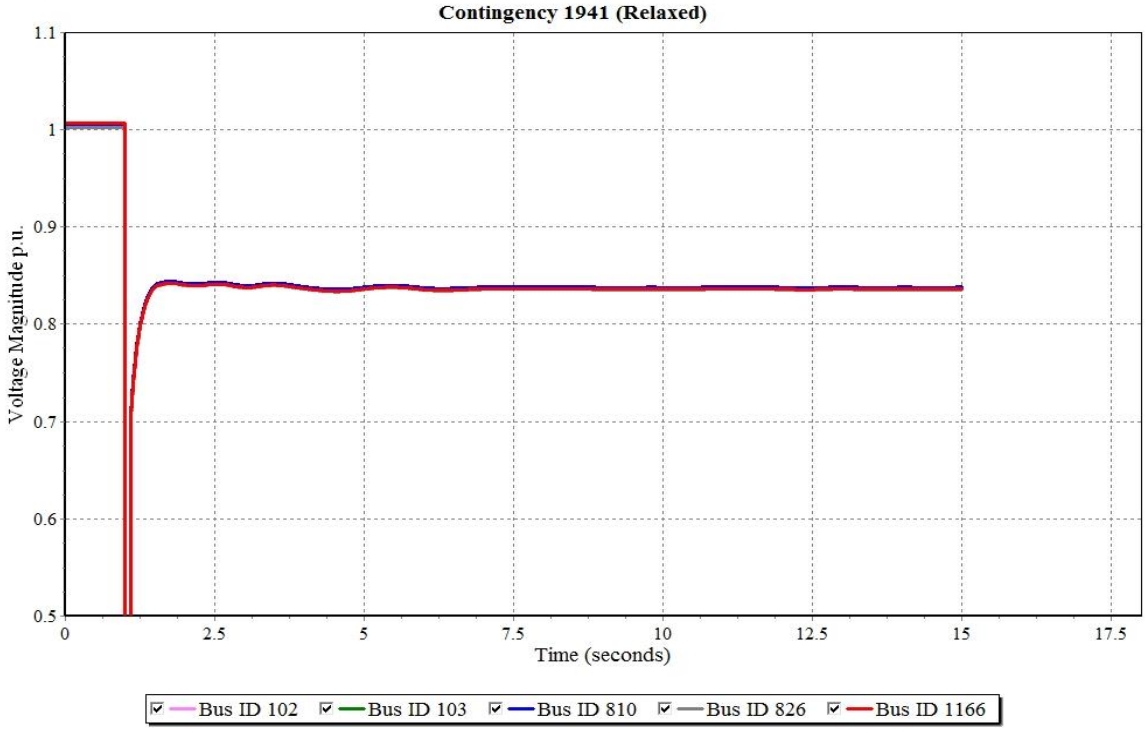

Figure 4.30. Voltage Profiles Following Contingency 1941 (Relaxed).

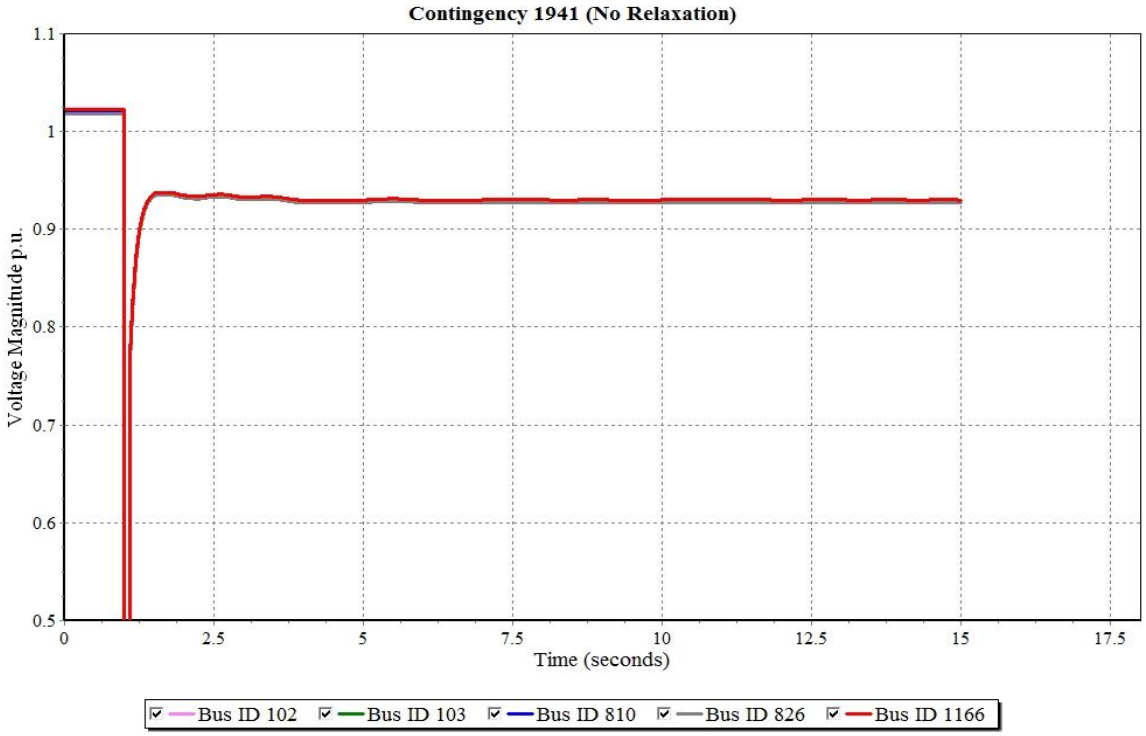

Figure 4.31. Voltage Profiles Following Contingency 1941 (No Relaxation).

Figure 4.28 - Figure 4.31 show that capturing the load dynamics had a significant impact on voltage profiles following a major contingency. Even scenarios with no relaxations suffered a slight voltage recovery delay as well. However, voltage stability issues were more apparent and severe in relaxed cases. For instance, Figure 4.28 shows a prolonged voltage recovery and a final voltage magnitude of 0.75 p.u. although the static load model analysis indicated instantaneous voltage recovery and a final voltage magnitude of 0.83 p.u., as a result of capturing load dynamic behavior. These results also confirm the high nonlinearity of dynamic loads, which was exhibited through the substantial reactive power consumption caused by depressed voltage levels, which led into even lower voltage magnitudes. The voltage stability analysis results shown here emphasize the importance of capturing load dynamic behavior by utilizing the appropriate load models. Capturing load dynamic behavior becomes even more crucial when constraint

relaxations are allowed, as the reactive power deficiency associated with constraint relaxations can cause motor loads to decelerate and stall as a result of depressed voltage profiles.

4.4 Risk Based Penalty Price Constraint Relaxations

Throughout this work, constraint relaxations impacts on system performance were investigated using a single penalty price to allow relaxations in the DC SCUC model, which replicates operators practices related to constraint relaxations. For instance, the PJM original penalty price of 1000 $/MWh for line thermal limits was used. Therefore, all lines were subject to the same penalty price in the day-ahead market model, regardless of the severity of contingencies associated with each line. The static and dynamic security assessment conducted in this work revealed the adverse impacts of potential constraint relaxations on system performance are attributed to two major factors, number of committed generators and the overloading of major transmission lines. Naturally, heavily loaded transmission lines are expected to have higher impact on the system operational security when they are tripped as a result of a contingent event, which is usually initiated by a fault. Tripping a heavily loaded transmission line results in its original power flow being distributed on other routes, which can overload (and even trip) other lines in a cascading sequence. Moreover, high voltage, high capacity transmission corridors consist of long transmission lines. As a result, they have higher probability of being exposed to contingent events, compared to short lines. Therefore, long transmission lines that are heavily loaded should be distinguished in the constraint relaxation process in a manner that

prevents or limits relaxing those lines, as they impose high risk to system security when they are overloaded.

4.4.1 High Risk Lines Identification

In order to categorize the transmission lines according to their associated risk on system security, a risk index was defined as:

$$R_{kj} = F_k \times OL_j^{norm} \qquad \forall k, j \text{ (4.1)}$$

$$OL_j^{norm} = \frac{OL_j^{post}}{OL_{MAX}^{post}} \qquad \forall j \text{ (4.2)}$$

where, R_{kj} is the risk index associated with line k outage and line j overload, F_k is the frequency of an unplanned outage on line k. F_k is expressed as the number of expected outage events in a given time period. OL_j^{norm} is the normalized post-contingency overload on line j, and OL_j^{post} and OL_{MAX}^{post} are the post-contingency overload on line j and the absolute maximum post-contingency overload for all contingencies, respectively, in MVA. Therefore, the risk index calculated by (4.1) incorporates both, the frequency (likelihood) of the occurrence of the contingency and, the impact of that contingency on system security. The maximum normalized post-contingency line overload was used in (4.1) as an indication of the impact or severity of a certain contingency, as high post-contingency overloads are expected to result in additional unplanned line outages in a cascading sequence.

The post-contingency operating conditions risk indices for the PJM peak hour were calculated in order to identify the events with high risk indices. A full *N*-1 contingency analysis was conducted on the relaxed PJM peak hour to identify the contingencies

that result in post-contingency line overloads (exceed emergency line thermal ratings). The next step in the process of evaluating risk indices was to determine the outage frequency of each line under consideration. The Canadian Electricity Association (CEA) 2012 Annual Report [80] was used to provide statistical and probabilistic information on transmission equipment forced outages. The CEA report used is based on five years (2008 – 2012) of historical data provided by Canadian utilities and operators. The CEA report was chosen for this work because of its comprehensive content and availability. However, other resources that provide similar data for transmission forced outages can be used. In addition, the lengths of transmission lines under consideration had to be estimated since the statistics and data provided by the CEA report are normalized for 100 km of length.

In order to estimate lines length, information such as lines impedance and conductor types and configurations used in the PJM system were utilized [81]. Table 4.13 shows a sample of contingencies and overloaded lines with the highest risk indices. Table 4.13 shows that line length plays a key role in determining the risk index associated with that line since it increases the likelihood of outage occurrence. Moreover, the magnitude of the post-contingency overload also has a direct effect on the risk index as it represents the impact of an outage event. Table 4.13 also shows that the outage of the relaxed line (ID 11001) results in two overloads with high risk indices. As can be seen in Table 4.8, this particular line was relaxed in the market solution and had an AC base-case overload of 106% of its normal thermal rating. Therefore, it was desired to attain a relaxed market solution that avoids (or limits) the relaxation of lines that are associated with high risk index outages.

Table 4.13. PJM High Risk Index Outage Events.

Overloaded line					Contingency					Risk index
Line ID	Voltage base kV	Emergency rating MVA	Maximum flow MVA	Normalized impact	Line ID	Voltage base kV	Line length mi	Base flow MVA	Outage freq. /year	
8253	345	897	912	0.524	8221	765	260	1905	1.15	0.603
11642	345	1718	1740	1.000	8542	765	86	1756	0.51	0.510
6949	345	1552	1626	0.934	6939	345	54	350	0.43	0.402
11474	138	142	254	0.146	11001*	138	171	136	2.64	0.385
11862	138	161	253	0.145	11001*	138	171	136	2.64	0.383
9966	230	626	791	0.455	9826	500	55	1087	0.41	0.187

* Relaxed line

4.4.2 Risk Based SCUC Solution

In order to incorporate the risk index information discussed in the previous subsection, three different penalty prices were defined in the DC SCUC algorithm instead of one. The penalty prices were defined in a manner that discourages the market model from relaxing lines that have high outage frequency, and the lines that have high outage impact. The penalty prices were defined as:

- High risk lines: this category includes transmission lines with thermal ratings greater than 999 MVA and, transmission lines which lengths are greater than 49 miles. A penalty price of 1500 $/MWh for relaxing line thermal limits was assigned for this category. This category includes 18% of the total number of lines.
- Medium risk lines: this category includes transmission lines with thermal ratings greater than 749 MVA and less than 1000 MVA and, transmission lines which lengths are greater than 9 miles and less than 50 miles. A penalty price of 1000 $/MWh for relaxing line thermal limits (original penalty price) was assigned for this category. This category includes 35% of the total number of lines.
- Low risk lines: all other lines are included in this category (thermal ratings less than 750 MVA and, lengths less than 10 miles). A penalty price of 500 $/MWh for relaxing line thermal limits was assigned for this category. This category includes 47% of the total number of lines.

It should be noted that the filters used to create these risk groups are not unique, however, the risk indices analysis presented in the previous subsection provided valuable information on the criteria of lines that are associated with high risk indices outages. For in-

stance, the long lines with high outage frequency and the heavily loaded lines with high outage impact shown in Table 4.13 fell into the high risk lines group. Moreover, additional risk groups with various penalty prices could be created depending on the system under consideration. Table 4.14 presents relaxations for the SCUC solution with risk based penalty prices. Table 4.14 also lists the relaxations results for the SCUC solution with single penalty price for comparison purposes.

Table 4.13. Risk Based Penalty Price Relaxations.

Risk based penalty price				
Relaxed line ID	Relaxation MW	Line rating MVA	Length mi	Risk group
190	2	553	4.3	Low
1703	51	670	2.7	Low
6470	8	115	45	Medium
6590	7	155	4	Low
7422	8	200	2	Low
7928	5	192	37	Medium
Single penalty price				
190	6	553	4.3	-
1703	4	670	2.7	-
6470	8	115	45	-
7557	85	1009	18	-
11001	2	128	171	-
11255	14	158	27	-

Table 14.14 shows that none of the high risk group lines was relaxed. Out of a total of six relaxed lines, only two lines are considered as medium risk lines, while the rest are in the low risk lines group. On the other hand, when a single penalty price was used, two high risk lines were relaxed (line IDs: 7557 and 11001). Moreover, although around half of the lines in the system were considered as low risk lines and were assigned low penalty price, the total relaxations magnitude was reduced when risk based penalty prices were used. The total magnitude of relaxations, for all relaxed lines, when risk

based penalty prices were used is 81 MW, compared to a total of 119 MW of line relaxations when a single penalty price was used. This result denotes that heavily loaded and long transmission lines are more likely to be relaxed because of their ability to have a noticeable impact on the SCUC solution and operating conditions. As a result, more generating units were committed in the risk based constraint relaxation SCUC solution as an alternative to relax high risk lines, as will be shown in the next subsection.

4.4.3 Risk Based Constraint Relaxations AC Analysis

In order to investigate the impacts of using risk based penalty prices on system performance, the market SCUC solution was used to solve an AC power flow. The same process explained in Section 4.4 was repeated to obtain an AC base-case solution. Out-of-market corrections were applied in the form of committing additional generators in order to eliminate active and reactive power mismatches caused by thermal losses and reactive power deficiency. Table 4.15 shows the number of committed generators and voltage violations for the risk based penalty price scenario, compared to the single penalty price and, non-relaxed solutions. It should be noted that the non-relaxed scenario presented in Table 4.15 is not *N*-1 secure in order to ensure comparison consistency with the other scenarios.

Table 4.14. Committed Generators and Voltage Violations (Risk Based Relaxation).

Risk based penalty price		
Committed generators (market)	Added generators	Voltage violations
1878	18	36
Single penalty price		
1837	26	52
No relaxation		
1935	12	6

Table 4.15 shows that fewer base-case voltage violations were reported in the risk based constraint relaxation solution as a result of the larger number of committed generators compared to single penalty price scenario. Fewer out-of-market generators were also required in the risk based penalty price case. Moreover, none of the high risk lines (long and high capacity lines) were relaxed when risk based penalty prices were used. Therefore, it can be concluded that using risk based penalty prices can have a positive impact on the system operational security by increasing the number of committed generators and, limit overflow violations.

4.5 Constraint Relaxations Impact on Energy Markets

The next step in the analysis was capturing the economic impact of constraint relaxations on energy markets, such as generation total cost. Therefore, it was necessary to obtain a base-case and *N*-1 secure solutions for both scenarios (relaxed and non-relaxed) for the RTS-96 and PJM system. This approach ensures that cost of out-of-market corrections performed to secure the system and remove violations introduced by constraint relaxations is captured. Fixing real-time base-case violations was performed using PSS/E ACOPF as it provides an economic and consistent transition from DC market solution to AC real-time system. On the other hand, achieving *N*-1 preventive security conditions manually is a very tedious and inconsistent process and even infeasible for large systems. For instance, securing the system against a specific contingency might worsen the violations of another contingency or introduce new violations, even in the base-case. Therefore, PSS/E PSCOPF tool was utilized in order to solve these problems more efficiently.

In order to run ACOPF, the DC SCUC solution was used as a starting point. The same objective function (total generation cost), linear constraints, and generation cost curves used in the energy market SCUC solution were used. The RTS-96 test case cost curves were provided by [75] while real bidding data provided by PJM was used to create the cost curves for PJM system. In addition to linear constraints, the voltage and reactive power limits were defined and enforced. Base-case bus voltage tolerances of ±5% and ±10% were enforced for the RTS-96 test case and PJM system respectively. A successful ACOPF run provided an AC feasible base-case with voltage magnitudes, lines MVA flows, and generators scheduled voltages within defined limits. However, ACOPF was not always capable of providing a feasible solution using the market SCUC solution, especially for PJM system. Therefore, additional units had to be committed to provide additional reactive power and alleviate line overloads as shown in Table 4.9.

After obtaining secure and optimal base-case operation conditions using ACOPF, the system had to be further secured against *N*-1 contingencies. The PSS/E built-in tool PSCOPF was used for this purpose through this work. The main advantage of using PSCOPF is its ability of considering off-line generators as one of the available controls. Therefore, PSCOPF has the ability of changing the dispatch schedules generated by the DC model in order to secure the system against any *N*-1 contingency. Since the starting point for PSCOPF is the ACOPF solution, it was desired to keep the generators statuses and dispatch levels as unchanged as possible. Therefore, lower weights were assigned to on-line and off-line generator controls in PSCOPF in order to change the optimal dispatch or turn on off-line generators only as a last resort. Therefore, PSCOPF attained *N*-1 secure cases by utilizing the available controls in the following order: tap setting adjust-

ments, switched shunts, on-line generators re-dispatch, and committing off-line generators as the last resort. Table 4.16 and Table 4.17 present generation total costs for RTS-96 test case and PJM system respectively. The RTS-96 test case total costs include the total costs of the entire 24 time-periods while the PJM total costs are for the peak time-period (hour 16:00) considered in this analysis. As expected, total generation cost for the relaxed scenarios is less than total generation cost for the non-relaxed scenarios. It can also be noticed that the cost of preventive actions and corrections that ensure *N*-1 security was lower for the relaxed scenario compared to the non-relaxed scenario for RTS-96 test case while it was higher for PJM system. This discrepancy in results can be explained due to the complexity and large scale of PJM system that resulted in more real-time violations in the relaxed scenarios compared to RTS-96 test case. Additional detailed discussion on the impacts of constraint relaxations on energy markets can be found in [73], [82].

Table 4.15. Total Generation Cost Comparison (RTS-96).

Settlement type	Original SCUC $k	*N*-1 secured $k	Cost increase %
Non-relaxed scenario	4,096	4,804	17%
Relaxed scenario	4,071	4,558	12%

Table 4.16. Total Generation Cost Comparison (PJM).

Settlement type	Original SCUC $k	*N*-1 secured $k	Cost increase %
Non-relaxed scenario	16,649	22,529	35%
Relaxed scenario	16,431	23,315	42%

It should be noted that the PJM relaxed SCUC was solved with PJM's real penalty prices of 1000 $/MWh and 2700 $/MWh for line limit and nodal relaxations respectively. The relaxed RTS-96 SCUC was solved using a line limit penalty price of $100/MWh.

5. POST-CONTINGENCY CONSTRAINT RELAXATIONS ANALYSIS AND RESULTS

5.1 Introduction

In this chapter, the investigation of constraint relaxations is extended to include post-contingency constraint relaxations. The purpose of this work is to investigate the impact of base-case and post-contingency constraint relaxations in energy market models on the real-time AC system performance and total generation costs. Although theoretically any constraint can be relaxed, only the thermal limits on the branches were considered in this study because these relaxations can be physically realized in the real-time system and have direct impact on security and reliability. Two types of constraint relaxations are considered in this study:

- Base-case relaxations: where the normal, continuous thermal ratings (Rate-A) [75] are allowed to be relaxed
- Post-contingency relaxations: where the relaxations are allowed for emergency thermal ratings (Rate-C) [75] following a contingency.

In order to compare the impact of each type of these relaxations separately, as well as when both types are allowed simultaneously, four scenarios were investigated:

- No relaxation allowed
- Base-case relaxations only
- Post-contingency relaxations only
- Base-case and post-contingency relaxations allowed.

The results from DC and AC analysis for each scenario were used to investigate the impact of each relaxation type on system security and reliability. Moreover, different penalty prices were also used for each scenario in order to investigate the correlation between penalty prices and real-time violations for each type of constraint relaxation. Since constraint relaxations also affect the total production cost, a thorough comparison between production costs for each scenario and for different penalty prices was also conducted.

In order to capture the direct effect of constraint relaxations on system security and reliability, the IEEE RTS-96 test case (presented in Subsection 4.3.1) was utilized. The test case was represented in the DC market model to obtain the SCUC solutions, and it was represented in PSS/E as well to capture AC and nonlinear characteristics such as reactive power, voltage magnitude and angles, and thermal losses. Different combinations of base-case and post-contingency relaxations were investigated. The same analysis was conducted twice for each scenario, once for cases with constraint relaxations and another time for cases that do not have any relaxations while ensuring analysis consistency.

5.2 SCUC Model with Base-Case and Post-Contingency Relaxations

Using Benders' decomposition, the SCUC problem was split into two sub-problems. The first part (master problem) is a regular base-case SCUC problem. Solving the master problem determines the status and dispatch of each generating unit. The base-case SCUC solution is then passed on to the second sub-problem (slave problem) where post-contingency feasibility is checked. The slave problem generates feasibility cuts and passes them to the master problem for each infeasible contingency. These feasibility cuts

act as additional constraints in the master problem and therefore reduce the feasibility region for the next SCUC solution. This process is iterative and will continue till a SCUC solution that is feasible for all contingencies is achieved.

The SCUC formulation is modified to allow both, base-case and post-contingency relaxations. Typically, relaxations are allowed by adding a slack variable to the constraint to be relaxed, and adding that slack multiplied by the penalty price to the objective function. Base-case relaxations were allowed in that manner since the objective function and relaxed constraints exist in the same sub-problem (master problem) as shown in Appendix A, Equation A.1 and Equation A.19. However, since the slave problem is merely a feasibility check for post-contingency conditions, the post-contingency relaxation decision cannot be made by the slave problem. Therefore, the slack variables were added to the feasibility cuts that are passed to the master problem as shown by Equation A.38 and Equation A.40. The post-contingency slack variables are also multiplied by the post-contingency penalty price and added to the main objective function. The post-contingency slack variables are sent back to the slave problem as fixed parameters in order for the relaxed lines to pass the post-contingency feasibility check as shown in Equations A.27, A.28, A.35, and A.36. The complete SCUC formulations (master and slave sub-problems) are presented in Appendix A [83].

5.3 Market Model Results

Using the security constrained unit commitment formulation presented in Section 2.5, the day-ahead SCUC solutions (i.e. 24-hours solutions) were obtained for different scenarios. First, a non-relaxed SCUC solution was attained in order to be used as a

benchmark for both, total production costs and system performance. Two base-case relaxed SCUC solutions were then achieved using two different penalty prices of values \$150/MWh and \$180/MWh. For the sake of comparison, a SCUC solution with post-contingency relaxation was performed using a penalty price of \$150/MWh (identical to base-case relaxation scenario). However, it was noticed that there were fewer post-contingency line relaxations -number and magnitude- compared to base-case relaxations. Therefore, another post-contingency SCUC solution was obtained using a penalty price of \$30/MWh. Finally, a SCUC solution was obtained allowing both base-case and post-contingency relaxations, using penalty prices of \$150/MWh and \$30/MWh for base-case and post-contingency respectively. The SCUC problem was formed in AMPL and solved using Gurobi solver with a MIP gap of 0.1%. Table 5.1 presents the different relaxations scenarios as well as line relaxations details (number and magnitude) over the 24 hours and the total production cost.

Table 5.1. Relaxation Scenarios Summary.

	Base-case		Post-contingency		Base-case and Post-contingency
	Penalty price: 180	Penalty price: 150	Penalty price: 150	Penalty price: 30	Penalty price: 30 / 150
Total cost %	99.63%	99.09%	98.27%	97.87%	96.85%
Number of relaxed lines	18	31	12	14	Base: 36 / Post: 22
Max. relaxation magnitude	9.5% (30 MW)	16% (50 MW)	2.2% (12.7 MW)	6% (33.5 MW)	Base: 14% (44 MW) / Post: 6% (33.5 MW)

As can be seen in Table 5.1 the total production cost dropped to 99.63% of the original (non-relaxed) case for base-case relaxations using a penalty price of \$180/MWh.

This relaxation resulted in a total of 18 relaxations with the highest relaxation being 9.5% beyond the line normal thermal rating. Decreasing the base-case penalty price to $150/MWh resulted in reducing the total production cost to 99.09% of the non-relaxed price. However, this relatively small reduction in total production costs was accompanied by a significant increase in the number and magnitude of line relaxations. Decreasing the base-case penalty price to $150/MWh has caused the line relaxations (violations) to rise to 31 relaxations with the maximum value being 16% above the line thermal rating. The base-case penalty price was not decreased below $150/MWh because of the excessive and unrealistic relaxations that would appear at lower penalty prices.

As for post-contingency relaxations, it can be noted from Table 5.1 that using a penalty price of $150/MWh caused total production cost to drop to 98.27% of the original price. This reduction was caused by relaxing the emergency thermal limits of 12 lines with a maximum violation of 2.2% beyond the line emergency thermal rating. Remarkably, the post-contingency penalty factor could be significantly reduced allowing for further reduction in total production costs without introducing unreasonable line flow violations. The total production cost was reduced to 97.87% of the original cost when a post-contingency penalty price of $30/MWh was used. Using this relatively low penalty price resulted in 14 line relaxations with the highest violation being 6% beyond the emergency line thermal rating.

Allowing both, base-case and post-contingency line relaxations together resulted in the lowest total production cost as well as the highest number and magnitude of line flow violations. The penalty prices used were $150/MWh and $30/MWh for base-case and post-contingency line relaxations, respectively. Using these penalty prices the total

production cost was reduced to 96.85% of the original cost. This reduction in cost was accompanied with 36 line flow relaxations in base-case with the highest relaxation being 14% beyond line normal thermal limits, and 22 line flow relaxations in post-contingency with the highest relaxation being 6% beyond line emergency thermal limits.

5.4 Base-Case AC Analysis

In order to investigate the impacts of line relaxations in the DC market model on real-time steady state security and reliability, the SCUC solutions were used to obtain AC solutions using PSS/E. Therefore, the test case (RTS-96) was modeled in PSS/E using the same data used in the DC market model. Moreover, generators economic data and other constraints used to solve the SCUC were modeled in PSS/E in order to run ACOPF. Using ACOPF rather than just an AC power-flow provides several advantages, such as:

- Distribute losses among committed units economically and consistently
- Control reactive power generation to ensure acceptable voltage levels throughout the system
- Identify infeasibilities in the system and quantify their sensitivities (severities)

The different scenarios presented in Section 5.1 were simulated in PSS/E. The DC SCUC solution was used as a starting point for the ACOPF. Five different time periods (hours) were chosen for AC analysis. Those hours were chosen in a manner that guarantees the inclusion of significant amount of line relaxations for both, base-case and post-contingency scenarios. Those hours also comprise peak load, medium load, and light load hours. Table 5.2 summarizes the steady state line flow and voltage violations in the ACOPF solution for the different scenarios considered. From Table 5.2 it can be seen that

even with no relaxations there were voltage and line flow violations. These violations are expected because of the approximations incorporated in the DC market model. In order to remove those violations and attain a completely feasible AC case, additional units need to be turned on. In this work no additional units were turned on in order to keep the operation conditions as close as possible to market solution.

Voltage and line flow violations are increased when constraint relaxations are allowed. As can be seen from Table 5.2 almost all base-case relaxations were translated into line flow violation in the AC case. The only exception was time period 19 in which only one violation appeared in AC solution. This exception can be explained again by the existing approximations in the DC market solution which result in slightly different AC solution. This also proves that relaxations in the market model could be considered another form of approximation and do not necessarily result in real-time violations all the time, provided that those relaxations are limited in number and magnitude. Table 5.2 also shows a noticeable increase in the number of voltage violations. These voltage violations are caused mainly by the fewer number of generators committed in the relaxed solution which resulted in less reactive power availability.

As for post-contingency relaxations, none of the line relaxations from the market solution appeared in real-time. This shows that post-contingency line relaxations have no direct adverse effect on real-time line flows. However, voltage violations increased in real-time due to the reduced number of committed generators.

When base-case and post-contingency relaxations are both allowed more real-time line flow and voltage violations are observed.

Table 5.2. Base-Case Violations.

	No relaxation					Base-case (PP: 150)					Post-contingency (PP: 30)					Base-case/Post-contingency (PP: 150/30)[1]				
Time period	7	8	11	19	22	7	8	11	19	22	7	8	11	19	22	7	8	11	19	22
Voltage violations	2	2	0	0	2	2	3	2	1	3	6	3	2	0	4	7	5	2	2	3
Flow violations	0	0	0	1	0	0	2	2	1	1	0	0	0	0	0	0	1	3	3	2
Number of relaxations	-	-	-	-	-	-	2	2	2	1	4	2	1	-	2	-/4	2/3	3/1	3/1	2/7
Maximum relaxation	-	-	-	-	-	-	7.4%	15.9%	10.5%	0.16%	2.9%	6%	-	-	2.3%	-/ 2.9%	5.7/ 6%	8.7/ 1.5%	12.4/ 0.54%	3.2/ 4.6%

[1] Base-case and post-contingency number and magnitude of relaxations for this scenario are displayed respectively

Base-case relaxations directly affect line flow violations as well as voltage violations, while post-contingency relaxations have a major impact on voltage violations. Therefore, when base-case and post-contingency relaxations are both allowed, the real-time AC case would encounter line flow violations as well as depressed voltage levels caused by reactive power deficiency.

5.5 Post-Contingency AC Analysis

In order to investigate the base-case and post-contingency relaxations impact on the system following a credible contingency event, a full-blown *N*-1 AC contingency analysis was run in PSS/E for each scenario shown in Section 5.1. The *N*-1 contingency analysis in this work included all branches (lines and transformers) as well as committed units. Following the loss of a unit the remaining units were re-dispatched according to their inertias.

Table 5.3 presents the post-contingency performance of the various considered scenarios. It can be seen that the original case (non-relaxed) was not *N*-1 secure since there were several line flow and voltage violations caused by various contingencies. There were also non-converged contingencies which implies that the AC power-flow either diverged or the maximum number of iterations was reached before reducing the mismatches to acceptable values for those contingencies. It should be noted here that *N*-1 security could be achieved for this test case by committing additional units, re-dispatching the system, and utilizing other control parameters such as tap settings and shunt devices. However, that is beyond the scope of this work as it is desired to keep the DC market solution as unchanged as possible.

Similar to AC base-case analysis, base-case and post-contingency relaxations have increased the number of real-time line flow and voltage violations. It should be noted here that despite the decrease in the number of violations for some hours that does not imply better reliability or security conditions because it is always accompanied with an increase in the number of the unsolved (non-converged) cases. Therefore, this implies that violations actually became more severe causing more contingencies not to solve. It should also be noted from Table 5.3 that violations in their various forms are generally higher when base-case and post-contingency relaxations were allowed simultaneously.

The significant degradation in post-contingency reliability performance when base-case and post-contingency relaxations are both allowed aroused concerns related to excessive line flow violations caused by violations from coinciding from both types of relaxations in a cascading like effect. Therefore, the lines that were relaxed in base-case and post-contingency SCUC solution were identified and their real-time flows were monitored throughout the *N*-1 analysis. Table 5.4 shows those lines.

As discussed in AC base-case analysis (Section 4.3), Table 5.4 shows that lines relaxed in the base-case SCUC solution are always violated in real-time. Table 5.4 also shows the flows on these lines following a contingency event. It can be seen that the violations on some lines have doubled following a contingency, such as line 114-116 in time period 11 and line 114-116 in time period 19 with real-time flow violations of 120% and 117% of the lines emergency thermal limits respectively. This significant increase in line flow violations could easily fall beyond the acceptable relaxation limits and impose serious security problems especially if another contingency event occurs (*N*-1-1 or *N*-2).

Table 5.3. Post-contingency violations.

	No relaxation					Base-case (PP: 150)					Post-contingency (PP: 30)					Base-case/Post-contingency (PP: 150/30)[1]				
Time period	7	8	11	19	22	7	8	11	19	22	7	8	11	19	22	7	8	11	19	22
Voltage violations	67	48	20	24	42	67	18	45	40	19	16	22	25	52	38	52	41	38	34	14
Flow violations	9	5	16	6	7	9	8	24	22	10	2	5	15	10	6	4	12	17	16	6
Non converged	13	9	3	2	13	13	17	5	4	10	20	21	7	8	18	18	15	11	13	19
Number of relaxations	-	-	-	-	-	-	2	2	2	1	4	2	-	-	2	-/4	2/3	3/1	3/1	2/7
Maximum relaxation	-	-	-	-	-	-	7.4%	15.9%	10.5%	0.16%	2.9%	6%	-	-	2.3%	-/ 2.9%	5.7/ 6%	8.7/ 1.5%	12.4/ 0.54%	3.2/ 4.6%

[1] Base-case and post-contingency number and magnitude of relaxations for this scenario are displayed respectively

Table 5.2. Flows on Lines Relaxed in Base-Case and Post-Contingency.

Time period 11:00		
Line	Base-case loading	Post-contingency loading
114-116	110%	120%
214-216	101%	105%
314-316	101%	109%
Time period 19:00		
114-116	108%	117%
214-216	102%	110%
314-316	103%	95%
Time period 22:00		
214-216	105%	106%
314-316	101%	91%

6. CONCLUSIONS

Constraint relaxation practices conducted by system operators have been reviewed and investigated in this research effort. In order to capture and quantify the effect of constraint relaxations on energy market efficiency and power system performance, a test case and real-life large-scale system were utilized to replicate the constraint relaxation practices conducted in practice. Realizing the precise and direct impact of relaxations provide a solid basis for decision makers for assessing the benefits and risks encountered with these practices. Assessing the associated benefits and risks constraints relaxations have on markets efficiency and operational security would also provide a sound basis for choosing appropriate values for the different penalty prices.

In this work, assessing the impacts of market constraint relaxations on real-time system performance was desired. Capturing the impacts of constraint relaxations on static and dynamic operational security makes operators more aware of the risks and benefits associated with constraint relaxations. Throughout this work static and dynamic base-case and post-contingency operating conditions were investigated to reveal any underlying adverse effects of constraints relaxations that operators may not notice or be aware of during normal operating conditions. Moreover, this analysis also provides better understanding of the correlation between DC market models and AC real-time systems, as this work analyzes how relaxations in market models propagate to real-time systems. Two test cases were used to replicate operators practices related to constraint relaxations. The first test case is the RTS-96 system that was used to demonstrate the constraint relaxations mechanism and the methodology of analysis on a relatively small and simple system. The second test case was a real-life large-scale system that represented PJM control

areas and their neighboring areas. PJM also provided the corresponding actual economic and dynamic data.

Static steady state and dynamic time-domain analysis were conducted for both test cases twice, once for cases with relaxed constraints and another time for non-relaxed cases. This approach has provided a systematic and consistent approach to demonstrate the impacts of relaxations on a real-time system. SCUC market solutions were used as starting points to achieve base-case AC feasible solutions. PSS/E ACOPF was utilized to achieve AC feasible solutions, as it provides an accurate and consistent transition from the dispatch schedules generated by the DC market models to an AC feasible solution. Thermal losses were distributed in an economic manner rather than being picked up by the slack bus. Other controls, such as scheduled voltages, transformers tap settings, and switched shunts, were adjusted automatically as well.

However, it was found that in some cases, out-of-market corrections were needed to achieve a successful and feasible ACOPF solution. Out-of-market corrections mainly consist of committing additional generators for voltage support purposes and/or lines overloading alleviation. It was noticed that more out-of-market corrections were needed for relaxed cases, which can be explained by the commitment of fewer generators in the relaxed cases in market solutions. For instance, PJM peak hour non-relaxed case has around 5.5% more generators (98 generators) than the relaxed case. It was also noticed that more out-of-market corrections were needed in the PJM test case compared to the RTS-96 case, as no out-of-market generations needed to be added to attain AC feasible solutions for the RTS-96 case, while 26 out-of-market generators were needed to solve the power flow for the PJM peak load hour. This can be explained by the effect of the

approximations inherent in market models, which became more evident in large-scale systems. It was also desired to attain *N*-1 security for the non-relaxed cases in order to be used as benchmarks for the corresponding relaxed cases. Attaining *N*-1 security required additional out-of-market corrections using PSS/E PSCOPF tool. In order to make the PJM system *N*-1 secure, a total of 84 and 63 additional out-of-market generators were committed in the load peak and off peak hours, respectively.

Static analysis of both test cases revealed that line relaxations in market models have a high tendency of appearing as AC line flow violations in real-time systems. A total of 6 lines were relaxed in the RTS-96 and they were all translated into real-time violations in the AC solution. However, in the PJM test case, most of the market solution relaxations appeared as AC flow violations alongside line flow violations that did not originate from market models, which can be explained due to the various approximations used in market models. For instance, the PJM peak hour had 13 line flow violations, of which 10 violations were originated from the market solution as line relaxations. However, flow violations that were not originated from the market solutions had relatively lower values.

Static analysis has also revealed reactive power deficiency in the relaxed cases that was translated into wide-spread voltage violations. Relaxed cases sustained reactive power deficiency because fewer generators were committed in those cases in the original market solutions, as well as in the out-of-market corrections compared to non-relaxed cases. *Q/V* analysis was also conducted for the PJM test cases to confirm the reactive power problem and it was found that significantly greater amount of reactive power was needed to regulate the voltage in relaxed cases. For instance, the *Q/V* analysis revealed

that an amount of 138 MVAr was needed to achieve a voltage magnitude of 1.0 p.u. at a test bus in a weak area in the relaxed PJM system, while an amount of 26 MVAr was needed for the same bus and same voltage magnitude in the non-relaxed PJM system. Static post-contingency analysis was also conducted and relaxed lines flows were monitored. It was noticed that relaxed lines were more likely to violate their thermal emergency limits following certain critical contingencies since they were already overloaded in base-case.

Dynamic time-domain analysis was also conducted to investigate the dynamic performance of relaxed cases compared to cases with no relaxation. Using *N*-1 analysis, the most severe contingencies were identified and ranked. A sequence of events representing *N*-2 contingencies was used to investigate the dynamic response of overloading and tripping relaxed lines. Relative rotor angles of the most affected generators were plotted and compared. Rotor angle stability analysis revealed higher oscillations in relaxed cases with prolonged settling time compared to non-relaxed cases. This observation was more evident in the PJM test case, as it represents a large-scale system with realistic dynamic models. Although all tested contingencies were stable, higher oscillations indicate narrower stability margins and, therefore, higher vulnerability to stability related problems. Dynamic post-contingency voltage profiles were also investigated for both test cases. Similar to stability studies, contingencies causing the most severe voltage violations were identified and ranked using *N*-1 analysis. Dynamic voltage analysis confirmed the static analysis results related to reactive power deficiency. It was noticed that relaxed cases sustained base-case and post-contingency depressed voltage levels compared to non-relaxed cases. Again, this is explained due to the fewer committed generators in the

relaxed case. Furthermore, more detailed voltage stability analysis was desired in order to capture the apparent reactive power deficiency issue in the relaxed cases. Therefore, loads in PJM peak load hour were modeled dynamically in order to reflect motors decelerating and stalling impact on voltage stability results. Using dynamic load models resulted in observing significant voltage delay recovery and sustained low voltage magnitudes following a severe contingency. For instance, in one of the studied contingences (Figure 4.28), the bus voltage magnitude recovered to 0.75 p.u. after around 2 seconds although static load model analysis indicated instantaneous voltage recovery and a final voltage magnitude of 0.83 p.u.

Security assessment conducted on the relaxed PJM system indicated that some high capacity transmission lines were relaxed in the market SCUC model and resulted in overloading those lines in the AC real-time solution. However, those high capacity lines tend to have severe impacts on the system security in the event of a fault or forced outage. Moreover, those lines are usually high voltage major transmission corridors that span long distances and should not be violated. Therefore, it was desired to design a risk based penalty price scheme that would avoid (or limit) relaxing high risk lines. Transmission lines were categorized in three distinctive groups depending on their risk indices. Risk indices were determined depending on the outage frequency (length of the lines) and, the impact on system operational security (post-contingency overloads) following a credible contingency. Increasing the penalty price for high capacity lines resulted in decreasing total relaxations magnitude. The total relaxations magnitude (for all relaxed lines) for the risk based penalty price scenario was 81 MW, while a total of 119 MW was reported for the traditional relaxed case. Therefore, more generating units were committed in the risk

based penalty price SCUC solution, compared to the traditional single penalty price scenario. As a result, voltage violations were reduced because of the additional reactive power availability. Moreover, none of the high risk lines (long and high capacity lines) were relaxed when risk based penalty prices were used.

This work has also investigated the effect of post-contingency constraint relaxations on system performance end energy markets utilizing the RTS-96 test case. The results presented in this work show that relaxations in energy market models have negative effects on real-time system performance in general since constraint relaxations are a form of violations in the market DC model. Base-case relaxations appeared consistently in real-time system as line flow violations. Base-case relaxations are based on the continuous normal thermal ratings of lines, therefore, they appeared as continuous violations in the real-time system. Scenarios that were base-case relaxed also encountered voltage violations caused by the limited availability of reactive power as a result of committing fewer generating units in the relaxed cases. Base-case relaxations have slightly increased the social welfare as they resulted in lower total production costs. Using lower penalty prices for base-case violations resulted in lower production costs. However, lowering the base-case penalty price below certain values resulted in unrealistic relaxations that would be translated into excessive violations.

Post-contingency constraint relaxations on the other hand were based on the emergency thermal ratings of lines following a contingency. Therefore, post-contingency relaxations appear as line flow violations in real-time system only following the event of a certain contingency. Hence, post-contingency relaxations are much less likely to appear in the real-time system as line flow violations compared to base-case relaxations. How-

ever, similar to base-case relaxations, voltage violations appeared in post-contingency relaxed cases because of reactive power deficiency. Post-contingency relaxations showed significant impact on lowering the total production costs. It was also possible to use much lower penalty prices (e.g. $30/MWh) without causing excessive violations because base-case constraints had to be enforced all the time.

Allowing base-case and post-contingency constraint relaxations simultaneously had the largest impact on real-time system performance. Line flow violations caused by base-case relaxations and voltage violations caused by both types of relaxations appeared in real-time system. Moreover, allowing both types of relaxations simultaneously could result in cascading violation events. This could happen when a single line is relaxed in base-case and post-contingency simultaneously. Therefore, that line could encounter large violations as a result of base-case and post-contingency relaxations overlapping at the same time following a specific contingency. A maximum line overload of 120% above the emergency thermal rate was reported when the same lines was relaxed in base-case and post-contingency simultaneously. Allowing both types of relaxations had also the most significant effect on lowering the total production cost, as the total cost was reduced to 96.5% of the non-relaxed cost when base-case and post-contingency constraint relaxations were allowed simultaneously. Penalty prices should be chosen carefully in this scenario, especially base-case penalty price, to ensure that relaxations do not cause excessive real-time violations.

While the risk analysis associated to line overloads was presented, a cost benefit analysis on the impacts on market surplus relative to the risk exposure should be completed. Such work will lead to more insight as to which lines should be penalized at high-

er or lower prices along with what are the appropriate values for those prices. Such a framework would provide industry with a more comprehensive analysis of the impacts of constraint relaxations on not just operational security but market efficiency, which then enables determination on appropriate penalty prices. It is also important to extend such risk assessment and cost benefit analysis to additional constraint relaxation practices, like reserve requirement relaxation. Other important aspects of constraint relaxation practices include the duration of the relaxation. The impact of relaxing a thermal limit for 5 minutes is not the same as the impact of relaxing the limit over 15 minutes; the thermal heating impact is not linear and, thus, it is important to account for such system operational security impacts when constructing the relaxation practices and penalty prices. Finally, further analysis and validation is needed. This thesis critiques and analyzes existing relaxation practices on actual PJM data; however, some data (e.g., load models) was limited. Additional analysis on a wider range of operating states and with complete system data would further improve the validation of the results and further provide quantifiable results regarding system specific impacts. With that said, the primary conclusions are, nonetheless, the same: constraint relaxations push system operations further to an extreme and, thus, impair system operational security; with this thesis, there is now a pathway to further analyze the tradeoffs of that risk exposure with the anticipated market benefits.

REFERENCES

[1] CAISO, "Market optimization details," Technical bulletin, June 2009.

[2] X. Ma, H. Song, M. Hong, et al., "The security constrained commitment and dispatch for Midwest ISO day-ahead co-optimized energy and ancillary service market," *IEEE Power and Energy Society General Meeting*, pp: 1-8, 2009.

[3] CAISO, "Minimum effective threshold report," Market Quality and Renewable Integration, March 1, 2010.

[4] NYISO, "NYISO's filing of revisions to its market administration and control area services tariff and its open access transmission tariff to apply an upper limit on transmission shortage costs reflected in locational based marginal prices." FERC, Docket ER07-720-000, Apr. 5, 2007.

[5] CAISO, "Price inconsistency market enhancements - revised straw proposal," 2012, [Online], Available: http://www.caiso.com/Documents/RevisedStrawProposal-PriceInconsistencyMarketEnhancements.pdf.

[6] CAISO, "Parameter tuning for uneconomic adjustments in the MRTU market optimizations," Market and Product Development, 2008, [Online], Available: http://www.caiso.com/1fbf/1fbfe3a2498e0.pdf.

[7] SPP, "Market protocols - SPP integrated market place revision 12.0," Market Design, 2012, [Online], Available: http://www.spp.org/publications/Integrated%20Marketplace%20Protocols%2012%200.pdf.

[8] K. Ogelman, "ERCOT business practice - setting the shadow price caps and power balance penalties in security constrained economic dispatch," ERCOT, 2012, [Online], Available: http://www.ercot.com/content/meetings/wms/keydocs/2011/0415/03_bus_pract_set_shadow_price_cap_wms_revised_april_15_2011.doc.

[9] MISO, "2011 State of the market report for miso electricity markets," Potomac Economics - Independent Market Monitor for MISO, 2012, [Online], Available: http://www.potomaceconomics.com/uploads/midwest_reports/2011_SOM_Report.pdf.

[10] MISO, "Constraint relaxation update," MISO Market Subcommittee, 2012, [Online], Available: https://www.misoenergy.org/Library/Repository/Meeting%20Material/Stakeholder/MSC/2012/20120501/20120501%20MSC%20Item%2004a%20Constraint%20Relaxation.pdf.

[11] MISO, "2010 State of the market report for miso electricity markets," Potomac Economics – Independent Market Monitor for MISO, 2011, [Online], Available: http://www.potomaceconomics.com/uploads/midwest_reports/2010_State_of_the_Market_Report_Final.pdf.

[12] NYISO "Day-ahead scheduling manual," New York ISO, 2013, [Online], Available: http://www.nyiso.com/public/webdocs/markets_operations/documents/Manuals_and_Guides/Manuals/Operations/dayahd_schd_mnl.pdf.

[13] V. Van Acker, P. Shamsollahi, C. Cathey, R. Dillon, D. Gray, "Impact of MW dependent constraint violation penalties on market results at southwest power pool," *IEEE PES Transmission and Distribution Conference and Exposition (T&D)*, pp.1,8, 7-10, 2012.

[14] V. T. Morgan, "Effect of elevated temperature operation on the tensile strength of overhead conductors," *IEEE Transactions on Power Delivery*, vol. 11, no. 1, pp. 345-352, 1996.

[15] V. T. Morgan, "The loss of tensile strength of hard-drawn conductors by annealing in service," *IEEE Transactions on Power Apparatus and Systems*, vol. PAS-98, no.3, pp. 700-709, 1979.

[16] J. R. Harvey, "Effect of elevated temperature operation on the strength of aluminum conductors," *IEEE Transactions on Power Apparatus and Systems*, vol. PAS-91, no 5, pp. 1769-1772, 1972.

[17] IEEE guide for determining the effects of high-temperature operation on conductors, connectors, and accessories, IEEE Standard 1283-2004, 2005.

[18] T.E.D. Liacco, "The adaptive reliability control system," *IEEE Transactions on Power Apparatus and Systems*, vol. PAS-86, no 5, pp. 517-531, 1967.

[19] R.J. Marceau, J. Endrenyl, "Power system security assessment," *CIGRE Task Force 38.03.12*, 1997.

[20] P. Kundur, L. Wang, and K. Morison, "Power system security assessment," *IEEE Power and Energy Magazine*, vol. 2, pp. 30-39, 2004.

[21] P. Kundur, V. Ajjarapu, V. Vittal, *et al*., "Definition and classification of power system stability," *IEEE Transactions on Power Systems*, pp. 1387 – 1401, 2004.

[22] A.A. Fouad, F. Aboytes, V.F. Carvalho, "Dynamic security assessment practices in North America," *IEEE Transactions on Power Systems*, vol. 3, pp. 1310, 1988.

[23] M. Schwan, H.J. Haubrich, A. Schnettler, "Investigation of power system security and availability," *INTELEC 27th Telecommunications Conference*, pp. 581-586, 2005.

[24] R.J. Marceau, M. Sirandi, S. Soumare, X.D. Do, "A review of signal energy analysis for the rapid determination of dynamic security limits," *Canadian Journal of Electrical and Computer Engineering*, vol. 21, pp. 125-132, 1996.

[25] International Electrotechnical Commission, ref: 191-21-03 [Online], Available: http://www.electropedia.org/iev/iev.nsf/display?openform&ievref=191-21-03.

[26] H. Ma, S.M. Shahideehpour, "Unit commitment with transmission security and voltage constraints," *IEEE Transactions on Power Systems*, vol. 14, pp. 757-764, 1999.

[27] N. Ming, J.D. McCalley, V. Vittal, T. Tayyib, "Online risk-based security assessment," *IEEE Transactions on Power Systems*, vol. 18, pp. 258-265, 2003.

[28] M. Abapour, M.R. Haghifam, "On-line assessment of the transient instability risk," *IET Generation, Transmission, and Distribution*, vol. 7, pp. 602-612, 2013.

[29] J. Geeganage, U.D. Annakkage, T. Weeks, B.A. Archer, "Application of energy-based power system features for dynamic security assessment," *IEEE Transactions on Power Systems*, vol. 30, pp. 1957-1965, 2015.

[30] V. Vittal, J.D. McCalley, V.V. Acker, W. Fu, N. Abi-Smara, "Transient instability risk assessment," *IEEE Power Engineering Society Summer Meeting*, vol. 1, pp. 206-211, 1999.

[31] U.S. – Canada Power System Outage Task Force, "Final report on the August 14, 2003 blackout in the United States and Canada: causes and recommendations," [Online], Available: http://energy.gov/sites/prod/files/oeprod/DocumentsandMedia/BlackoutFinal-Web.pdf.

[32] I.A. Hiskens, M.A. Pai, "Trajectory Sensitivity Analysis of Hybrid Systems," *IEEE Circuits and Systems I: Fundamental Theory and Applications*, vol. 47, pp. 2014-220, 2000.

[33] I.A. Hiskens, J. Alseddiqui, "Sensitivity, approximation, and uncertainty in power system dynamic simulation, *IEEE Transactions on Power Systems*, vol. 21, pp. 1808-1820, 2006.

[34] R. Diao, S. Kai, V. Vittal, *et al*., "Decision tree-based online voltage security assessment using PMU measurements," *IEEE Transactions on Power Systems*, vol. 24, pp. 832-839, 2009.

[35] I. Genc, R. Diao, V. Vittal, *et al*. "Decision tree-based preventive and corrective control applications for dynamic security enhancement in power systems," *IEEE Transactions on Power Systems*, vol. 25, pp. 1611-1619, 2010.

[36] Y. Xu, Y. Dong, Z Xu, *et al*, "An intelligent dynamic security assessment framework for power systems with wind power," *IEEE Transactions on Power Systems*, vol. 8, pp. 995-1003, 2012.

[37] D.N. Kosterev, C.W. Taylor, W.A. Mittelstadt, "Model validation for the August 10, 1996 WSCC system outage," *IEEE Transactions on Power Systems*, vol. 14, pp. 967-979, 1999.

[38] J. Undrill, L. Pereira, D.N. Kosterev, *et al*., "Generating unit model validation: WECC lessons and moving forward," *IEEE Power and Energy Society General Meeting*, pp. 1-5, 2009.

[39] A. J. Wood and B. F. Wollenberg. Power Generation Operation and Control – 2nd Ed. Hoboken, NJ: Wiley, 1996.

[40] B. Stott, J Jardim, O. Alsaç, "DC power flow revisited," *IEEE Transactions on Power Systems*, pp: 1290 – 1300, 2009.

[41] PSS/E 33.5, "Program operational manual," Siemens, Oct. 2013.

[42] H. Wei, H. Sasaki, J. Kubokawa, R. Yokoyama, "An interior point nonlinear programming for optimal power flow problems with a novel data structure," *IEEE Transactions on Power Systems*, vol. 13, pp. 870-877, 1998.

[43] Q. Jiang, Z. Huang, "An enhanced numerical discretization method for transient stability constrained optimal power flow," *IEEE Transactions on Power Systems*, vol. 25, pp. 1790-1797, 2010.

[44] A. Bhardwaj, V. Kamboj, V. Shukla , B. Singh, P. Khurana, "Unit commitment in electrical power system – A literature review," *IEEE International Power Engineering and Optimization Conference (PEDCO)*, pp: 275 – 280, 2012.

[45] ERCOT, "Report on existing and potential electric system constraints and needs," 2007, [Online], http://www.er¬cot.com/news/presentations/2008/35171_ERCOT_2007_Transmission_Constraints_Needs_Report.pdf.

[46] Y. Li, J. McCalley, "A general Benders' decomposition structure for power system decision problems," *IEEE International Conference on Electro/Information Technology*, pp: 72 – 77, 2008.

[47] S. Cvijic, J. Xiong, "Security constrained unit commitment and economic dispatch through Benders' decomposition: A comparative study," *IEEE Power and Energy Society General Meeting*, pp: 1 – 8, 2001.

[48] M. Shahidehpour, Y. Fu, "Benders' decomposition in restructured power systems," *IEEE Power and Energy Magazine*, pp: 20 - 21, 2005.

[49] M. Cadoli, F. Patrizi, "On the separability of subproblems in Benders' decompositions," [Online], Available: http://www.dis.uniroma1.it/~patrizi/docs/papers/cadoli-patrizi-CPAIOR06-final.pdf.

[50] C. Taylor, "Power system voltage stability," MC Graw Hill, New York, 1994.

[51] P. Kundur, "Power system stability and control," McGraw Hill, New York, 1994.

[52] T. Yong, M. Shiying and Z. Wuzhi, "Mechanism research of short-term large-disturbance voltage stability," *International Conference on Power System Technology*, pp. 1-5, 2006.

[53] P. Li, B. Zhang, C. Wang, J. Shu, M. You, Y. Wang, Z. Bo, and A. Klimek, "Time-domain simulation investigates short-term voltage stability with dynamic loads," *Asia-Pacific Power and Energy Engineering Conference*, pp. 1-5, 2009.

[54] J. Diaz de Leon II, and C. Taylor, "Understanding and solving short-term voltage stability problems," *IEEE Power Engineering Society Summer Meeting*, vol. 2, pp. 745 – 752, 2002.

[55] C. Sharma, and M. Ganness, "Determination of power system voltage stability using modal analysis," *International Conference on Power Engineering, Energy and Electrical Drives*, pp. 381 – 387, 2007.

[56] M.Hasani and M.Parniani, "Method of combined static and dynamic analysis of voltage collapse in voltage stability assessment," *IEEE Transmission and Distribution Conference and Exhibition: Asia and Pacific*, pp. 1-6, 2005.

[57] T. Cutsem, and C. Vournas, "Voltage stability of electric power systems," Kluwer Academic Publishers, 1998.

[58] IEEE Task Force on Load Representation for Dynamic Performance, "Load representation for dynamic performance analysis," *IEEE Transactions on Power Systems*, vol. 8, pp. 472-482, 1993.

[59] IEEE Task Force for Load Representation for Dynamic Performance, "Standard models for power flow and dynamic performance simulation," *IEEE Transactions on Power Systems*, vol. 10, pp. 1302-1313, 1995.

[60] K. Morison, H. Hamdani, L. Wang, "Practical issues in load modeling for voltage stability studies," *IEEE Power Engineering Society General Meeting*, vol. 3, pp. 1392-1397, 2003.

[61] B. Lesieutre, D. Kosterev, J. Undrill, "Phasor modeling approach for single phase ac motors," *IEEE Power Engineering Society General Meeting*, pp. 1-7, 2008.

[62] D. Kosterev, A. Meklin, J. Undrill, *et al.*, "Load modeling in power system studies: WECC progress update," *IEEE Power Engineering Society General Meeting*, pp. 1-9, 2008.

[63] G. K. Stefopoulos, A. P. Meliopoulos, "Induction motor load dynamics: Impact on voltage recovery phenomena," *IEEE Power Engineering Society Transmission and Distribution Conference and Exhibition*, pp. 752-759, 2006.

[64] L. Taylor, R. Jones, S. Halpin, "Development of load models for fault induced delayed voltage recovery dynamic studies," *IEEE Power and Energy Society General Meeting*, pp. 1-7, 2008.

[65] X. Zheng, R. He, J. Ma, "A new load model suitable for transient stability analysis with large voltage disturbances," *Electrical Machines and Systems (ICEMS)*, pp. 1898 – 1902, 2010.

[66] K. Rudion, H. Guo, H. Abildgaard, Z. A. Styczynski, "Non-linear load modeling - requirements and preparation for measurement," *IEEE Power & Energy Society General Meeting*, pp. 1-7, 2009.

[67] P. Pourbeik and B. Agrawal, "A hybrid model for representing air-conditioner compressor motor behavior in power system studies," *IEEE Power Engineering Society General Meeting*, pp. 1-8, 2008.

[68] B. Sapkota, V. Vittal, "Dynamic VAr planning in a large power system using trajectory sensitivities," *IEEE Transactions on Power Systems*, pp. 461 – 469, 2010.

[69] P. Pourbeik, D. Wang, K. Hoang, "Load modeling in voltage stability studies," *Power Engineering Society General Meeting*, pp. 1893 – 1900, 2005.

[70] V. Stewart, E. H. Camm, "Modeling of stalled motor loads for power system short term voltage stability analysis," *IEEE Power Engineering Society General Meeting*, vol. 2, pp. 1887-1892, 2008.

[71] P. Pourbeik, B. Agrawal, "A hybrid model for representing air-conditioner compressor motor behavior in power system studies," *IEEE Power Engineering Society General Meeting*, pp. 1-8, 2008.

[72] CAISO, "Minimum effective threshold report," Market Quality and Renewable Integration, March 1, 2010.

[73] Yousef M. Al-Abdullah, PhD Dissertation, Arizona State University, 2016.

[74] NERC Reliability Assessment Guidebook, Version 3.1, 2012, [Online], Available: http://www.nerc.com/files/Reliability%20Assessment%20Guidebook%203%201%20Final.pdf.

[75] University of Washington, "Power system test case archive," Dept. of Elect. Eng., 2007, [Online], Available: http://www.ee.washington.edu/research/pstca.

[76] PJM Planning Committee, "Dynamic load modeling," TPL-001-4, 2015, [Online], Available:http://www.pjm.com/~/media/committees-groups/committees/pc/20150507/20150507-item-08-dynamic-load-modeling-for-tpl-001-4.ashx.

[77] ISO New England, Summary of stability base cases for TPL 001-4 studies, 2015, [Online], Available: http://www.iso-ne.com/static-assets/documents/2015/10/final_summary_of_stability_basecases_for_tpl_001_4_studies.pdf.

[78] New York ISO, Intermediate area transmission review of the New York state bulk power transmission system (study years 2015, 2019, 2024), 2015, [Online], Available: http://www.nyiso.com/public/webdocs/markets_operations/services/planning/Documents_and_Resources/Reliability-Compliance/2014_NYISO_IntermediateATR_FINAL_2015-06-03.pdf.

[79] MISO, MOD-032 Model data requirements and reporting procedures, version 2, 2015, [Online], Availabe: https://www.misoenergy.org/Library/Repository/Communication%20Material/Compliance%20Corner/MOD-32%20Model%20Data%20Requirements%20and%20Reporting%20Procedures.pdf.

[80] Canadian Electricity Association, Annual report - forced outage performance of transmission equipment, 2012.

[81] PJM, Interconnection Training Program, 2011, [Online], Available: https://www.pjm.com/~/media/training/nerc-certifications/to1-transmissionops.ashx.

[82] Y. Al-Abdullah, A. Salloum, K. Hedman, V. Vittal, "Analyzing the impacts of constraint relaxation practices in electric energy markets," *IEEE Transactions on Power Systems*, 2015.

[83] K. Hedman, EEE-598 Operations Research Applied to Power Systems, Arizona State University, 2014.

APPENDIX A

SCUC FORMULATION

Extensive Form *N*-1 Reliable Unit Commitment Formulation: [83]

Min: $\sum_{g,t}\left(c_g P_{gt} + c_g^{NL} u_{gt} + c_g^{SU} v_{gt} + PF_M(S_M^+ + S_M^-) + PF_S(S_{NK}^- + S_{NK}^+ + S_{NG}^- + S_{NG}^+)\right)$ A.1

s.t.:

Base-case modeling of generation

$P_g^{min} u_{gt} \le P_{gt}$, $\forall g,t$ A.2

$P_{gt} + r_{gt} \le P_g^{max} u_{gt}$, $\forall g,t$ A.3

$0 \le r_{gt} \le R_g^{10} u_{g,t}$, $\forall g,t$ A.4

$\sum_{q\in G} r_{qt} \ge P_{gt} + r_{gt}$, $\forall g,t$ A.5

$P_{gt} - P_{g,t-1} \le R_g^{hr} u_{g,t-1} + R_g^{SU} v_{gt}$, $\forall g, t \ge 2$ A.6

$P_{g,t-1} - P_{gt} \le R_g^{hr} u_{g,t} + R_g^{SD}(v_{gt} - u_{gt} + u_{g.t-1})$, $\forall g, t \ge 2$ A.7

$P_{g1} - P_{g,T} \le R_g^{hr} u_{g,T} + R_g^{SU} v_{g1}$, $\forall g$ A.8

$P_{g,T} - P_{g1} \le R_g^{hr} u_{g,1} + R_g^{SD}(v_{g1} - u_{g1} + u_{g,T})$, $\forall g$ A.9

$\sum_{q=t-UT_g+1}^{t} v_{g,q} \le u_{gt}$, $\forall g, t \ge UT_g$ A.10

$\sum_{q=T+t-UT_g+1}^{T} v_{g,q} + \sum_{q=1}^{t} v_{g,q} \le u_{gt}$, $\forall g, t \le UT_g - 1$ A.11

$\sum_{q=t+1}^{t+DT_g} v_{g,q} \le 1 - u_{g,t}$, $\forall g, t \le T - DT_g$ A.12

$\sum_{q=1}^{t+DT_g-T} v_{g,q} + \sum_{q=t+1}^{T} v_{g,q} \le 1 - u_{g,t}$, $\forall g, t \ge T - DT_g + 1$ A.13

$$v_{gt} \geq u_{gt} - u_{g,t-1}, \qquad \forall g, t \geq 2 \qquad \text{A.14}$$

$$v_{g1} \geq u_{g1} - u_{g,T}, \qquad \forall g \qquad \text{A.15}$$

$$0 \leq v_{gt} \leq 1, \qquad \forall g, t \qquad \text{A.16}$$

$$u_{gt} \in \{0,1\}, \qquad \forall g, t \qquad \text{A.17}$$

Base-case modeling of power flow

$$P_{kt} - b_k(\theta_{nt} - \theta_{mt}) = 0, \qquad \forall k, t \qquad \text{A.18}$$

$$-(S_M^- + P_k^{max}) \leq P_{kt} \leq (S_M^+ + P_k^{max}), \qquad \forall k, t \qquad \text{A.19}$$

$$\sum_{g \in g(n)} P_{g,t} + \sum_{k \in \delta^+(n)} P_{k,t} - \sum_{k \in \delta^-(n)} P_{k,t} = d_{n,t}, \qquad \forall n, t \qquad \text{A.20}$$

The formulation for each contingency and for each hour of the slave problem

Min: s A.21

s.t.:

For each line contingency (($\forall\, c \in N^k$)) in each hour ($\forall\, t$)

$$-P_g + s\left(R_g^{10}\overline{u_g} - \overline{P_g}\right) \leq R_g^{10}\overline{u_g} - \overline{P_g}, \qquad \forall g \qquad \left(\alpha_{gct}^-\right) \qquad \text{A.22}$$

$$P_g + s\left(R_g^{10}\overline{u_g} + \overline{P_g}\right) \leq R_g^{10}\overline{u_g} + \overline{P_g}, \qquad \forall g \qquad \left(\alpha_{gct}^+\right) \qquad \text{A.23}$$

$$-P_g + s\left(-P_g^{min}\overline{u_g}\right) \leq -P_g^{min}\overline{u_g}, \qquad \forall g \qquad \left(\zeta_{gct}^-\right) \qquad \text{A.24}$$

$$P_g + s\left(P_g^{max}\overline{u_g}\right) \le P_g^{max}\overline{u_g}, \qquad \forall g \quad \left(\zeta_{gct}^{+}\right) \qquad \text{A.25}$$

$$P_k - N_{c,k}^{k} b_k(\theta_n - \theta_m) = 0, \qquad \forall k \quad \left(s_{kct}^{k}\right) \qquad \text{A.26}$$

$$-P_k \le N_{c,k}^{k}(\overline{S_{NK}^{-}} + P_k^{max,c})(1-s), \qquad \forall k \quad \left(F_{kct}^{k-}\right) \qquad \text{A.27}$$

$$P_k \le N_{c,k}^{k}(\overline{S_{NK}^{+}} + P_k^{max,c})(1-s), \qquad \forall k \quad \left(F_{kct}^{k+}\right) \qquad \text{A.28}$$

$$\sum_{g\in g(n)} P_g + \sum_{k\in\delta^{+}(n)} P_k - \sum_{k\in\delta^{-}(n)} P_k + s(d_n) = d_n, \qquad \forall n \quad (LMP_{nct}) \qquad \text{A.29}$$

For each generator contingency ($\forall\, c \in N^g$) in each hour ($\forall\, t$)

$$-P_g + s\left(R_g^{10}\overline{u_g} - N_{c,g}^{g}\overline{P}_g\right) \le R_g^{10}\overline{u_g} - N_{c,g}^{g}\overline{P}_g, \qquad \forall g \quad \left(\beta_{gct}^{-}\right) \qquad \text{A.30}$$

$$P_g + s\left(R_g^{10}\overline{u_g} + N_{c,g}^{g}\overline{P}_g\right) \le R_g^{10}\overline{u_g} + N_{c,g}^{g}\overline{P}_g, \qquad \forall g \quad \left(\beta_{gct}^{+}\right) \qquad \text{A.31}$$

$$-P_g + s\left(-P_g^{min}\overline{u_g}N_{c,g}^{g}\right) \le -P_g^{min}\overline{u_g}N_{c,g}^{g}, \qquad \forall g \quad \left(\gamma_{gct}^{-}\right) \qquad \text{A.32}$$

$$P_g + s\left(P_g^{max}\overline{u_g}N_{c,g}^{g}\right) \le P_g^{max}\overline{u_g}N_{c,g}^{g}, \qquad \forall g \quad \left(\gamma_{gct}^{+}\right) \qquad \text{A.33}$$

$$P_k - b_k(\theta_n - \theta_m) = 0, \qquad \forall k \quad \left(s_{kct}^{g}\right) \qquad \text{A.34}$$

$$-P_k \le (\overline{S_{NG}^{-}} + P_k^{max,c})(1-s), \qquad \forall k \quad \left(F_{kct}^{g-}\right) \qquad \text{A.35}$$

$$P_k \le (\overline{S_{NG}^{+}} + P_k^{max,c})(1-s), \qquad \forall k \quad \left(F_{kct}^{g+}\right) \qquad \text{A.36}$$

The formulation of feasibility cuts for line contingency

$$\sum_g\left(R_g^{10}u_{g,t} - P_{gt}\right)\alpha_{gct}^{r-} + \sum_{\forall g}\left(R_g^{10}u_{g,t} + P_{g,t}\right)\alpha_{gct}^{r+} + \sum_{\forall g}\left(-P_g^{min}u_{gt}\right)\eta_{gct}^{r-} + \sum_{\forall g}\left(P_g^{max}u_{gt}\right)\eta_{gct}^{r+} + C_{c,t}^{r} \le 0 \qquad \text{A.37}$$

Where

$$C_{c,t}^{r} = \sum_{\forall k}\left(N_{c,k}^{k}(S_{NK}^{-} + P_{k}^{max,c})\right)F_{kct}^{r\,k-} + \sum_{\forall k}\left(N_{c,k}^{k}(S_{NK}^{+} + P_{k}^{max,c})\right)F_{kct}^{r\,k+} + \sum_{\forall n}\left(d_{n,t}\right)LMP_{nct}^{r} \quad \forall r, c \in N^{k}, t \qquad \text{A.38}$$

The formulation of feasibility cuts for generator contingency

$$\sum_{\forall g}\left(R_{g}^{10}u_{g,t} - N_{c,g}^{g}P_{gt}\right)\beta_{gct}^{r-} + \sum_{\forall g}\left(R_{g}^{10}u_{g,t} + N_{c,g}^{g}P_{g,t}\right)\beta_{gct}^{r+} + \sum_{\forall g}\left(-P_{g}^{min}u_{gt}N_{c,g}^{g}\right)\gamma_{gct}^{r-} + \sum_{\forall g}\left(P_{g}^{max}u_{gt}N_{c,g}^{g}\right)\gamma_{gct}^{r+} + C_{c,t}^{r} \leq 0 \quad \forall r, c \in N^{g}, t \qquad \text{A.39}$$

Where

$$C_{c,t}^{r} = \sum_{\forall k}\left(S_{NG}^{-} + P_{k}^{max,c}\right)F_{kct}^{r\,g-} + \sum_{\forall k}\left(S_{NG}^{+} + P_{k}^{max,c}\right)F_{kct}^{r\,g+} + \sum_{\forall n}\left(d_{n,t}\right)LMP_{nct}^{r} \quad \forall r, c \in N^{g}, t \qquad \text{A.40}$$